PLANE-STRAIN DIFFRACTION OF TRANSIENT ELASTIC WAVES BY A CIRCULAR CAVITY

Thesis by

Jerry Clifford Pcck

In Partial Fulfillment of the Requirements

For the Degree of

Doctor of Philosophy

California Institute of Technology

Pasadena, California

1965

(Submitted May 19, 1965)

ACKNOWLEDGEMENTS

The author is greatly indebted to Professor J. Miklowitz for suggesting the present problem and for his stimulating encouragement and wise guidance. The author's wife, Zoe, is gratefully thanked for her confidence and fortitude. Special thanks are also due to Professor E. E. Sechler for his help in many matters; to the Western Data Processing Center at UCLA (especially Off-Campus Consultant Gale Montgomery), where a large part of the numerical calculations were performed; to the staff of the Caltech Computing Center; and last, but so helpful and competent, to Mrs. Elizabeth Fox for her preparation of the typed manuscript and Mrs. Betty Wood for her preparation of the figures.

ABSTRACT

The plane-strain problem of the diffraction of a transient plane dilatation wave by a circular cavity in an elastic medium is treated. The method used determines the (total) solution only in the shadow zone, i.e., those points which cannot be connected to the source of disturbance by straight-line rays. Numerical results are obtained for the velocities and displacements on the "back" surface of the cavity caused by a step-stress incident wave.

The analysis is based on a method devised by Friedlander (see his book Sound Pulses, Cambridge, 1958) for the analogous acoustic diffraction problem. This method converges most rapidly at short time, in contrast to Fourier series methods. The Friedlander method essentially employs integral transforms on both time and θ, the circumferential coordinate. In the shadow zone, the θ-inversion can be performed by residue theory, the residues resulting from poles at the roots of a "frequency equation." The roots are infinite in number, and may be regarded as forming a dispersion spectrum relating the frequencies and angular wave numbers of a series of circumferential propagation modes. The time-transform inversion is carried out by contour integration and subsequent numerical evaluation.

The transient response results are found to compare well with the Fourier-series solutions at moderate to long times, but at short time the differences are marked, as would be expected. The fact that the present technique yields good long-time results suggests it is even more powerful than might be expected. The major limitation of the numerical method is its restriction to the shadow zone.

TABLE OF CONTENTS

TABLE OF CONTENTS (Cont'd)

TABLE OF CONTENTS (Cont'd)

LIST OF FIGURES

LIST OF FIGURES (Cont'd)

LIST OF FIGURES (Cont'd)

NOMENCLATURE

Latin Symbols

a	radius of cavity
a_j	zeros of Ai(z)
$A(\nu,p)$	(see Equation 2.21)
Ai(z)	Airy function
$B(\nu,p)$	(see Equation 2.22)
c	general wave velocity
C	integration contour for inversion of Laplace transform (Figure 6)
c_d	dilatation wave velocity
c_R	Rayleigh wave velocity
c_s	shear wave velocity
$D(\nu,p)$	frequency function (see Equation 2.23)
$D_p(\nu,p) = \frac{\partial}{\partial p} D(\nu,p)$	
$D_\nu(\nu,p) = \frac{\partial}{\partial \nu} D(\nu,p)$	
$f(r,\theta,t)$	general response function, e.g., displacement, etc.
$f_j^*(r,\theta,t)$	response in jth mode of f in wave sum form
$f_{jF}^*(r,\theta,t)$	integral for f_j^* on imaginary p axis
$f_{j0}^*(r,\theta,t)$	branch point contribution to f_j^*
$f_{j\Delta}^*(r,\theta,t)$	contribution to f_j^* from $0 \leq \Omega \leq \Delta$
$\hat{f}_j(r,\Omega)$	non-oscillatory factor in integrand (Equation 4.12)
$H(t)$	Heaviside step function
$H_\nu(z)$	Hankel function of the first kind
j	mode number
$k_d = p/c_d$	
$k_s = p/c_s$	

p		Laplace transform parameter
m		number associated with terms or "waves" in wave sum
P1,P2,...		designations for series of modes associated with c_d
r		radial coordinate
R		Rayleigh mode designation
S1,S2,...		designation for series of modes associated with c_s
t		time
T	=	$\frac{c_d t}{a}$
u		radial displacement
u_0	=	$\frac{\sigma_0 a}{\lambda+2\mu}$ normalization constant for displacements
$\dot{u}_0$	=	$\frac{\sigma_0 c_d}{\lambda+2\mu}$ normalization constant for velocities
v		circumferential displacement
x		Cartesian coordinate
y		Cartesian coordinate
z		general complex variable

Greek Symbols

α	=	$\frac{c_d}{c_s}$
ϵ	=	$\nu - 1$
ζ		(see Equation A.2)
θ		circumferential coordinate
κ		lineal wave number
λ		Lamé elastic constant
μ		Lamé elastic constant
ν		Fourier transform parameter angular wave number

ν_j root of D = 0

ν_j^+ the roots ν_j satisfying Im $\nu_j > 0$

ρ density

σ_r radial stress

σ_θ circumferential stress

σ_0 stress amplitude of incident wave

$\tau_{r\theta}$ shear stress

ϕ scalar displacement potential

Ψ non-zero component of vector displacement potential

$\omega = ip$ frequency

$\Omega = \frac{\omega a}{c_d}$ nondimensional frequency

$\Omega_s = \frac{\omega a}{c_s} = \alpha\Omega$

Subscripts and Superscripts

$(\ )_{inc}$ incident part of solution

$(\ )_{sc}$ scattered part of solution

$(\ )^*$ wave sum form of a function

$\bar{(\ )}$ Laplace transform

$\tilde{(\ )}$ double (Laplace-Fourier) transform

$\dot{(\ )}$ time derivative

$(\ )_j$ function associated with jth mode

1. INTRODUCTION

The purpose of this investigation is to obtain analytical and numerical results for the diffraction of a stress pulse by a circular cylindrical cavity in an infinite elastic medium. We consider the two dimensional, plane-strain, problem in which the incident pulse is the same at all points of any straight line parallel to the axis of the cylinder. The specific incident pulse considered is a plane-fronted dilatation wave whose stress has step-function time dependence.

There has been considerable interest in this problem in recent years because it has a bearing on the design of underground structures to withstand severe ground shock environments (1). However, beyond this, it has fundamental significance as one of the simplest examples of the diffraction of stress waves by a smooth curvilinear boundary.

Previous numerical treatments of the problem (2-5) have used a Fourier series representation of the dependence on θ, the circumferential coordinate. The Fourier series may be expected to converge rapidly at long time, since the exact static solution is a two term series. However at short time the convergence has been found to be poor. Thus the need arose for a form of solution which would yield accurate numerical results for short times.

An approach to the diffraction of pulses by a circular boundary in an acoustic medium, which yielded short time approximations, was developed by Friedlander (6) in 1954. This method utilizes double integral transforms, on time and θ. In the diffracted region,

the spatial inversion is performed by residue theory, producing an infinite series of circumferential propagation modes, whose frequency-wave length relations comprise a dispersive spectrum. Gilbert (7,8) utilized this technique to develop wave-front approximations for elastodynamic problems. Miklowitz proposed that the technique would be useful for obtaining analytical and numerical results (9), in a manner similar to that used in rod and plate theory (10). Miklowitz noted that a branch of the spectrum was associated with the Rayleigh velocity and developed an approximation for the associated circumferentially propagating Rayleigh pulse (9, 11, 12).

The present investigation is devoted to exploiting the numerical possibilities of the double transform-residue method, as suggested by Miklowitz. The inversion by residues reduces the problem to the Laplace (time) inversion of a series of circumferential propagation modes, which is carried out numerically. This mode series converges rapidly near the wave fronts and thus complements the previous numerical work based on the use of Fourier series.

The inversion of the θ-transform by residues is essential to the numerical evaluation, because it reduces the double inversion integral to a single integral. However, the price paid for this simplification is a restriction of the area of applicability of the method to the so-called shadow or diffraction zone. For the case of an incident plane pulse the shadow zone is that shown in Figure 1.* For points on the surface of the cavity, this restriction means that

* The residue solution for the diffracted waves can be obtained outside the shadow zone in Figure 1, but it is not the total response in this region.

the total response can be found only on the "back" side of the cavity.

The first step in the numerical analysis is the determination of the roots of the frequency equation relating the frequency and circumferential wave number, for the residue series is formed by poles associated with these roots. The frequency equation involves Bessel functions of complex order, the wave number and frequency being the order and argument of the Bessel functions, respectively. The zeros are found numerically and checked by approximations valid at high and low frequency. The behavior is found to be similar to that associated with the simpler equations governing electromagnetic diffraction problems, which have been studied by similar means quite recently (13).

The inversion of the Laplace transform is carried out by contour integration and subsequent numerical evaluation of the resultant integrals. The transient response is obtained for the displacements and velocities on the surface of the cavity. Comparison of these results with Baron's Fourier series results (3) shows good agreement at moderate to long times, indicating a desirable overlap of the region of convergence of the respective series. The short time response obtained with the present method differs considerably from Baron's, as would be expected. Thus the present technique provides an estimate of the region of validity of the Fourier series results, in addition to its usefulness in its own right.

2. METHOD OF ANALYSIS

2.1 Statement of Problem

Consider the plane-strain problem shown in Figure 1. A plane dilatation wave, propagating freely in a homogeneous, isotropic, linearly elastic solid impinges on a circular cavity, passing the center of the cavity at time t = 0.

The problem is treated by displacement potentials ϕ and $\vec{\Psi}$, where the displacement $\vec{u}$ is given by

$$\vec{u} = \nabla\varphi + \nabla\times\vec{\psi}, \qquad \nabla\cdot\vec{\psi} = 0$$

Then the governing displacement equation of motion,

$$(\lambda+2\mu)\,\nabla(\nabla\cdot\vec{u}) - \mu\,\nabla\times\nabla\times\vec{u} = \rho\,\frac{\partial^2\vec{u}}{\partial t^2}$$

is satisfied by solutions of the wave equations

$$\nabla^2\varphi = \frac{1}{c_d^2}\,\frac{\partial^2\varphi}{\partial t^2}, \qquad c_d^2 = \frac{\lambda+2\mu}{\rho} \tag{2.1a}$$

$$\nabla^2\psi = \frac{1}{c_s^2}\,\frac{\partial^2\psi}{\partial t^2}, \qquad c_s^2 = \frac{\mu}{\rho} \tag{2.1b}$$

where Ψ is the component of $\vec{\Psi}$ perpendicular to the x-y plane, and, for problems in plane strain, the other components of $\vec{\Psi}$ may be taken to be zero. λ and μ are Lamé's elastic constants, c_d and c_s are the dilatation and shear wave velocities, respectively, and ρ is the density.

In the polar coordinate system (r,θ) one has for the Laplacian operator

$$\nabla^2 = \frac{\partial^2}{\partial r^2} + \frac{1}{r}\,\frac{\partial}{\partial r} + \frac{1}{r^2}\,\frac{\partial^2}{\partial\theta^2}$$

and for the radial and circumferential displacement components u and v,

$$u = \frac{\partial \varphi}{\partial r} + \frac{1}{r}\frac{\partial \psi}{\partial \theta} \tag{2.2a}$$

$$v = \frac{1}{r}\frac{\partial \varphi}{\partial \theta} - \frac{\partial \psi}{\partial r} \tag{2.2b}$$

Using the strain-displacement and stress-strain relations the stresses may be expressed in terms of the potentials as

$$\sigma_r = (\lambda+2\mu)\nabla^2\varphi + 2\mu\left(-\frac{1}{r}\frac{\partial \varphi}{\partial r} - \frac{1}{r^2}\frac{\partial^2 \varphi}{\partial \theta^2} - \frac{1}{r^2}\frac{\partial \psi}{\partial \theta} + \frac{1}{r}\frac{\partial^2 \psi}{\partial r \partial \theta}\right) \tag{2.3a}$$

$$\sigma_\theta = (\lambda+2\mu)\nabla^2\varphi - 2\mu\left(\frac{\partial^2 \varphi}{\partial r^2} - \frac{1}{r^2}\frac{\partial \psi}{\partial \theta} + \frac{1}{r}\frac{\partial^2 \psi}{\partial r \partial \theta}\right) \tag{2.3b}$$

$$\tau_{r\theta} = \mu\left(\frac{2}{r}\frac{\partial^2 \varphi}{\partial r \partial \theta} - \frac{2}{r^2}\frac{\partial \varphi}{\partial \theta} + \frac{1}{r^2}\frac{\partial^2 \psi}{\partial \theta^2} - \frac{\partial^2 \psi}{\partial r^2} + \frac{1}{r}\frac{\partial \psi}{\partial r}\right) \tag{2.3c}$$

The solution is separated into an incident and a scattered part. The incident part is that corresponding to the case when the cavity is absent. It is taken as given, and must satisfy the wave equations. The scattered part must be such as to satisfy the boundary conditions at the cavity, in addition to satisfying the wave equations. Thus the boundary conditions for the problem are

$$\sigma_{r_{sc}}(a,\theta,t) = -\sigma_{r_{inc}}(a,\theta,t) \tag{2.4a}$$

$$\tau_{r\theta_{sc}}(a,\theta,t) = -\tau_{r\theta_{inc}}(a,\theta,t) \tag{2.4b}$$

so that the total stress at the surface of the cavity, r = a, is zero. The subscripts $(\,)_{sc}$ and $(\,)_{inc}$ denote the scattered and incident

parts, respectively.

The incident plane dilatation wave is specified by the function $\phi_0(t)$ in

$$\varphi_{inc}(r,\theta,t) = \varphi_0\left(t + \frac{r\cos\theta}{c_d}\right) H\left(t + \frac{r\cos\theta}{c_d}\right) \qquad (2.5a)$$

For a step-function stress of amplitude σ_0

$$\varphi_0(t) = \frac{\sigma_0 c_d^2}{\lambda+2\mu} \frac{t^2}{2} \qquad (2.5b)$$

Since the incident wave first touches the cavity at $t = -\frac{a}{c_d}$ the initial conditions for the scattered waves are

$$\varphi_{sc} = \frac{\partial \varphi_{sc}}{\partial t} = \psi_{sc} = \frac{\partial \psi_{sc}}{\partial t} = 0; \qquad t = -\frac{a}{c_d}$$

2.2 Geometry of Rays and Wave Fronts

The positions of the various wave fronts in the present problem can be found through geometrical reasoning based on the concept of rays. Since the method of solution is intimately connected with the wave front propagation, these geometrical arguments will be presented at this point.

A ray may be defined as the minimum time path along which a signal is propagated from a source of disturbance to a "receiver" or field point. For the sake of simplicity, first consider the acoustic (one-velocity) problem. The plane-fronted incident wave may be regarded as the disturbance emanating from a source at $r = \infty$ and $\theta = 0$. Then the incident rays are straight lines parallel to the horizontal axis as shown in Figure 2. Points outside the shadow zone

receive signals via straight lines which are either purely incident rays or incident plus reflected rays. However, points in the shadow zone can receive signals only via rays which lie in part along the surface r = a. On all rays the signals propagate at the wave speed c and by using this property the wave fronts may be constructed. The position of the diffracted wave fronts on r = a is particularly easy to determine. For waves propagating in the positive θ direction the fronts on r = a are given simply by

$$\theta - \frac{\pi}{2} = \frac{ct}{a} \tag{2.6}$$

since t = 0 is taken when the incident wave is at the center of the cavity.

The development of the wave fronts as time increases is shown in Figure 3. The comparison between Figures 3(b) and 3(c) is especially significant. A time difference of ct/a = 2π has elapsed between these cases, so the diffracted front on r = a has propagated an additional angle of 2π. This "winding" of the diffracted waves around the cavity continues ad infinitum.

The above discussion also applies to the dilatational fronts in the elastodynamic problem. However, in this case the dilatation-shear mode conversion at the cavity surface gives rise to shear waves also. Since these details become rather involved, and are not of major concern for present purposes, they will not be discussed here. Gilbert gives a thorough treatment of dilatation and shear wave diffraction in References 7 and 8. Diffracted Rayleigh wave pulses also occur, with their arrival times governed by Equation 2.6 with c = c_R, the Rayleigh velocity, as discussed in Miklowitz's work (9, 11, 12).

2.3 Friedlander's Representation of the θ-Dependence

It has long been known that for harmonic wave diffraction problems by spheres and circular cylinders the Fourier series type of solution converges increasingly slowly in the shadow zone as the frequency is increased. It was discovered that this difficulty could be resolved by changing the form of the solution through the use of Poisson's summation formula (14), which may be stated

$$\sum_{n=-\infty}^{\infty} F(n) = \sum_{m=-\infty}^{\infty} \int_{-\infty}^{\infty} F(\xi) e^{i2m\pi\xi} d\xi$$

Applied to a Fourier series for the function $g(\theta)$ this gives

$$g(\theta) = \sum_{n=-\infty}^{\infty} G(n) e^{in\theta} = \sum_{m=-\infty}^{\infty} \int_{-\infty}^{\infty} G(\xi) e^{i\xi(\theta+2m\pi)} d\xi$$

i.e.,

$$g(\theta) = \sum_{m=-\infty}^{\infty} g^*(\theta+2m\pi) \tag{2.7a}$$

where

$$g^*(\theta) = \int_{-\infty}^{\infty} G(\xi) e^{i\xi\theta} d\xi \tag{2.7b}$$

For reasons which will become clear presently, the sum on m of g^* will be called the "wave sum" representation of $g(\theta)$.

It turns out that this way of representing the θ dependence of the solutions to harmonic diffraction problems permits them to be evaluated in ways for which the convergence becomes more rapid as the frequency is increased.

Since high frequency is associated with short time through integral transform theory, it might be expected that in transient problems the wave sum representation would lead to a solution appropriate for wave front evaluations. Friedlander (6) was apparently the first to try this idea. He attacked the diffraction of transient acoustic waves by a circular cylinder, and showed that not only did the wave sum form give good wave front solutions but also that this form of solution corresponds remarkably well with the physical phenomena of the problem.

Before discussing Friedlander's results in detail, the appropriate notation for the present problem will be given and the initial-boundary value problem will be set. Let $f(r,\theta,t)$ denote any of the response functions of interest, i.e., potentials, displacements, etc. Then the wave sum representation will be written

$$f(r,\theta,t) = \sum_{m=-\infty}^{\infty} f^*(r,\theta+2m\pi,t) \tag{2.8}$$

The incident potential ϕ_{inc} is the only given function in the problem, so once it is written in the wave sum form one can set the problem for the scattered potentials $\phi^*_{sc}(r,\theta,t)$ and $\Psi^*_{sc}(r,\theta,t)$ as follows:

$$\frac{\partial^2 \varphi^*_{sc}}{\partial r^2} + \frac{1}{r}\frac{\partial \varphi^*_{sc}}{\partial r} + \frac{1}{r^2}\frac{\partial^2 \varphi^*_{sc}}{\partial \theta^2} = \frac{1}{c_d^2}\frac{\partial^2 \varphi^*_{sc}}{\partial t^2} \tag{2.9a}$$

$$\frac{\partial^2 \psi^*_{sc}}{\partial r^2} + \frac{1}{r}\frac{\partial \psi^*_{sc}}{\partial r} + \frac{1}{r^2}\frac{\partial^2 \psi^*_{sc}}{\partial \theta^2} = \frac{1}{c_s^2}\frac{\partial^2 \psi^*_{sc}}{\partial t^2} \tag{2.9b}$$

$$\sigma^*_{r_{sc}}(a,\theta,t) = -\sigma^*_{r_{inc}}(a,\theta,t) \tag{2.10a}$$

$$\tau^*_{r\theta_{sc}}(a,\theta,t) = -\tau^*_{r\theta_{inc}}(a,\theta,t) \tag{2.10b}$$

$$\varphi^*_{sc} = \frac{\partial \varphi^*_{sc}}{\partial t} = \psi^*_{sc} = \frac{\partial \psi^*_{sc}}{\partial t} = 0; \quad t = -\frac{a}{c_d}$$

where $\sigma^*_{r_{inc}}$ and $\tau^*_{r\theta_{inc}}$ are found from ϕ^*_{inc}. It is apparent that the wave sum of the solutions to the above problem will be the solution to the original problem, provided the wave sums involved all converge. But it will shortly be seen that the wave sum has a finite number of terms, so convergence does not enter.

The solution will be obtained through the use of integral transforms, and it turns out that the transform of ϕ^*_{inc} has a simple expression, whereas ϕ^*_{inc} itself does not, so it will not be given at this point.

Now the discussion of Friedlander's results will be resumed. He obtained wave front approximations for f^* (in the analogous acoustic problem) for which the wave front positions coincide exactly with those obtained on the basis of the geometrical reasoning of Section 2.2. That is, the diffracted fronts wind around the cavity. Plotted against θ as a rectilinear coordinate, a typical response function f^* on $r = a$, is shown in Figure 4(a), propagating outward from $\theta = 0$ as time increases. With this picture of the behavior of $f^*(a,\theta,t)$ the physical significance of the wave sum can be appreciated. It is simply the sum of those parts of f^* that have overlapped each other at a given θ as f^* winds around the cavity. Since for finite

time it will have overlapped itself only a finite number of times, the wave sum is finite. The appearance of the wave sum for θ constant and $r = a$ is shown in Figure 4(b). There is a succession of arrivals corresponding to wave fronts passing θ as they propagate in the positive and negative θ directions.

It is convenient at this time to give some of the qualitative results that Friedlander obtained from his wave front approximations. He showed that the diffracted wave front behavior is smooth regardless of the character of the incident wave. Furthermore, the amplitudes near the wave fronts decay rather rapidly as the wave propagates into the shadow.

The wave sum representation has been used by Payton (16) and Levey and Mahoney (17) for acoustic problems, and Gilbert (7,8), Miklowitz (9,11,12), and Grimes (18) for elastodynamic problems. These authors obtained various types of approximations to the response valid near wave arrival times. The present work is devoted to the numerical evaluation of the solution in the shadow zone, for short to moderate time. This is one of the regions where Gilbert (8) obtained his approximations, but it appears that a sizable extension of his work would be necessary before his approximations could be made applicable to the present problem. Therefore no quantitative comparisons between Gilbert's approximations and the present work will be made. However, it may be remarked that qualitative properties of the diffracted dilatational fronts obtained by Gilbert are the same as Friedlander found in the acoustic problem, and these properties will be observed in the numerical results presented

in Chapter 4.

Grimes' work considered the reflected wave fronts which are not treated in the present problem. The approximations obtained by Miklowitz applied to the Rayleigh pulse in the deep shadow, i.e., after the pulse has propagated around the cavity one or more times. In this sense it is long time, even though it is concerned with short times away from pulse arrivals. The numerical methods used here are not suitable for long times, so no direct comparison can be made with Miklowitz's work either. However, the occurrence of a pulse-like disturbance at the diffracted Rayleigh wave arrival time is observed in the numerical results even at short time.

2.4 Application of Integral Transforms

The bilateral Laplace transform on time will be denoted by

$$\bar{f}(h,\theta,p) = \int_{-\infty}^{\infty} f(h,\theta,t)\, e^{-pt}\, dt \qquad (2.11a)$$

where

$$f(h,\theta,t) = \frac{1}{2\pi i} \int_{Br} \bar{f}(h,\theta,p)\, e^{pt}\, dp \qquad (2.11b)$$

Br is the Bromwich contour, $\mathrm{Re}\, p = c$, $-R \leq \mathrm{Im}\, p \leq R$, $R \to \infty$, and c must lie in the strip of convergence of the definition integral, Equation 2.11a (see, for example, Reference 15). The subsequent Fourier transform on θ will be denoted by

$$\tilde{f}(h,\nu,p) = \int_{-\infty}^{\infty} \bar{f}(h,\theta,p)\, e^{i\nu\theta}\, d\theta \qquad (2.12a)$$

where

$$\bar{f}(r,\theta,p) = \frac{1}{2\pi}\int_{-\infty}^{\infty} \tilde{f}(r,v,p)\, e^{-iv\theta}\, dv \qquad (2.12b)$$

Applying these to the field equations 2.9 and boundary conditions 2.10 gives

$$\frac{d^2\tilde{\varphi}^*_{sc}}{dr^2} + \frac{1}{r}\frac{d\tilde{\varphi}^*_{sc}}{dr} - \left(\frac{v^2}{r^2} + k_d^2\right)\tilde{\varphi}^*_{sc} = 0 \qquad (2.13a)$$

$$\frac{d^2\tilde{\psi}^*_{sc}}{dr^2} + \frac{1}{r}\frac{d\tilde{\psi}^*_{sc}}{dr} - \left(\frac{v^2}{r^2} + k_s^2\right)\tilde{\psi}^*_{sc} = 0 \qquad (2.13b)$$

$$\tilde{\sigma}^*_{r_{sc}}(a,v,p) = -\tilde{\sigma}^*_{r_{inc}}(a,v,p) \qquad (2.14a)$$

$$\tilde{\tau}^*_{r\theta_{sc}}(a,v,p) = -\tilde{\tau}^*_{r\theta_{inc}}(a,v,p) \qquad (2.14b)$$

where

$$k_d = \frac{p}{c_d}, \qquad k_s = \frac{p}{c_s}$$

The transformed displacement and stress expressions may be written

$$\tilde{u}^* = \frac{d\tilde{\varphi}^*}{dr} - \frac{iv}{r}\tilde{\psi}^* \qquad (2.15a)$$

$$\tilde{v}^* = -\frac{iv}{r}\tilde{\varphi}^* - \frac{d\tilde{\psi}^*}{dr} \qquad (2.15b)$$

$$\tilde{\sigma}^*_r = \mu r^{-2}\left[\left(k_s^2 r^2 + 2v^2\right)\tilde{\varphi}^* - 2r\frac{d\tilde{\varphi}^*}{dr} + 2iv\left(\tilde{\psi}^* - r\frac{d\tilde{\psi}^*}{dr}\right)\right] \qquad (2.16a)$$

$$\tilde{\sigma}_\theta^* = \mu r^{-2}\left[\left(k_s^2 r^2 - 2v^2 - 2k_y^2 r^2\right)\tilde{\varphi}^* + 2r\frac{d\tilde{\varphi}^*}{dr} - 2iv\left(\tilde{\psi}^* - r\frac{d\tilde{\psi}^*}{dr}\right)\right] \qquad (2.16b)$$

$$\tilde{\tau}_{r\theta}^* = \mu r^{-2}\left[2iv\left(\tilde{\varphi}^* - r\frac{d\tilde{\varphi}^*}{dr}\right) - \left(2v^2 + k_s^2 r^2\right)\tilde{\psi}^* + 2r\frac{d\tilde{\psi}^*}{dr}\right] \qquad (2.16c)$$

The double transform of the incident potential, $\tilde{\phi}_{inc}^*$, is found by applying the Poisson summation formula to the Fourier series of the Laplace transform of ϕ_{inc}. From Equations 2.5

$$\bar{\varphi}_{inc}(r,\theta,p) = \bar{\varphi}_o(p)\, e^{k_y r\cos\theta} \qquad (2.17a)$$

where

$$\bar{\varphi}_o(p) = \frac{\sigma_o c_d^2}{\lambda+2\mu}\, p^{-3} \qquad (2.17b)$$

The Fourier series is

$$\bar{\varphi}_{inc}(r,\theta,p) = \sum_{n=-\infty}^{\infty} \bar{\varphi}_o(p)\left\{\frac{1}{2\pi}\int_{-\pi}^{\pi} e^{k_y r\cos\theta - in\theta}\, d\theta\right\} e^{in\theta}$$

$$= \sum_{n=-\infty}^{\infty} \bar{\varphi}_o(p)\, I_n(k_y r)\, e^{in\theta}$$

from the integral definition of $I_n(z)$, given, for example, in Reference 30. Since $I_n(z) = I_{-n}(z)$ one has also

$$\bar{\varphi}_{inc}(r,\theta,p) = \sum_{n=-\infty}^{\infty} \bar{\varphi}_o(p)\, I_{|n|}(k_y r)\, e^{in\theta}$$

Then, applying Equation 2.7b,

$$\bar{\varphi}^{*}_{inc}(\lambda,\theta,p) = \int_{-\infty}^{\infty} \bar{\varphi}_o(p)\, I_{|\xi|}(k_d\lambda)\, e^{i\xi\theta}\, d\xi$$

so

$$\tilde{\varphi}^{*}_{inc}(\lambda,\nu,p) = \bar{\varphi}_o(p) \int_{-\infty}^{\infty}\int_{-\infty}^{\infty} I_{|\xi|}(k_d\lambda)\, e^{i\theta(\xi+\nu)}\, d\xi\, d\theta$$

Since $I_\nu(z)$ approaches zero exponentially as $\nu \to \infty$ (see Reference 23, for example) the Fourier integral theorem may be applied to give

$$\tilde{\varphi}^{*}_{inc}(\lambda,\nu,p) = 2\pi\bar{\varphi}_o(p)\, I_{|\nu|}(k_d\lambda) \tag{2.18}$$

It will later be seen that when the sum of the incident and scattered solution is formed, the sum is even in ν when I_ν is substituted for $I_{|\nu|}$, even though $I_\nu(z) \neq I_{-\nu}(z)$. For the sake of convenience, this result will be anticipated in the writing of some of the expressions which follow, by writing I_ν for $I_{|\nu|}$ (but the individual statements will be made rigorous by the temporary restriction that $\nu > 0$). Thus, the transforms of the incident stresses are found to be, for $\nu > 0$,

$$\tilde{\sigma}^{*}_{\lambda_{inc}} = 2\pi\mu\,\bar{\varphi}_o(p)\,\lambda^{-2}\left[(2\nu^2+k_s^2\lambda^2)\,I_\nu(k_d\lambda) - 2k_d\lambda\, I'_\nu(k_d\lambda)\right] \tag{2.19a}$$

$$\tilde{\tau}_{\lambda\theta_{inc}} = 2\pi\mu\,\bar{\varphi}_o(p)\,\lambda^{-2}\,(2i\nu)\left[\, I_\nu(k_d\lambda) - k_d\lambda\, I'_\nu(k_d\lambda)\,\right] \tag{2.19b}$$

2.5 Solution of the Transformed Equations

The solutions of the transformed wave equations 2.13 for the scattered potentials which vanish as $r \to \infty$ are

$$\tilde{\varphi}^{*}_{sc}(r,\nu,p) = A(\nu,p)\, K_\nu(k_d r)$$

$$\tilde{\psi}^{*}_{sc}(r,\nu,p) = B(\nu,p)\, K_\nu(k_s r)$$

where A and B are determined from the boundary conditions 2.14 at r = a, which when written out in full for $\nu > 0$, are

$$\mu a^{-2}\Big\{\Big[(2\nu^2+k_s^2a^2)K_\nu(k_da)-2k_da\,K'_\nu(k_da)\Big]A + 2i\nu\Big[K_\nu(k_sa)-k_sa\,K'_\nu(k_sa)\Big]B\Big\} = -\mu a^{-2}2\pi\bar{\varphi}_o(p)\Big[(2\nu^2+k_s^2a^2)I_\nu(k_da)-2k_da\,I'_\nu(k_da)\Big] \qquad (2.20a)$$

$$\mu a^{-2}\Big\{2i\nu\Big[K_\nu(k_da)-k_da\,K'_\nu(k_da)\Big]A - \Big[(2\nu^2+k_s^2a^2)K_\nu(k_sa)-2k_sa\,K'_\nu(k_sa)\Big]B\Big\} = -\mu a^{-2}2i\nu\,\bar{\varphi}_o(p)\Big[I_\nu(k_da)-k_da\,I'_\nu(k_da)\Big]2\pi \qquad (2.20b)$$

Solving Equations 2.20 for A and B gives

$$A(\nu,p) = \Big[D(\nu,p)\Big]^{-1}2\pi\bar{\varphi}_o(p)\Big\{\Big[(2\nu^2+k_s^2a^2)I_\nu(k_da)-2k_da\,I'_\nu(k_da)\Big]\cdot\Big[(2\nu^2+k_s^2a^2)K_\nu(k_sa)-2k_sa\,K'_\nu(k_sa)\Big] - 4\nu^2\Big[I_\nu(k_da)-k_da\,I'_\nu(k_da)\Big]\cdot\Big[K_\nu(k_sa)-k_sa\,K'_\nu(k_sa)\Big]\Big\} \qquad (2.21)$$

$$B(\nu,p) = \Big[D(\nu,p)\Big]^{-1}2\pi\bar{\varphi}_o(p)\,(2i\nu)(2\nu^2+k_s^2a^2-2) \qquad (2.22)$$

where

$$D(\nu,p) = -\Big\{\Big[(2\nu^2+k_s^2a^2)\,K_\nu(k_da) - 2k_da\,K_\nu'(k_da)\Big]$$
$$\cdot\Big[(2\nu^2+k_s^2a^2)K_\nu(k_sa) - 2k_sa\,K_\nu'(k_sa)\Big]$$
$$-4\nu^2\Big[K_\nu(k_da) - k_da\,K_\nu'(k_da)\Big]\cdot\Big[K_\nu(k_sa) - k_sa\,K_\nu'(k_sa)\Big]\Big\} \tag{2.23}$$

The Wronskian

$$K_\nu(z)I_\nu'(z) - K_\nu'(z)I_\nu(z) = z^{-1}$$

has been used to simplify the expression for $B(\nu,p)$.

The expressions for the transformed displacements and stresses are, for $\nu > 0$,

$$\tilde{u}_{sc}^*(r,\nu,p) = r^{-1}\Big[k_dr\,K_\nu'(k_dr)\,A(\nu,p) - i\nu K_\nu(k_sr)\,B(\nu,p)\Big] \tag{2.24a}$$

$$\tilde{v}_{sc}^*(r,\nu,p) = -r^{-1}\Big[i\nu K_\nu(k_dr)\,A(\nu,p) + k_sr\,K_\nu'(k_sr)\,B(\nu,p)\Big] \tag{2.24b}$$

$$\tilde{\sigma}_{rr_{sc}}^*(r,\nu,p) = \mu r^{-2}\Big\{\Big[(2\nu^2+k_s^2r^2)K_\nu(k_dr) - 2k_dr\,K_\nu'(k_dr)\Big]\,A(\nu,p)$$
$$+2i\nu\Big[K_\nu(k_sr) - k_sr\,K_\nu'(k_sr)\Big]\,B(\nu,p)\Big\} \tag{2.25a}$$

$$\tilde{\sigma}^{*}_{\theta_{sc}}(\lambda,\nu,p) = \mu\lambda^{-2}\left\{2i\nu\left[K_\nu(k_d\lambda) - k_d\lambda K_\nu'(k_d\lambda)\right]A(\nu,p)\right.$$

$$\left. - \left[(2\nu^2 + k_s^2\lambda^2)K_\nu(k_s\lambda) - 2k_s\lambda K_\nu'(k_s\lambda)\right]B(\nu,p)\right\} \quad (2.25b)$$

$$\tilde{\tau}^{*}_{r\theta_{sc}}(\lambda,\nu,p) = \mu\lambda^{-2}\left\{\left[(k_s^2\lambda^2 - 2\nu^2 - k_d^2\lambda^2)K_\nu(k_d\lambda) + 2k_d\lambda K_\nu'(k_d\lambda)\right]A(\nu,p)\right.$$

$$\left. - 2i\nu\left[K_\nu(k_s\lambda) - k_s\lambda K_\nu'(k_s\lambda)\right]B(\nu,p)\right\} \quad (2.25c)$$

2.6 The Bromwich Contour for the Laplace Transform

In the inversion integral for the bilateral Laplace transform, Equation 2.11b, the Bromwich contour, $\mathrm{Re}\,p = c$, $-R \leq \mathrm{Im}\,p \leq R$, $R \to \infty$, must be chosen so that it lies in the strip of convergence, $c_1 < c < c_2$, of the definition integral given by Equation 2.11a. Let $f(r,\theta,t)$ denote any of the potentials, displacements, or stresses. It is physically reasonable to assume that f and f^* grow with time at most like t^n, so that

$$f^*(\lambda,\theta,t) = o(e^{at})$$

as $t \to \infty$ for any $a > 0$. This establishes the convergence of the definition integral at the upper limit for $\mathrm{Re}\,p > 0$. Since the functions associated with the scattered and incident waves are identically zero for $t < -a/c_d$ and $t < -x/c_d$, respectively, the definition integral converges at the lower limit for all finite p. Finally, assuming integrability of f^* for any bounded t interval, the strip of convergence is seen to be $0 < c < \infty$.

Under the conditions given above, the $\bar{f}^*$ are regular in the

interior of any closed region inside Re p > 0. To see this, integrate around any closed path Γ in the interior of such a closed region:

$$\int_{\Gamma} \bar{f}^*(r,\theta,p)\,dp = \int_{\Gamma}\int_{-\infty}^{\infty} f^*(r,\theta,t)e^{-pt}\,dt\,dp$$

For f^* integrable on any bounded t interval, e^{pt} continuous on p and t, and the t integral uniformly convergent, Theorem 14-26 of Reference 19 shows that the integrals on p and t may be interchanged, since the integral on p can be written as the sum of four real integrals. Regularity of $\bar{f}^*$ then follows from Morera's theorem.

2.7 Inversion of the θ-Transform by Residue Theory

Now the properties of the transforms will be considered in the complex ν-plane, so the transforms must thus be continued off the real ν axis. In order to do this, the use of $I_{|\nu|}(k_d r)$ for $\tilde{\phi}^*_{inc}$, as specified by Equation 2.18, will be re-examined. Consider

$$\tilde{\varphi}^*(r,\nu,p) = \tilde{\varphi}^*_{sc}(r,\nu,p) + \tilde{\varphi}^*_{inc}(r,\nu,p)$$

For $\nu > 0$, one has from Equations 2.18 and 2.21,

$$\tilde{\varphi}^*(r,\nu,p) = A(\nu,p)K_\nu(k_d r) + 2\pi\bar{\varphi}_0(p)I_\nu(k_d r)$$

Using the identity

$$I_{-\nu}(z) = I_\nu(z) + 2\pi^{-1}\sin\nu\pi\, K_\nu(z)$$

it is easy to show that

$$A(-\nu,p) = A(\nu,p) - 4\bar{\varphi}_0(p)\sin\nu\pi$$

and then one finds

$$\tilde{\varphi}^*(k,-\nu,p) = \tilde{\varphi}^*(k,\nu,p)$$

From this result it follows that, as far as the sum $\tilde{\phi}^* = \tilde{\phi}^*_{sc} + \tilde{\phi}^*_{inc}$ is concerned, it is irrelevant whether I_ν or $I_{|\nu|}$ is used for $\tilde{\phi}^*_{inc}$. Since I_ν occurs in the general response function transforms $\tilde{f}^*$ only through their dependence on $\tilde{\phi}^*$, the same holds true for $\tilde{f}^*$. Thus, in summary, the expressions obtained above for $\tilde{f}^*_{sc}$, when used in $\tilde{f}^* = \tilde{f}^*_{sc} + \tilde{f}^*_{inc}$, hold for all real ν. Then the continuation into the complex ν-plane is immediate.

The singularities of the functions $\tilde{f}^*(r,\nu,p)$ considered as a function of the complex variable ν will now be investigated. First, it is seen that ν occurs in $\tilde{f}^*$ only in two ways: as the order of K_ν and I_ν, and as ν raised to integral powers. Then, since $K_\nu(z)$ and $I_\nu(z)$ are entire functions with respect to their order, singularities of $\tilde{f}^*$ can arise only if there are zeros of $D(\nu,p)$, which occurs in the denominator of $A(\nu,p)$, and $B(\nu,p)$ in $\tilde{f}^*_{sc}$. In Chapter 3 it will be seen that $D(\nu,p)$ has an infinity of simple complex zeros, which are denoted $\nu_j(p)$. Therefore $\tilde{f}^*_{sc}$ has an infinity of simple poles at $\nu_j(p)$, and the inversion on ν can be performed using residue theory. By completing the ν contour by a sequence of curves C_j passing between the zeros, as shown in Figure 5,* and applying the residue theorem one obtains

$$f^*(k,\theta,t) = \sum_{j=-\infty}^{\infty} f_j^*(k,\theta,t) \qquad (2.26)$$

---

* For later convenience, θ is taken negative, so for convergence the C_j are taken in the upper half-plane. Results for positive θ are obtained by symmetry.

where

$$f_j^*(\lambda,\theta,t) \equiv \frac{1}{2\pi i}\int_{Br} \bar{f}_j^*(\lambda,\theta,p)e^{pt}dp \tag{2.27}$$

$$\bar{f}_j^*(\lambda,\theta,p)\Big|_{\theta<0} = i\tilde{f}_{sc}^*(\lambda,\nu_j^+,p)e^{-i\nu_j^+\theta}\frac{D(\nu_j^+,p)}{D_\nu(\nu_j^+,p)} \tag{2.28}$$

and

$$D_\nu(\nu,p) \equiv \frac{\partial D(\nu,p)}{\partial \nu}$$

The notation ν_j^+ has been used to signify that only the roots having Im $\nu_j > 0$ are used.

Since $D(\nu_j,p) = 0$ one has

$$\frac{d\nu_j}{dp} = -\frac{D_p(\nu_j,p)}{D_\nu(\nu_j,p)} \tag{2.29}$$

so that Equation 3.28 may be written

$$\bar{f}_j^*(\lambda,\theta,p)\Big|_{\theta<0} = -i\tilde{f}_{sc}^*(\lambda,\nu_j^+,p)e^{-i\nu_j^+\theta}\frac{D(\nu_j^+,p)}{D_p(\nu_j^+,p)}\frac{d\nu_j^+}{dp} \tag{2.30}$$

In the above it is assumed that the integral on p and the summation on j may be interchanged, and that the integrals on C_j vanish as $j\to\infty$. For the acoustic case it has been shown (17) that the integrals on C_j vanish only if the field point (r,θ) lies in the shadow zone and it is assumed that the same result holds for the present case.

The series (2.26) will henceforth be referred to as the "mode

sum."[11] Each term is the transient response in a circumferential propagation mode, as discussed in Chapter 3. The ordering of j from $-\infty$ to ∞ rather than 1 to ∞ is a matter of convenience.

2.8 Completion of the Bromwich Contour

The Bromwich contour is completed down the imaginary axis, as shown in Figure 6, by the contour $C + C_R + C_{-R}$, where $C = C_U + C_L + C_0$. From Equation 2.29 it is seen that ν_j is regular in p except at $p = 0$, where $D(\nu,p)$ has a branch point associated with the Bessel functions, and at the zeros, if any, of $D_\nu(\nu_j,p)$, i.e., multiple zeros in ν of $D(\nu,p)$. In Chapter 3 it is shown that the zeros of $D(\nu,p)$ are simple for p on C for large and small $|p|$. For intermediate $|p|$, the simplicity of the zeros has been verified by explicit numerical calculation for the first few j. With ν_j regular the only singularities of $\bar{f}_j^*$ arise from the branch points of the Bessel functions and the pole of $\bar{\phi}_0(p)$ at $p = 0$. Thus $\bar{f}_j^*$ is regular on C and Cauchy's theorem may be applied to give

$$f_j^*(h,\theta,t) = -\frac{1}{2\pi i}\int_C \bar{f}_j^*(h,\theta,p)e^{pt}dp \qquad (2.31)$$

where it has been assumed that the integrals on C_R and C_{-R} vanish as $R \to \infty$. The analytical proof of this assumption would require complicated and delicate arguments based on the large order approximations for the Bessel functions. It is made plausible by the fact that numerical results which follow from it are reasonable.

The integration contour is taken on the imaginary axis because this gives p the character of frequency, allowing more physical insight into the transforms. Such contours have been successfully used for the numerical treatment of transient elastic wave propagation problems, see, for example, Miklowitz (20) and Lloyd and Miklowitz (29). Further analysis and numerical evaluation of Equation 2.31 will be carried out in Chapter 4, after the detailed discussion of the roots ν_j in Chapter 3.

3. ROOTS OF THE FREQUENCY EQUATION

3.1 Introduction

The functions

$$\varphi^*(r,\theta,t) = \Phi(r)\, e^{-i\omega t - i\nu\theta}$$

$$\psi^*(r,\theta,t) = \Psi(r)\, e^{-i\omega t - i\nu\theta}$$

are obviously solutions of the wave equations 2.9 if Φ and Ψ satisfy the Bessel equations 2.13 with p replaced by $-i\omega$. The addition of homogeneous boundary conditions on σ_r^* and $\tau_{r\theta}^*$ at r = a then is found to lead to the requirement

$$D(\nu, -i\omega) = 0$$

for non-trivial solutions, where $D(\nu, p)$ is given by Equation 2.23. Thus for a given ω only certain values of ν, the roots ν_j, satisfy the boundary conditions, i.e., this is an eigenvalue problem.

Regarding ω as frequency and ν as an angular wave number, i.e., 2π/(wavelength in radians), it is seen that the above solutions are "harmonic wave-train" solutions for circumferential propagation. In this respect they are identical to the familiar Pochammer solutions for circular rods and Rayleigh-Lamb solutions for plates (10), in which the propagation direction is a rectangular coordinate. Thus the ν_j-ω relations may be said to form a dispersive spectrum governed by the frequency equation D = 0.

The purpose of the above discussion is to point out the intimate relation between the transient and harmonic problems. The correspondence could be carried a step further by using integral

superposition on ω of the wave train solutions to produce transient solutions. However, the more direct, but essentially equivalent, method of integral transforms has been used instead.

The unique aspect of the present use of wave trains is that the physical requirement of 2π periodicity in θ has been circumvented by the Friedlander representation.

In this section the behavior of the roots will be investigated for values of p on the Laplace inversion contour C (Figure 6). For points on the imaginary axis, $p = -i\omega$, with ω real, will be used. Approximations will be found for large ω and small $|p|$. Numerical results will be obtained for $0.01 \leq \Omega \leq 40$, where $\Omega \equiv \omega a/c_d$.

3.2 Forms of the Frequency Equation

The frequency equation written out in full is, from Equation (2.23),

$$D(\nu,p) = -\Big\{\Big[(2\nu^2+k_s^2a^2)K_\nu(k_da) - 2k_da\,K_\nu'(k_da)\Big]$$
$$\cdot\Big[(2\nu^2+k_s^2a^2)K_\nu(k_sa) - 2k_sa\,K_\nu'(k_sa)\Big]$$
$$- 4\nu^2\Big[K_\nu(k_da) - k_da\,K_\nu'(k_da)\Big]\cdot\Big[K_\nu(k_sa) - k_sa\,K_\nu'(k_sa)\Big]\Big\} = 0 \qquad (3.1)$$

where $k_d = \frac{p}{c_d}$ and $k_s = \frac{p}{c_s}$.

For $p = -i\omega \equiv \omega e^{-i\frac{\pi}{2}}$ and using

$$K_\nu(ze^{-i\frac{\pi}{2}}) = \tfrac{1}{2}\,i\pi e^{\frac{1}{2}\nu\pi i}H_\nu(z)$$

one obtains

$$D(\nu,-i\omega) = \left(\frac{\pi}{2}\right)^2 e^{\nu\pi i}\Big\{\left[(2\nu^2-\Omega_s^2)H_\nu(\Omega)-2\Omega H_\nu'(\Omega)\right]$$
$$\cdot\left[(2\nu^2-\Omega_s^2)H_\nu(\Omega_s)-2\Omega_s H_\nu'(\Omega_s)\right]$$
$$-4\nu^2\left[H_\nu(\Omega)-\Omega H_\nu'(\Omega)\right]\cdot\left[H_\nu(\Omega_s)-\Omega_s H_\nu'(\Omega_s)\right]\Big\}$$
$$= 0 \qquad (3.2)$$

where $\Omega = \frac{\omega a}{c_d}$, $\Omega_s = \frac{\omega a}{c_s}$ and $H_\nu(z)$ denotes the Hankel function of the first kind.*

Through the use of the identities

$$K_\nu(z) - zK_\nu'(z) = \left(\frac{z}{2}\right)^2 \nu^{-1}\left[K_{\nu+2}(z) - K_{\nu-2}(z)\right]$$

and

$$\left(2\nu^2+\frac{c_d^2}{c_s^2}z^2\right)K_\nu(z) - 2zK_\nu'(z)$$
$$= \left(\frac{c_d^2}{c_s^2}-1\right)z^2K_\nu(z) + \frac{1}{2}z^2\left[K_{\nu+2}(z)+K_{\nu-2}(z)\right]$$

the frequency equation 3.1 can be written in the forms

$$D(\nu,p) = -\frac{1}{2}k_d^2k_s^2a^4\Big\{K_{\nu+2}(k_da)K_{\nu-2}(k_sa)+K_{\nu-2}(k_da)K_{\nu+2}(k_sa)$$
$$+\left(\frac{c_d^2}{c_s^2}-1\right)K_\nu(k_da)\left[K_{\nu+2}(k_sa)+K_{\nu-2}(k_sa)\right]\Big\}$$
$$= 0 \qquad (3.3)$$

and

* The superscript used in the conventional notation $H_\nu^{(1)}$ has been omitted since the Hankel functions of the second kind will not be used.

$$D(\nu,-i\omega) = \frac{1}{2}\Omega^2\Omega_s^2\left(\frac{\pi}{2}\right)^2 e^{\nu\pi i}\left\{H_{\nu+2}(\Omega)H_{\nu-2}(\Omega_s) + H_{\nu-2}(\Omega)H_{\nu+2}(\Omega_s)\right.$$

$$\left. - \left(\frac{c_d^2}{c_s^2} - 1\right)H_\nu(\Omega)\left[H_{\nu+2}(\Omega_s) + H_{\nu-2}(\Omega_s)\right]\right\}$$

$$= 0 \qquad (3.4)$$

3.3 Previous Work on the Frequency Equation

The frequency equation was first obtained in the form given in Equation 3.4 by Victorov (21), who obtained an asymptotic approximation for a root for which the corresponding velocity c_j, where

$$c_j \equiv \frac{\omega}{\nu_j a} = \frac{\Omega}{\nu_j} c_d$$

approached the Rayleigh velocity (22) as $\Omega \to \infty$. Victorov showed that this root, which will be referred to as the Rayleigh root, was complex for finite Ω, but the imaginary part vanished as $\Omega \to \infty$.

Gilbert (8) used the frequency equation in the form given in Equation 3.1 and found asymptotic approximations for an infinity of roots for which $c_j \to c_d$ as $p \to \infty$ for p real. These roots have, to two terms, the same asymptotic approximation as the zeros of $K_\nu(k_d a)$, and are purely imaginary for p real.

The simpler frequency equations which occur in the acoustic and electromagnetic wave diffraction problems have received considerable attention in recent years. Friedlander (6) and Levey and Mahoney (17) obtained asymptotic approximation for the zeros of $K_\nu(z)$ for large real z. Keller, et al., (13) gave approximations

for the zeros ν_j of $H_\nu(z)$ and $H'_\nu(z)$ for small $|z|$, large j and large $|z|$ and numerical results for z real, $0.01 < z < 7$, $j = 1,\ldots,5$.

3.4 Symmetry Properties of the Roots

Let $\nu_0(p)$ denote a root of the frequency equation. Considering the form given in Equation 3.1 it is first seen that

$$D(\nu,p) = D(-\nu,p) \tag{3.5}$$

since

$$K_{-\nu}(z) = K_\nu(z)$$

and ν appears otherwise in D raised to the second power. Thus $-\nu_0(p)$ is a root also.

Second, since $K_\nu(z)$ is real for ν real and z real and positive, so is $D(\nu,p)$ for ν real and p real and positive. Then it follows from the reflection principle that

$$D(\bar{\nu},\bar{p}) = \overline{D(\nu,p)} \tag{3.6}$$

where barred quantities denote complex conjugates. Therefore $\bar{\nu}_0(p)$ and $-\bar{\nu}_0(p)$ are roots of $D(\nu,\bar{p}) = 0$.

Then it follows that the roots need be found only in half-planes of ν and p, the roots in other regions being obtainable by symmetry.

3.5 Asymptotic Approximations for Large $|\nu|$ and Imaginary p

The roots on the integration paths C_U and C_L depend on imaginary p only, so putting $p = -i\omega$, ω real will be considered, and

the frequency equation is taken in the form given in Equation 3.2. By virtue of the symmetry property only $\omega > 0$ need be considered.

For $|\nu|$ large the approximations developed in Appendix A for $H_\nu(\nu z)$ may be applied. There separate approximations are obtained for the transitional zone, defined as

$$z-1 = O(\nu^{-2/3}), \quad \text{i.e.,} \quad \lim_{|\nu|\to\infty} |\nu^{2/3}(z-1)| < \infty$$

and the non-transitional zone, defined as

$$\lim_{|\nu|\to\infty} |\nu^{2/3}(z-1)| = \infty$$

When these restrictions are applied to the frequency equation three cases arise:

(i) P-transitional case: $\frac{\Omega}{\nu} - 1 = O(\nu^{-2/3})$

(ii) S-transitional case: $\frac{\Omega_s}{\nu} - 1 = O(\nu^{-2/3})$

(iii) Non-transitional case: $\lim_{|\nu|\to\infty} |\nu^{2/3}(\frac{\Omega}{\nu} - 1)| = \lim |\nu^{2/3}(\frac{\Omega_s}{\nu} - 1)| = \infty$

where the use of P for reference to dilatation waves and S for shear waves has been adopted. The reason that $\Omega/\nu \doteq 1$ is associated with P waves is that the lineal wave number κ on r = a is ν/a, so that the phase velocity c is given by

$$c = \frac{\omega}{\kappa} = \frac{\omega a}{\nu} = c_d \frac{\omega a}{c_d \nu} = c_d \frac{\Omega}{\nu} \quad \Rightarrow \quad \frac{\Omega}{\nu} = \frac{c}{c_d}$$

Therefore $\Omega/\nu \doteq 1$ implies $c \doteq c_d$ and, similarly, $\Omega_s/\nu \doteq 1$ implies $c \doteq c_s$.

In the P-transitional case the transitional Hankel function

approximations are used for $H_\nu(\Omega)$ and the non-transitional approximations are used for $H_\nu(\Omega_s)$. In the S-transitional case, just the opposite applies.

3.5.1 Transitional Cases

First consider the P-transitional case. The requirement $\frac{\Omega}{\nu} - 1 = O(\nu^{-2/3})$ is written as

$$\Omega = \nu + \tau\nu^{1/3} \tag{3.7}$$

Then $\Omega_s = \frac{c_d}{c_s}\Omega \sim \frac{c_d}{c_s}\nu$ so that

$$\lim_{|\nu|\to\infty} \left| \nu^{2/3}\left(\frac{\Omega_s}{\nu} - 1\right)\right| = \infty$$

Then Equations A.14 and A.15 of Appendix A apply to $H_\nu(\Omega)$ and $H'_\nu(\Omega)$ and Equations A.21 and A.22 apply to $H_\nu(\Omega_s)$ and $H'_\nu(\Omega_s)$. Using these in Equation 3.2 gives

$$D(\nu, -i\omega) = \left(\frac{\pi}{2}\right)^2 e^{\nu\pi i} \exp\left\{(-1)^n \frac{2}{3}\left[\zeta(\Omega_s/\nu)\right]^{3/2}\nu\right\}$$

$$\cdot\left\{\left[O(\nu^{5/3}) + O(\nu^{1/3})\right]\cdot\left[O(\nu^{3/2}) + O(\nu^{1/2})\right]\right.$$

$$\left. + \nu^2\left[O(\nu^{-1/3}) + O(\nu^{1/3})\right]\cdot\left[O(\nu^{-1/2}) - O(\nu^{1/2})\right]\right\}$$

where the O terms have been arranged in the same order as the terms in Equation 3.2. Thus the dominant term is

$$D(\nu, -i\omega) \sim \left(\frac{\pi}{2}\right)^2 e^{\nu\pi i}\left(2\nu^2 - \Omega_s^2\right)^2 H_\nu(\Omega)\, H_\nu(\Omega_s)$$

An examination of Equation A.21 shows that $H_\nu(\Omega_s)$ does not have zeros in this zone, but Equation A.14 shows that $H_\nu(\Omega)$ has zeros

asymptotically at

$$Ai\left(-2^{1/3}\tau e^{2/3\pi i}\right) = 0$$

i.e., at

$$\tau = -2^{-1/3} e^{-2/3\pi i} a_j$$

where a_j are the zeros of Ai(z), which are real and negative. Since, from Equation 3.7

$$\nu \sim \Omega - \tau \Omega^{1/3}$$

then

$$\nu_j \sim \Omega + 2^{-1/3} e^{-2/3\pi i} a_j \Omega^{1/3} \qquad (3.8)$$

Thus there are an infinite number of roots of D which are associated with the dilatation velocity, and these will be referred to as the P roots. These roots are the same as the zeros of $H_\nu(\Omega)$ to this degree of approximation.

A similar treatment for the S-transitional case leads to an infinite set of S roots

$$\nu_j \sim \Omega_s + 2^{-1/3} e^{-2/3\pi i} a_j \Omega_s^{1/3} \qquad (3.9)$$

3.5.2 Non-Transitional Case

In the non-transitional case the asymptotic approximations given by Equation A.21 and Equation A.22 hold for both $H_\nu(\Omega)$ and and $H_\nu(\Omega_s)$ and their derivatives. Then the frequency equation 3.2 becomes

$$D(\nu,-i\omega) = \left(\frac{\pi}{2}\right)^2 e^{\nu\pi i}\, 2\pi^{-1}\nu^{-1} \exp\left[(-1)^{n_d}\nu\tfrac{2}{3}\zeta_d^{3/2} + (-1)^{n_s}\nu\tfrac{2}{3}\zeta_s^{3/2}\right]$$

$$\cdot\left\{\left[O(\nu^{3/2}) + O(\nu^{1/2})\right]\cdot\left[O(\nu^{3/2}) + O(\nu^{1/2})\right]\right.$$

$$\left. + \nu^2\left[O(\nu^{-1/2}) + O(\nu^{1/2})\right]\cdot\left[O(\nu^{-1/2}) + O(\nu^{1/2})\right]\right\} \qquad (3.10)$$

where the O terms have been arranged in the same order as the terms in Equation 3.2. n_d and n_s are the values of n in Equation A.19 according to $z_d \equiv \Omega/\nu$ and $z_s \equiv \Omega_s/\nu$, respectively, and ζ_d and ζ_s are the corresponding values of $\zeta(z)$.

From Equation 3.10 it is seen that there are two terms of equal order in ν, giving

$$D(\nu,-i\omega) \sim -\frac{\pi}{2}\nu^{-1}\exp\left[\nu\pi i + (-1)^{n_d}\nu\tfrac{2}{3}\zeta_d^{3/2} + (-1)^{n_s}\nu\tfrac{2}{3}\zeta_s^{3/2} + (n_d+n_s)\tfrac{\pi}{2}i\right]$$

$$\cdot\left(1-\Omega^2\nu^{-2}\right)^{-1/4}\left(1-\Omega_s^2\nu^{-2}\right)^{-1/4}$$

$$\cdot\left\{\left(2\nu^2-\Omega_s^2\right)^2 - 4\nu^4\left(1-\Omega^2\nu^{-2}\right)^{1/2}\left(1-\Omega_s^2\nu^{-2}\right)^{1/2} e^{(n_d+n_s)\pi i}\right\}$$

Only the factor in braces can have zeros in the non-transitional zone. Setting it equal to zero gives

$$\left(2\nu^2-\Omega_s^2\right)^2 = 4\nu^4\left(1-\Omega^2\nu^{-2}\right)^{1/2}\left(1-\Omega_s^2\nu^{-2}\right)^{1/2}(-1)^{n_d+n_s} \qquad (3.11)$$

Using the definition of phase velocity, $c = \frac{\omega a}{\nu}$, Equation 3.11 can be written

$$\left(2 - \frac{c^2}{c_s^2}\right)^2 = 4\left(1 - \frac{c^2}{c_s^2}\right)^{1/2}\left(1 - \frac{c^2}{c_d^2}\right)^{1/2}(-1)^{n_d + n_s} \qquad (3.12)$$

Squaring Equation 3.12 gives

$$\frac{c^2}{c_s^2}\left[\frac{c^6}{c_s^6} - 8\frac{c^4}{c_s^4} + \frac{c^2}{c_s^2}\left(24 - 16\frac{c_s^2}{c_d^2}\right) - 16\left(1 - \frac{c_s^2}{c_d^2}\right)\right] = 0 \qquad (3.12a)$$

Equations 3.12 and 3.12a are discussed at length in Reference 22, p. 31 ff. They show that, besides the $c = 0$ root, Equation 3.12 has one real root $c < c_s$, the Rayleigh velocity c_R, for $(-1)^{n_d+n_s} = 1$ and two real roots $c > c_d$ for $(-1)^{n_d+n_s} = -1$.

The use of somewhat delicate reasoning, based on the discussion in the paragraphs following Equation A.19 of Appendix A, will now be used to show only the Rayleigh root applies in the present case. First, for $-\frac{\pi}{2} < \arg \nu < 0$, the abovementioned discussion shows $n_d = n_s = 0$, excluding the non-Rayleigh roots in this region. Second, consider $0 \leq \arg \nu < \frac{\pi}{2}$. If the roots $c > c_d$ existed, then z_d and z_s are not in the domain K, in which case $n_d = n_s = 0$, which is a contradiction. Thus the non-Rayleigh roots don't exist. On the other hand, for $c < c_s$ and sufficiently small $\arg \nu$, z_d and z_s are in K, and for sufficiently small $\arg \nu$, $n_d = n_s = 0$, so the Rayleigh root does exist.

In summary, there is only one root for the non-transitional case, which approaches the real ν axis as $|\nu| \to \infty$ and whose limiting phase velocity is the Rayleigh velocity. It will be referred to as the Rayleigh or R root, and denoted ν_0. The discussion above shows

that

$$v_0 \sim \frac{c_d}{c_R}\Omega$$

3.5.3 Victorov's Higher Approximation to the Rayleigh Root

The approximation obtained by Victorov (21) for the Rayleigh root, which was mentioned earlier, contains higher order terms which will be useful in comparing asymptotic and numerical results. Victorov's expressions may be written

$$v_0 \sim \frac{c_d}{c_R}\Omega + v_0^{(2)} \tag{3.13a}$$

where

$$\mathrm{Re}\, v_0^{(2)} = \frac{Q+S}{2SQ(Q-S)}$$

$$\cdot \frac{(2SQ+Q-S)(1-S)^2(1+Q)^2+(2SQ-Q+S)(1+S)^2(1-Q)^2-4S^3Q^2(Q-S)}{(1-S)^2(1+Q)^2-(1+S)^2(1-Q)^2+4SQ(Q+S)} \tag{3.13b}$$

$$\mathrm{Im}\, v_0^{(2)} = \frac{c_d}{c_R}\Omega \frac{Q^2S^2}{(Q-S)(Q-S+2QS^2)} \exp\left[-2\left(\frac{c_d}{c_R}\Omega + \mathrm{Re}\, v_0^{(2)}\right)\left(\tanh^{-1}S_1 - S_1\right)\right] \tag{3.13c}$$

in which

$$Q^2 = 1 - \frac{c_R^2}{c_d^2}$$

$$S^2 = 1 - \frac{c_R^2}{c_s^2}$$

$$S_1^2 = 1 - \frac{\left(\frac{c_d}{c_s}\Omega\right)^2}{\left(\frac{c_d}{c_R}\Omega + \mathrm{Re}\, v_0^{(2)}\right)^2} \sim S^2$$

These expressions have the forms

$$\mathrm{Re}\ \nu_0^{(2)} = \text{const}$$

$$\mathrm{Im}\ \nu_0^{(2)} \sim \text{const}\ \Omega\ e^{-\text{const}\,\Omega}$$

where const > 0.

3.6 Approximations for Small p

For $0 < |p| \ll 1$ the frequency equation may be expressed as a power series in p. Consider the frequency equation in the form given in Equation 3.1. The power series for $K_\nu(z)$ may be written as

$$K_\nu(z) = \frac{1}{2}\left(\frac{z}{2}\right)^{-\nu}\sum_{m=0}^{\infty}(-1)^m(\nu-1-m)!\,(m!)^{-1}\left(\frac{z}{2}\right)^{2m}$$

$$+\ \frac{1}{2}\left(\frac{z}{2}\right)^{\nu}\sum_{m=0}^{\infty}(-1)^m(-\nu-1-m)!\,(m!)^{-1}\left(\frac{z}{2}\right)^{2m}$$

Substituting the series for $K_\nu(z)$ into the expression for $D(\nu,p)$ and carrying out the required differentiation and multiplication of series gives, after considerable algebra,

$$D(\nu,p) = -\sum_{m=0}^{\infty}\left\{b_m(\nu)\left(\frac{k_d a}{2}\right)^{-2\nu} + c_m(\nu) + b_m(-\nu)\left(\frac{k_d a}{2}\right)^{2\nu}\right\}\left(\frac{k_d a}{2}\right)^{2m} \qquad (3.14)$$

where

$$k_d = \frac{p}{c_d}$$

The coefficients b_m and c_m are functions of ν with the ratio of velocities $a \equiv c_d/c_s$ as a parameter. These coefficients become progressively more complicated as m increases, and although general

expressions for them can be written, they are lengthy. For present purposes only the expressions for m = 0, 1 are needed:

$$
\left.
\begin{aligned}
b_0 &= 0 \\
c_0 &= 2\nu^2(\nu^2-1)(\alpha^{\nu}+\alpha^{-\nu})(\nu-1)!(-\nu-1)! \\
b_1 &= 2\alpha^{-\nu}(\alpha^2-1)\nu(\nu+1)\left[(\nu-1)!\right]^2 \\
c_1 &= \left[-2\nu(1-\nu^2-2\nu)\alpha^{2+\nu}+2\nu(1-\nu^2+2\nu)\alpha^{2-\nu}-2\nu(1-\nu^2)\alpha^{-\nu}\right. \\
&\qquad \left.+2\nu(1-\nu^2)\alpha^{\nu}\right](\nu-1)!(-\nu-1)!
\end{aligned}
\right\} \quad (3.15)
$$

The series given by Equation 3.14 may be used to generate approximations for roots found numerically, but does not appear to be a useful tool for investigations of the behavior of the roots for general ν as $p \to 0$. Therefore, the numerical results are anticipated, which show that $\nu \to \pm 1$ as $p \to 0$ along imaginary p. As a result of the symmetry properties of the roots the region of interest can be narrowed to $\nu \doteq 1$.

Putting $\nu = 1 + \epsilon(p)$ it is found that as $\epsilon \to 0$

$$
\begin{aligned}
c_0(\nu) &= O(1) \\
b_1(\nu) &= O(1) \\
c_1(\nu) &= O(\epsilon^{-1}) \\
b_1(\nu) &= O(\epsilon)
\end{aligned}
$$

Then

$$
D(\nu,p) = c_0(\nu) + b_1(\nu)\left(\tfrac{1}{2}k_d a\right)^{2-2\nu} + O(p^2\epsilon^{-1}) = 0 \qquad (3.16)
$$

i.e.,

$$\left(\frac{1}{2}k_d a\right)^{-2\epsilon} = -\frac{\alpha^{2+2\epsilon}+1}{\alpha^2-1}\,\frac{(-\epsilon)!}{\epsilon!}\left[1+O(p^2\epsilon^{-1})\right] \qquad (3.16a)$$

Taking logarithms of each side gives

$$-2\epsilon\log\left(\frac{1}{2}k_d a\right) = \log\left(-\frac{\alpha^{2+2\epsilon}+1}{\alpha^2-1}\right)+\log\frac{(-\epsilon)!}{\epsilon!}+O(p^2\epsilon^{-1}) \qquad (3.17)$$

Expanding for small ϵ gives

$$\log\left(-\frac{\alpha^{2+2\epsilon}+1}{\alpha^2-1}\right) = \log\left(-\frac{\alpha^2+1}{\alpha^2-1}\right)+\sum_{m=1}^{\infty} d_m \epsilon^m$$

where

$$d_1 = \frac{\alpha^2}{\alpha^2+1}\log\alpha^2$$

$$d_2 = \frac{1}{2}\left(\frac{\alpha^2}{\alpha^2+1}\right)\left(1-\frac{\alpha^2}{\alpha^2+1}\right)(\log\alpha^2)^2$$

$$d_3 = \left(\frac{\alpha^2}{\alpha^2+1}\right)\left[\frac{1}{6}-\frac{1}{3}\frac{\alpha^2}{\alpha^2+1}+\frac{1}{4}\left(\frac{\alpha^2}{\alpha^2+1}\right)^2\right](\log\alpha^2)^3$$

and

$$\log\frac{(-\epsilon)!}{\epsilon!} = 2\gamma\epsilon+2\sum_{m=1}^{\infty}\frac{\zeta(2m+1)}{2m+1}\epsilon^{2m+1}$$

where γ is Euler's constant and ζ is the Riemann zeta function. The latter series was used by Keller, et al., (13) to find small z expansions for the zeros of $H_\nu(z)$.

Using these expansions in Equation 3.17 gives

$$\sum_{m=0}^{\infty} A_m \epsilon^m + O(p^2 \epsilon^{-1}) = 0 \tag{3.18}$$

where

$$A_0 = \log\left(-\frac{\alpha^2+1}{\alpha^2-1}\right) \tag{3.19a}$$

$$A_1 = 2\left[\log\left(\tfrac{1}{2}k_d a\right) + \gamma\right] + \frac{\alpha^2}{\alpha^2+1}\log\alpha^2 \tag{3.19b}$$

$$A_2 = \tfrac{1}{2}\left(\frac{\alpha^2}{\alpha^2+1}\right)\left(1 - \frac{\alpha^2}{\alpha^2+1}\right)(\log\alpha^2)^2 \tag{3.19c}$$

$$A_3 = \tfrac{2}{3}\zeta(3) + \frac{\alpha^2}{\alpha^2+1}\left[\tfrac{1}{6} - \tfrac{1}{3}\frac{\alpha^2}{\alpha^2+1} + \tfrac{1}{4}\left(\frac{\alpha^2}{\alpha^2+1}\right)^2\right](\log\alpha^2)^3 \tag{3.19d}$$

in which $\zeta(3) = 1.202\ldots$.

Reversion of the series in Equation 3.18 yields a series in ascending powers of A_1^{-1}

$$\epsilon(p) = \sum_{m=1}^{M} B_m A_1^{-m} + O(A_1^{-M-1}) \tag{3.20}$$

where

$$B_1 = -A_0, \quad B_2 = 0, \quad B_3 = -A_2 A_0^2, \quad B_4 = A_3 A_0^3$$

An infinite number of roots $\nu_j = 1 + c_j$ are obtained by considering the multiplicity

$$\log\left(-\frac{\alpha^2+1}{\alpha^2-1}\right) = \log\frac{\alpha^2+1}{\alpha^2-1} + (2j+1)\pi i \tag{3.20a}$$

in A_0. $\epsilon_j(p)$ may also be expressed as a series in ascending powers of $(\log p)^{-1}$ but considerable accuracy is lost (cf. Reference 26 for the similar case of $H_\nu(z)$). The first term of this series,

$$\nu_j(p) = 1 + \epsilon_j(p)$$

$$= 1 - \frac{1}{2}\left[\log\frac{\alpha^2+1}{\alpha^2-1} + (2j+1)\pi i\right]\left(\log\frac{pa}{2c_d}\right)^{-1} + O\left[(\log p)^{-2}\right] \qquad (3.21)$$

is of interest because it shows clearly the dependence of ϵ_j on j. For small p, log p is approximately real and negative, cancelling the minus sign. Then it is seen that roots leave $\nu = 1$ at the slope

$$\frac{(2j+1)\pi}{\log\frac{\alpha^2+1}{\alpha^2-1}}$$

in the ν plane. For $j \geq 0$, Im $\nu_j > 0$, for $j < 0$, Im $\nu_j < 0$. By symmetry in $\nu = 0$ the $j < 0$ roots correspond to roots leaving $\nu = -1$ with positive imaginary parts.

The approximation for $d\nu_j/dp$ will be needed for the analysis of the small $|p|$ behavior of $\bar{f}_j^*(r,\theta,p)$ in Chapter 4. It has already been pointed out in Chapter 2 that $\nu_j(p)$ is regular for $|p| > 0$ as long as it is a simple zero of $D(\nu,p)$. The preceding analysis has shown the zeros are simple near $p = 0$. Thus ν_j is regular, and the asymptotic approximation for $d\nu_j/dp$ can be found by differentiating the asymptotic approximation given in Equation 3.21 for ν_j, according to the theorem on p. 21 of Reference 27. One finds

$$\frac{d\nu_j}{d\left(\frac{pa}{c_d}\right)} \sim \frac{1}{4}\left[\log\frac{\alpha^2+1}{\alpha^2-1} + (2j+1)\pi i\right]\left(\log\frac{pa}{2c_d}\right)^{-2}\left(\frac{pa}{2c_d}\right)^{-1} \qquad (3.22)$$

3.7 Numerical Determination of the Roots for Imaginary p

For p on the imaginary axis, $pa/c_d = -i\Omega$ with Ω real, the

roots were determined numerically* for $c_d^2/c_s^2 = 3$** in the range $0.01 < \Omega < \Omega_{max}$, where Ω_{max} is 20 or 40, depending on the root. The results are shown in Figures 7 and 8 for Im $\nu > 0$; the roots in $\Omega < 0$ and Im $\nu < 0$ follow from symmetry.

For large Ω the roots separate into three groups, identified by their asymptotic phase velocities, as predicted by the asymptotic expansions. The P1, P2 and P3 roots are the first three of an infinite set of roots whose associated velocity is the P-wave velocity, c_d. The S1, S2 and S3 roots are part of the infinite set of c_s velocity roots. The ordering is based on increasing imaginary ν, and corresponds with the ordering in the asymptotic approximations given in Equations 3.8 and 3.9. The third "group" is a single root, the R or Rayleigh root, whose imaginary part approaches zero as $\Omega \to \infty$.

For small Ω the roots approach the points $\nu = \pm 1$, as predicted by the small p approximations. The numerical results show that the P roots approach $\nu = -1$ and the S and R roots approach $\nu = 1$. The correspondence with the j-ordering in the approximation given in Equation 3.21 is as follows: $j = 0$ is the R root; $j = 1, 2, \ldots$ are the S1, S2,... roots; and $j = -1, -2, \ldots$ are the P1, P2,... roots. Since this ordering of the mode numbers is systematic and encompasses all of the modes, it is adopted as the definitive ordering.

3.8 Comparison of Asymptotic and Numerical Results

In Figures 9 and 10 the numerical and asymptotic results for

---

* See Appendix E for a discussion of the numerical methods.

** $c_d^2/c_s^2 = 3$ corresponds to $\lambda = \mu$ and Poisson's ratio = 1/4.

the P and S roots are compared. There appears to be a difference of $O(\Omega^0)$, i.e., the next higher term for the approximations given in Equations 3.8 and 3.9 appears to be a constant. This is in contrast to the zeros of $H_\nu(\Omega)$, in which the next term is $O(\Omega^{-1/3})$ (see Reference 13, for example). The possibility that this could be due to numerical error is quite unlikely, since the same computer program gives a very close comparison with the zeros of $H_\nu(\Omega)$ (see Appendix E).

Such a second order term would have a significant effect on approximations to the transient response, such as those of Gilbert's (8), in which it was apparently assumed that the second order term was $O(\Omega^{-1/3})$.

For the Rayleigh root, it is seen from Figure 11 that Victorov's second approximation compares well with the numerical results.

For small Ω the asymptotic and numerical results are compared in Figures 12 and 13. The asymptotic results are shown for the series given in Equation 3.20 to m = 4 and for the numerical solution of the approximate frequency equation given in Equation 3.16. It is seen that Equation 3.20 is not a very powerful approximation and becomes poorer rapidly with increased mode number.

4. EVALUATION OF TRANSIENT RESPONSE

4.1 Introduction

The ultimate goal of the present work is the numerical evaluation of the solution. In Chapter 2, the solution was reduced to a series of Laplace inversion integrals involving the roots $\nu_j(p)$. In Chapter 3 the properties of these roots were studied and numerical evaluations given. These results will now be used to evaluate the solution.

The first step is the reduction of the contour integral on C to the sum of a real integral on the imaginary axis and an integral on the indentation C_0. It happens that the integrals on the imaginary axis are improper at $p = 0$, so the next step is the assessment of these singularities. Then the singularities are eliminated by the use of the convolution theorem. After convolution the contributions near $p = 0$ are found to be negligible, reducing the solution to the integrals on the imaginary p axis, which are then evaluated numerically. The evaluations are made at $r = a$, where σ_r and $\tau_{r\theta}$ are zero. Therefore detailed discussion of these stresses is omitted in this chapter.

The results obtained are found to be circumferentially propagating pulses with definite fronts corresponding to those predicted in Section 2.2. Except near the wave fronts, the results compare favorably with those obtained by the Fourier series method. The results also compare well with the long-time solution given in Appendix D.

4.2 Normalization of Response Quantities

The response functions u, v, $\dot{u}$ and $\dot{v}$ can be normalized in terms of the following constants:

$$u_o = \frac{\sigma_o}{\lambda+2\mu}\, a \tag{4.1}$$

$$\dot{u}_o = \frac{\sigma_o}{\lambda+2\mu}\, c_d \tag{4.2}$$

where σ_0 is the amplitude of the stress in the incident wave. Physically, u_0 is the change in length of a reference length a behind the incident wave, and $\dot{u}_0$ is the particle velocity behind the incident wave.

4.3 Simplification of Integral on the Imaginary p Axis

In Chapter 2 the solution for the response functions f_j^* was reduced to the integral

$$f^*(r,\theta,t) = -\frac{1}{2\pi i}\int_C \bar{f}_j^*(r,\theta,p)\, e^{pt}\, dp \tag{4.3}$$

where $\bar{f}_j^*$ is given by

$$\bar{f}_j^*(r,\theta,p)\Big|_{\theta<0} = -i\,\tilde{f}_{sc}^*(r,v_j^+,p)\, e^{-ipv_j^+\theta}\,\frac{D(v_j^+,p)}{D_p(v_j^+,p)}\,\frac{dv_j^+}{dp} \tag{4.4}$$

The contour C, shown in Figure 6, consists of the imaginary p axis, except for an indentation C_0 about p = 0.

Now let the radius of C_0 be δ, with $\delta \to 0$, and let $p = -i\omega$, so that ω is real on the imaginary p axis. Then Equation 4.3 becomes

$$f_j^*(r,\theta,t) = f_{j_F}^*(r,\theta,t) + f_{j_o}^*(r,\theta,t) \tag{4.5}$$

where

$$f_{j_F}^*(r,\theta,t) \equiv \lim_{\substack{R\to\infty \\ \delta\to 0}} \frac{1}{2\pi}\left[\int_{\delta}^{R} + \int_{-R}^{-\delta}\right] \bar{f}_j^*(r,\theta,-i\omega)\, e^{-i\omega t}\, d\omega \tag{4.6}$$

$$f_{j_0}^*(r,\theta,t) \equiv -\frac{1}{2\pi i} \lim_{\delta\to 0} \int_{C_0} \bar{f}_j^*(r,\theta,p)\, e^{pt}\, dp \tag{4.7}$$

The integral in Equation 4.6 can be written on the interval $\delta \leq \omega \leq R$ only, as follows. The transforms $\bar{f}_j^*$ are real for p real by virtue of the definition integral, Equation 2.11a. Therefore

$$\bar{f}_j^*(r,\theta,i\omega) = \overline{\bar{f}_j^*(r,\theta,-i\omega)}$$

by the reflection principle, where the "long" bar indicates the complex conjugate. Then

$$f_{j_F}^*(r,\theta,t) = \lim_{\substack{R\to\infty \\ \delta\to 0}} \frac{1}{2\pi}\left\{\int_{\delta}^{R} \bar{f}_j^*(r,\theta,-i\omega)\, e^{-i\omega t}\, d\omega + \int_{\delta}^{R} \bar{f}_j^*(r,\theta,+i\omega)\, e^{+i\omega t}\, d\omega\right\}$$

$$= \int_0^{\infty} \mathrm{Re}\left[\pi^{-1}\bar{f}_j^*(r,\theta,-i\omega)\; e^{-i\omega t}\right] d\omega \tag{4.8}$$

The integrand in Equation 4.8 is, from Equation 4.4,

$$\mathrm{Re}\left[\pi^{-1}\bar{f}_j^*(r,\theta,-i\omega)\, e^{-i\omega t}\right]$$

$$= \mathrm{Re}\left[-i\pi^{-1}\tilde{f}_{sc}^*(r,\nu_j^+,-i\omega)\, \frac{D(\nu_j^+,-i\omega)}{D_\omega(\nu_j^+,-i\omega)}\, \frac{d\nu_j^+}{d\omega}\, e^{-i(\omega t+\nu_j^+\theta)}\right] \tag{4.9}$$

Equation 4.9 is valid for $\theta < 0$. For $\theta > 0$, the symmetry property given in Equation B.3 and the result given in Equation B.7 may be used to give

$$\begin{aligned}
&Re\left[\pi^{-1}\bar{f}_j^*(k,\theta,-i\omega)\,e^{-i\omega t}\right] \\
&= Re\left[-S(f)\,i\pi^{-1}\tilde{f}_{sc}^*(k,v_j^+,-i\omega)\,\frac{D(v_j^+,-i\omega)}{D_\omega(v_j^+,-i\omega)}\,\frac{dv_j^+}{d\omega}\,e^{-i(\omega t - v_j^+\theta)}\right] \\
&= Im\left[S(f)\,\pi^{-1}\tilde{f}_{sc}^*(k,v_j^+,-i\omega)\,\frac{D(v_j^+,-i\omega)}{D_\omega(v_j^+,-i\omega)}\,\frac{dv_j^+}{d\omega}\,e^{-i(\omega t - v_j^+\theta)}\right]
\end{aligned} \tag{4.10}$$

where

$$S(f) = \begin{cases} +1, & \text{for } f \text{ even in } \theta \\ -1, & \text{for } f \text{ odd in } \theta \end{cases}$$

It is convenient to express Equation 4.10 in terms of the non-dimensional frequency $\Omega \equiv \omega a/c_d$. Furthermore, it turns out that Equation 4.10 can be expressed as the product of a non-oscillatory factor, which will be denoted $\hat{f}_j(r,\Omega)$, and an exponential factor, as follows:

$$\begin{aligned}
&Re\left[\pi^{-1}\bar{f}_j^*(k,\theta,-i\omega)\,e^{-i\omega t}\right] \\
&\quad = Im\left\{\frac{a}{c_d}\,\hat{f}_j(k,\Omega)\,exp\left[-i\left(\Omega\,\frac{c_d t}{a} - v_j^+\left(\theta - \frac{\pi}{2}\right)\right)\right]\right\}
\end{aligned} \tag{4.11}$$

where

$$\hat{f}_j(k,\Omega) \equiv S(f)\,\pi^{-1}\frac{c_d}{a}\,\tilde{f}^*_{sc}(k,\nu_j^+,-i\omega)\,\frac{D(\nu_j^+,-i\omega)}{D_\omega(\nu_j^+,-i\omega)}\,\frac{d\nu_j^+}{d\omega}\,e^{i\nu_j^+\frac{\pi}{2}} \tag{4.12}$$

$$= i\pi^{-1}\frac{c_d}{a}\,e^{-i\nu_j^+(\theta-\frac{\pi}{2})}\,\bar{f}_j^*(k,\theta,-i\omega) \tag{4.13}$$

Then Equation 4.8 becomes

$$f^*_{j_F}(k,\theta,t) = \int_0^\infty Im\left\{\hat{f}_j(k,\Omega)\,e^{-i\left[\Omega\frac{c_d t}{a}-\nu_j^+(\theta-\frac{\pi}{2})\right]}\right\}d\Omega \tag{4.14}$$

4.4 Behavior of Integrands for Small Ω

Consider the integrand given in Equation 4.14. The exponential factor of the integrand

$$e^{-i\left[\Omega\frac{c_d t}{a}-\nu_j^+(\theta-\frac{\pi}{2})\right]} \longrightarrow e^{i\,sgn(j)(\theta-\frac{\pi}{2})}$$

as $\Omega \to 0$, since ν_j^+ approaches ± 1, according to the sign of j. Thus both the real and imaginary parts behave like Ω^0 as $\Omega \to 0$. The behavior of the factors $\hat{f}$ in Equation 4.14 is examined in Appendix B. From Equations B.23, B.24 and B.25 it is seen that

$$\frac{\hat{u}_j(a,\Omega)}{u_o} \sim const\,(\log\Omega)^{-1}\Omega^{-2} \tag{4.15a}$$

$$\frac{\hat{v}_j(a,\Omega)}{u_o} \sim const\,(\log\Omega)^{-1}\Omega^{-2} \tag{4.15b}$$

$$\frac{\hat{\sigma}_{\theta_j}(a,\Omega)}{\sigma_o} \sim const\,(\log\Omega)^{-2}\Omega^{-2} \tag{4.16}$$

Since the transforms of the velocities $\dot{u}$ and $\dot{v}$ are found by simply multiplying the transforms of u and v by p, and since $\hat{f}$ is proportional to $\overline{f}^*$, by Equation 4.13, it is seen that

$$\frac{\hat{\dot{u}}_j(a,\Omega)}{\dot{u}_o} \sim \text{const}\,(\log\Omega)^{-1}\Omega^{-1} \tag{4.17a}$$

$$\frac{\hat{\dot{v}}_j(a,\Omega)}{\dot{u}_o} \sim \text{const}\,(\log\Omega)^{-1}\Omega^{-1} \tag{4.17b}$$

Attention has been focussed on r = a, where σ_r and $\tau_{r\theta}$ are zero, so their approximations have been omitted.

These results indicate that the integrals given by Equation 4.14 are improper at $\Omega = 0$. As far as convergence of the improper integrals is concerned, it turns out that the integral for σ_0^* converges and the others diverge. However, it will be shown below that by using convolution the integrands can, in essence, be multiplied by powers of p near p = 0, thus eliminating the singularities of the integrand. This will certainly remove any convergence problems, but convergence is not the most important problem. Since the integrals will be evaluated numerically, it is highly desirable to make them proper at the origin, so that straightforward numerical methods can be used. It is seen from Equations 4.15 and 4.16 that the integrals for u, v and σ_θ will be proper at the origin if the integrands are multiplied by Ω^2. For $\dot{u}$ and $\dot{v}$ the integrals will be proper if the integrands are multiplied by Ω.

4.5 Behavior of Integrands for Large Ω

As $\Omega \to \infty$, the ν_j^+ for the P modes have the form

$$\nu_j^+ \sim \Omega + 2^{-1/3} e^{-2/3\pi i} a_j \Omega^{1/3}$$

and for the S modes

$$\nu_j^+ \sim \alpha\Omega + 2^{-1/3} e^{-2/3\pi i} a_j (\alpha\Omega)^{1/3}$$

from Equations 3.8 and 3.9. Since $a_j < 0$, in both cases

$$Im\ \nu_j^+ \sim const\ \Omega^{1/3}$$

where const > 0. Thus the exponential factor in Equation 4.14 is $O[\exp(-\text{const}\ \Omega^{1/3})]$ for the P and S roots, provided $\theta > \frac{\pi}{2}$. For the R root

$$\lim_{\Omega \to \infty} Im\ \nu_o^+ = 0$$

so the exponential factor is $O(\Omega^0)$.

The non-oscillatory factors, $\hat{f}_j(r, \Omega)$, have been investigated numerically. The results for the P1, S1 and R modes are shown in Figures 14, 15, and 16. The behavior for the higher P and S modes is essentially the same. It is seen that for the P modes

$$\hat{u}_j(a, \Omega) \doteq O(\Omega^{-2})$$
$$\hat{v}_j(a, \Omega) \doteq O(\Omega^{-2})$$
$$\hat{\sigma}_{\theta_j}(a, \Omega) \doteq O(\Omega^{-1})$$

and for the S modes

$$\hat{u}_j(a, \Omega) = o(\Omega^{-2})$$
$$\hat{v}_j(a, \Omega) = o(\Omega^{-2})$$
$$\hat{\sigma}_{\theta_j}(a, \Omega) = o(\Omega^{-2})$$

For the R mode

$$\hat{u}_j(a,\Omega) = O(e^{-\beta\Omega})$$
$$\hat{v}_j(a,\Omega) = O(e^{-\beta\Omega})$$
$$\hat{\sigma}_{\theta_j}(a,\Omega) = O(e^{-\beta\Omega})$$

where $\beta > 0$.

Now the convergence of the integrals given in Equation 4.14 as $\Omega \to \infty$ will be investigated. For the P and S modes, convergence is assured by the decay of the exponential factor, provided $\theta > \pi/2$. If $0 < \theta < \frac{\pi}{2}$, the integrals diverge. This is an additional reason that the present technique is limited to the shadow zone (which is $\theta > \frac{\pi}{2}$ on r = a). Notice also that the integrals converge uniformly with respect to t.

For the R mode the convergence depends on the decay of the factor $\hat{f}_j(a,\Omega)$. Since $\hat{f}_j(a,\Omega) = O(e^{-\beta\Omega})$, $\beta > 0$, these integrals also converge, uniformly with respect to t.

Later the convergence of integrals like Equation 4.14 with the integrands multiplied by Ω^n will be considered. It is seen that such integrals also converge, uniformly on t.

4.6 Application of the Convolution Theorem

In the shadow zone the response functions $f(r,\theta,t)$ are identically zero for $t < 0$. Thus the bilateral Laplace transforms reduce to one-sided Laplace transforms, and the convolution theorem can be applied in the form

$$\frac{1}{2\pi i}\int_{Br} \bar{g}_1(p)\,\bar{g}_2(p)\,e^{pt}\,dp = \int_0^t g_1(\tau)\,g_2(t-\tau)\,d\tau$$

To apply this to the present problem, consider

$$f_j^*(\lambda,\theta,t) = \frac{1}{2\pi i}\int_{Br} \bar{f}_j^*(\lambda,\theta,p)\,e^{pt}\,dp$$

$$= \frac{1}{2\pi i}\int_{Br} \left[p^n \bar{f}_j^*(\lambda,\theta,p)\right]\left[p^{-n}\right] e^{pt}\,dp$$

i.e., let

$$\bar{g}_1 = p^n \bar{f}_j^*(\lambda,\theta,p)$$

$$\bar{g}_2 = p^{-n}$$

Then

$$g_2 = \frac{t^{n-1}}{(n-1)!}$$

$$g_1 = \frac{1}{2\pi i}\int_{Br} p^n \bar{f}_j^*(\lambda,\theta,p)\,e^{pt}\,dp$$

and

$$f_j^*(\lambda,\theta,t) = \int_0^t \frac{(t-\tau)^{n-1}}{(n-1)!}\,\frac{1}{2\pi i}\int_{Br} p^n \bar{f}_j^*(\lambda,\theta,p)\,e^{p\tau}\,dp\,d\tau$$

The exponent n will be referred to as the "degree of convolution." Proceeding as in Chapter 2, the path Br is completed by the path C, which is then written as an integral on C_0 and an integral on $0 \leq \Omega \leq \omega$, as in the immediately preceding sections.

Consider the integrals

$$f_{j_o}^{*}(r,\theta,t;n) \equiv -\frac{1}{2\pi i}\lim_{\delta\to 0}\int_{C_o} p^n \bar{f}_j^{*}(r,\theta,p)\, e^{pt}\, dp$$

$$= -\frac{1}{2\pi i}\lim_{\delta\to 0}\int_{\frac{\pi}{2}}^{-\frac{\pi}{2}} i\delta^{n+1}\bar{f}_j^{*}(r,\theta,\delta e^{i\varphi})\, e^{\delta e^{i\varphi}t}\, e^{i(n+1)\varphi}\, d\varphi$$

From Equations B.20, B.21 and B.22 it is seen that

$$\left.\begin{matrix}\bar{u}_j^{*}(a,\theta,p)\\ \bar{v}_j^{*}(a,\theta,p)\end{matrix}\right\} \sim \text{const}\,(\log p)^{-1} p^{-2}$$

$$\left.\begin{matrix}\bar{\dot{u}}_j^{*}(a,\theta,p)\\ \bar{\dot{v}}_j^{*}(a,\theta,p)\end{matrix}\right\} \sim \text{const}\,(\log p)^{-1} p^{-1}$$

$$\bar{\sigma}_{\theta_j}^{*}(a,\theta,p) \sim \text{const}\,(\log p)^{-2} p^{-2}$$

Then, since

$$\lim_{\delta\to 0}\int_{C_o}\frac{dp}{p\log p} = \lim_{\delta\to 0}\int_{\frac{\pi}{2}}^{-\frac{\pi}{2}}\frac{i\,d\varphi}{\log\delta + i\varphi} = 0$$

$$\lim_{\delta\to 0}\int_{C_o}\frac{dp}{p(\log p)^2} = \lim_{\delta\to 0}\int_{\frac{\pi}{2}}^{-\frac{\pi}{2}}\frac{i\,d\varphi}{(\log\delta + i\varphi)^2} = 0$$

one has

$$\left.\begin{matrix} u_{j_o}^*(a,\theta,t;n) \\ v_{j_o}^*(a,\theta,t;n) \end{matrix}\right\} = 0, \quad \text{for } n \geq 1$$

$$\left.\begin{matrix} \dot{u}_{j_o}^*(a,\theta,t;n) \\ \dot{v}_{j_o}^*(a,\theta,t;n) \end{matrix}\right\} = 0, \quad \text{for } n \geq 0 \tag{4.18}$$

$$\sigma_{\theta j_o}^*(a,\theta,t;n) = 0, \quad \text{for } n \geq 1$$

Therefore for n selected as above

$$f_j^*(a,\theta,t) = \int_0^t \frac{(t-\tau)^{n-1}}{(n-1)!} f_{j_F}^*(a,\theta,\tau;n)\, d\tau \tag{4.19}$$

where

$$f_{j_F}^*(a,\theta,t;n) = \lim_{\substack{R\to\infty \\ \delta\to 0}} \frac{1}{2\pi}\left[\int_\delta^R + \int_{-R}^{-\delta}\right] p^n \bar{f}_j^*(a,\theta,-i\omega)\, e^{-i\omega t}\, d\omega \tag{4.20}$$

The integrals in Equation 4.20 can be manipulated in the same way as the integrals in Equation 4.6, finally resulting in

$$f_{j_F}^*(a,\theta,t;n) = \int_0^\infty Im\left\{\left(-i\Omega\frac{c_4}{a}\right)^n \hat{f}_j(a,\Omega)\exp\left[-i\Omega\frac{c_4 t}{a} + i v_j^+(\theta-\tfrac{\pi}{2})\right]\right\} d\Omega \tag{4.21}$$

Then, from Equation 4.19,

$$f_j^*(a,\theta,t) = \int_0^t \frac{(t-\tau)^{n-1}}{(n-1)!} \int_0^\infty Im\left\{\left(-i\Omega\frac{c_d}{a}\right)^n \hat{f}_j(a,\Omega)\right.$$

$$\left. \cdot \exp\left[-i\Omega\frac{c_d\tau}{a} + i\nu_j^+\left(\theta-\frac{\pi}{2}\right)\right]\right\} d\Omega d\tau$$

The discussion of the large Ω behavior of $\hat{f}_j$ showed the integral over Ω is uniformly convergent on τ for all n, as far as the upper limit is concerned. If it is further stipulated that n be such as to make the integrals proper at the lower limit, then the integrals on τ and Ω can be interchanged, and the τ integration carried out, giving

$$f_j^*(a,\theta,t) = \int_0^\infty Im\left\{\hat{f}_j(a,\Omega)\, e^{i\nu_j^+\left(\theta-\frac{\pi}{2}\right)}\left[e^{-i\Omega T} - \sum_{k=0}^{n-1}\frac{(-i\Omega T)^k}{k!}\right]\right\} d\Omega \qquad (4.22)$$

where $T \equiv c_d t/a$. Since

$$e^{-i\Omega T} = \sum_{k=0}^{\infty}\frac{(-i\Omega T)^k}{k!}$$

it is seen that

$$e^{-i\Omega T} - \sum_{k=0}^{n-1}\frac{(-i\Omega T)^k}{k!} = O(\Omega^n) \quad as \quad \Omega \to 0$$

thus the integral on Ω remains proper at the lower limit after the τ integration.

Finally, it is noted that the minimum values of n to make the integrals proper at $\Omega = 0$ are, from Equations 4.15, 4.16 and 4.17,

$$u, v, \sigma_\theta : n=2 ; \quad \dot{u}, \dot{v} : n=1 \tag{4.23}$$

The integrals given by Equation 4.22 are in the form required for numerical integration, except for two items. The limitations of the numerical techniques used in calculating the Bessel functions prevent evaluation of the roots and integrands for $\Omega < 0.01$ and $\Omega > 40$. Therefore, the contributions from these intervals will be estimated in the next two sections.

4.7 Contributions from Small Ω

The contributions to the integrals in Equation 4.22 from $0 \leq \Omega \leq 0.01$ will now be estimated. It will be shown that they may be neglected for the time interval of interest, namely, $c_d t/a < 10$.

The $\Omega \to 0$ approximations for $\hat{f}_j$, given in Equations B.23, B.24 and B.25, are

$$\hat{u}_j(a,\Omega)/u_0 \sim \left\{(-1)^j (i)^{1+\mathrm{sgn}(j)} (\alpha^4-1)^{-1/2} (\log\Omega)^{-1} \Omega^{-2}\right\} \tag{4.24a}$$

$$\hat{v}_j(a,\Omega)/u_0 \sim i\,\mathrm{sgn}(j)\left\{\text{same as Eqn. 4.24a}\right\} \tag{4.24b}$$

$$\hat{\sigma}_{\theta_j}(a,\Omega)/\sigma_0 \sim (-1)^j (i)^{1+\mathrm{sgn}(j)} 2\alpha^{-2} \left(\frac{\alpha^2-1}{\alpha^2+1}\right)^{1/2} \cdot \left[\log\frac{\alpha^2+1}{\alpha^2-1} + (2j+1)\pi i\right] (\log\Omega)^{-2} \Omega^{-2} \tag{4.24c}$$

Let $f^*_{j_\Delta}(r,\theta,t)$ denote the small Ω contribution to the integrals in Equation 4.22, i.e.,

$$f^*_{j_\Delta}(a,\theta,t) \equiv \int_0^\Delta Im\left\{\hat{f}_j(a,\Omega) e^{i v_j^+ (\theta-\frac{\pi}{2})} \left[e^{-i\Omega T} - \sum_{k=0}^{n-1} \frac{(-i\Omega T)^k}{k!}\right]\right\} d\Omega \tag{4.25}$$

where n is the least integer making the integrals proper at $\Omega = 0$, i.e., n is chosen according to Equation 4.23. Note

$$e^{-i\Omega T} - \sum_{k=0}^{n-1} \frac{(-i\Omega T)^k}{k!} \sim \frac{(-i\Omega T)^n}{n!} \tag{4.26}$$

Substituting the above approximations into Equation 4.25 gives

$$u^*_{j_\Delta}(a,\theta,t)/u_o \sim (-1)^{j+1} \frac{1}{2} (\alpha^4-1)^{-1/2} T^2 (\cos\theta)\, \Delta (\log\Delta)^{-1} \tag{4.27a}$$

$$v^*_{j_\Delta}(a,\theta,t)/u_o \sim (-1)^{j} \frac{1}{2} (\alpha^4-1)^{-1/2} T^2 (\sin\theta)\, \Delta (\log\Delta)^{-1} \tag{4.27b}$$

$$\dot{u}^*_{j_\Delta}(a,\theta,t)/\dot{u}_o \sim (-1)^{j+1} (\alpha^4-1)^{-1/2} T (\cos\theta)\, \Delta (\log\Delta)^{-1} \tag{4.27c}$$

$$\dot{v}^*_{j_\Delta}(a,\theta,t)/\dot{u}_o \sim (-1)^{j} (\alpha^4-1)^{-1/2} T (\sin\theta)\, \Delta (\log\Delta)^{-1} \tag{4.27d}$$

$$\sigma^*_{\theta_{j_\Delta}}(a,\theta,t)/\sigma_o \sim (-1)^{j+1} \alpha^{-2} \left(\frac{\alpha^2-1}{\alpha^2+1}\right)^{1/2}$$
$$\cdot \left[\log\left(\frac{\alpha^2+1}{\alpha^2-1}\right) \cos\theta - \mathrm{sgn}(j)(2j+1)\pi \sin\theta\right]$$
$$\cdot T^2 \Delta (\log\Delta)^{-2} \tag{4.27e}$$

where the asymptotic approximations

$$\int_0^\Delta (\log\Omega)^{-1} d\Omega \sim \Delta (\log\Delta)^{-1} \tag{4.28a}$$

$$\int_0^\Delta (\log\Omega)^{-2} d\Omega \sim \Delta (\log\Delta)^{-2} \tag{4.28b}$$

valid for $\Delta \to 0$ have been used. Equations 4.28 are derived in Appendix C.

Numerical estimates of the contributions $f^*_{j_\Delta}$ may be made by inserting $\Delta = 0.01$ and $a^2 = 3$. The contributions are normalized on the long-time values of $f(a,\theta,t)$, given in Appendix D, namely *

$$u(a,\theta,t)/u_0 \sim T\cos\theta$$

$$v(a,\theta,t)/u_0 \sim -T\sin\theta$$

$$\dot{u}(a,\theta,t)/\dot{u}_0 \sim \cos\theta$$

$$\dot{v}(a,\theta,t)/\dot{u}_0 \sim -\sin\theta$$

$$\sigma_\theta(a,\theta,t)/\sigma_0 \sim \frac{8}{3}\sin^2\theta$$

as $T \to \infty$. Then

$$\left|\frac{u^*_{j_\Delta}(a,\theta,t)}{u(a,\theta,t)}\right| \doteq \left|\frac{v^*_{j_\Delta}(a,\theta,t)}{v(a,\theta,t)}\right| \doteq 3.8\times10^{-4}T$$

$$\left|\frac{\dot{u}^*_{j_\Delta}(a,\theta,t)}{\dot{u}(a,\theta,t)}\right| \doteq \left|\frac{\dot{v}^*_{j_\Delta}(a,\theta,t)}{\dot{v}(a,\theta,t)}\right| \doteq 7.6\times10^{-4}T$$

$$\left|\frac{\sigma_{\theta j_\Delta}(a,\theta,t)}{\sigma_\theta(a,\theta,t)}\right| \doteq 0.41\times10^{-4}\,\frac{[0.693\cos\theta - \mathrm{sgn}(j)(2j+1)\pi\sin\theta]}{\sin^2\theta}\,T^2$$

---

* The following results are for $a^2 = 3$.

Thus, for the displacements and velocities the contribution is about 1% or less for $T \leq 10$. These contributions will be regarded as negligible.

For σ_θ, the contribution for $\theta = \frac{3}{4}\pi$, $j = -1$ and $T = 10$ is about 1%. The contribution to σ_θ of the higher modes $j > 0$ and $j < -1$ would be larger than 1% according to the above estimate. However, it will be seen below that convergence difficulties at the upper limit prevent evaluation of the σ_θ response by the present techniques, so the analysis of the small Ω contribution to σ_θ will not be pursued further.

Therefore the integrals in Equation 4.22 over $0 \leq \Omega \leq \infty$ will be approximated for $r = a$, $c_d t/a < 10$ by the integrals

$$f_j^*(a,\theta,t) \doteq \int_{0.01}^{\infty} Im\left\{ \hat{f}_j(a,\Omega)\, e^{i v_j^+ (\theta - \frac{\pi}{2})} \cdot \left[e^{-i\Omega T} - \sum_{k=0}^{n-1} \frac{(-i\Omega T)^k}{k!} \right] \right\} d\Omega \qquad (4.29)$$

4.8 Truncation of the Infinite Integrals

The numerical evaluation of the infinite integrals in Equation 4.29 requires truncation at a finite upper limit, which will be denoted Ω_{upper}. Furthermore, the limitations of the Bessel function program require that $\Omega \leq 40$. Thus it is necessary to study the degree of convergence as a function of Ω_{upper}.

Although the answer to the truncation question will lie principally in an examination of the numerical results, the process will be simplified by using the available knowledge regarding the large Ω

behavior of the integrands. In Section 4.5 it was seen that the large Ω behavior of $\hat{f}_j$ is

P modes: $\hat{u}_j,\ \hat{v}_j = O(\Omega^{-2});\quad \hat{\sigma}_{\theta j} = O(\Omega^{-1})$

S modes: $\hat{u}_j,\ \hat{v}_j,\ \hat{\sigma}_{\theta j} = o(\Omega^{-2})$

R mode: $\hat{u}_j,\ \hat{v}_j,\ \hat{\sigma}_{\theta j} = O(e^{-\beta\Omega}),\quad \beta>0$

Since, from Chapter 3,

P,S modes: $Im\ v_j^+ \sim b_j \Omega^{1/3}$ where $\begin{cases} 0<b_{-1}<b_{-2}<\dots \\ 0<b_1<b_2<\dots \end{cases}$

R mode: $Im\ v_j^+ \sim 0$

then the large Ω behavior of the integrand factors

$$e^{iv_j^+(\theta-\frac{\pi}{2})}\left[e^{-i\Omega T}\sum_{k=0}^{n-1}\frac{(-i\Omega T)^k}{k!}\right] \equiv f_j^{(e)}(\Omega,T)$$

is

P,S modes: $f_j^{(e)} = O\left[\Omega^{n-1}e^{-b_j\Omega^{1/3}(\theta-\frac{\pi}{2})}\right]$

R mode: $f_j^{(e)} = O\left(\Omega^{n-1}e^{-\beta\Omega}\right)$

where n is chosen according to Equation 4.23.

Combining these results, it is found that the total integrands behave as follows:

P modes: Integrands for $u, v, \dot{u}, \dot{v} = O\left[\Omega^{-1}e^{-b_j\Omega^{1/3}(\theta-\frac{\pi}{2})}\right]$

Integrands for $\sigma_\theta = O\left[e^{-b_j\Omega^{1/3}(\theta-\frac{\pi}{2})}\right]$

S modes: Integrands for $u, v, \dot{u}, \dot{v}, \sigma_\theta = o\left[\Omega^{-1} e^{-b_j \Omega^{1/3}(\theta - \frac{\pi}{2})}\right]$

R mode: Integrands for $u, v, \dot{u}, \dot{v}, \sigma_\theta = O\left[\Omega e^{-\beta\Omega}\right]$

Thus the following conclusions can be drawn:

(i) Convergence will be slowest for the P1 mode.

(ii) For the P and S modes convergence becomes slower as $(\theta - \pi/2)$ becomes smaller.

(iii) For the P modes convergence is slower for σ_θ than for u, v, $\dot{u}$ or $\dot{v}$.

The smallest value of θ considered in the numerical evaluations is $\theta = \frac{3}{4}\pi$.

The convergence of the P1 mode integrals for $\sigma_{\theta_j}(a, \frac{3}{4}\pi, t)$ is shown in Figure 17.* It is seen that $\Omega_{upper} = 40$ is not nearly large enough to obtain satisfactory convergence. There are various ways in which the analytical/numerical technique could be modified to accelerate the convergence of the σ_θ integrals. One method would be to reduce the degree of convolution for σ_θ from two to one. This makes the integrals improper but still convergent at $\Omega = 0$. Then by refining the small Ω approximations, they could be made powerful enough to allow evaluation of the improper integral. However, it appears that any such modified method would require a sizable

---

* These curves are jagged because a limited number of values of Ω_{upper} were used.

extension of the techniques developed in the present work. Since the present technique is adequate for the displacements and velocities, σ_θ is simply dropped from further consideration.

The convergence of the P1 mode integrals for $\dot{u}_j^*$ and u_j^* is shown in Figures 18 and 19, which are also representative of the convergence for $\dot{v}_j^*$ and v_j^*. From these figures it is seen that the only instance where convergence is not rapid is for the velocities at short time, say $c_d t/a \doteq 1$ or less. This lack of strong convergence manifests itself as small oscillations in time about the true value, which will be seen in the transient response graphs discussed later, such as Figure 21. These oscillations are sufficiently minor to be of little consequence. At larger values of θ, $\theta = \pi, \frac{5}{4}\pi$, they disappear completely because of the more rapid convergence. Thus it is concluded that with $\Omega_{upper} = 40$ the convergence for the P modes is satisfactory. For the S and R modes similar studies have shown the convergence is rapid enough so that $\Omega_{upper} = 20$ may be used.

Thus the integral given in Equation 4.29 is reduced to

$$f_j^*(a,\theta,t) \doteq \int_{0.01}^{\Omega_{upper}} Im\left\{ \hat{f}_j(a,\Omega)\, e^{i v_j^+ (\theta - \frac{\pi}{2})} \cdot \left[e^{-i\Omega T} - \sum_{k=0}^{n-1} \frac{(-i\Omega T)^k}{k!} \right] \right\} d\Omega \qquad (4.30)$$

This is the final form for numerical evaluation.

4.9 Numerical Evaluations of Transient Response

4.9.1 Scope of the Response Calculations

The integrals given in Equation 4.30 for the transient response have been evaluated in the shadow zone on the surface of the cavity, $r = a$, for $c_d t/a \leq 10$. The case $a^2 = c_d^2/c_s^2 = 3$, corresponding to $\lambda = \mu$ and Poisson's ratio = 1/4, is considered. The results are presented as timewise variations of the velocities and displacements at the points $\theta = \frac{3}{4}\pi$ and $\theta = \pi$ in the physical plane. The waves m = 0 and m = -1 are evaluated, so for $\theta = \frac{3}{4}\pi$ the response in the wave sum form must also be calculated at $\theta - 2\pi = -\frac{5}{4}\pi$ or, by using symmetry, $\theta = \frac{5}{4}\pi$. The modes evaluated are P1, P2, P3, R, S1, and S2. For the most part these modes are sufficient for good convergence of the mode sum, but in certain cases higher P modes would be desirable, as pointed out below.

In the time region $c_d t/a \leq 10$ the m = -2 and m = 1 waves have also reached the points $\theta = \frac{3}{4}\pi$ and $\theta = \pi$ but numerical results showed that the contribution from these waves is less than 1% in this time region, so they have been omitted. For $c_d t/a \geq 10$ the higher $|m|$ waves' contribution will increase, and the Rayleigh mode response will begin to predominate as predicted by Miklowitz's approximations (9, 11, 12) but this region is outside the scope of the present numerical techniques.

4.9.2 Discussion of Transient Response Results

The first cases to be examined are the radial and circumferential velocities at $\theta = \frac{3}{4}\pi$. The response for m = 0 wave is shown in Figures 20 and 21, in which both the response in each mode and

the mode sum is given.

The major response occurs in the P1 and R modes. The contribution from the higher P modes decreases rapidly as the mode number increases. The S1 mode contributes little and the S2 mode contribution is too small to be shown. It would probably be desirable to calculate the P4 mode response in the case of $\dot{v}^*$, since the P3 response is still fairly large.

The arrival times of the P and R waves are indicated. The P1 mode has distinctive wave front behavior at the P arrival time, but there is little pulse-like behavior at the R arrival time. For times less than the P arrival time the modal response curves are too crowded to allow the mode sum to be shown, but in Figures 24 and 25, the mode sum response in this region can be seen. It is essentially zero, but there are rather minor perturbations about zero, which arise from the lack of complete convergence of the P1 mode integrals. In the case of $\dot{v}$, these perturbations persist slightly beyond the P arrival time, so that the peak appears to be jagged, which is, of course, erroneous. For larger θ's or higher modes, the convergence is strong enough to eliminate these perturbations.

The response for $\theta = \frac{5}{4}\pi$, which is used to construct the $m = -1$ wave at $\theta = \frac{3}{4}\pi$, is shown in Figures 22 and 23. The mode convergence is seen to be quite rapid; the P3 and S modes are too small to be shown. The amplitudes have decayed markedly from those at $\theta = \frac{3}{4}\pi$. The mode sum is clearly seen to be zero ahead of the P arrival time. A pulse-like behavior has begun to appear at the R arrival time.

The wave sum of the response at $\theta = \frac{3}{4}\pi$ is then constructed from the above wave response, as shown in Figures 24 and 25. Note that the circumferential velocity $\dot{v}^*$ for the m = -1 wave is the negative of the $\theta = \frac{5}{4}$ response, since v is odd in θ. The wave sums compare well with the long time solutions given in Appendix D. The comparison would probably be enhanced by using more modes in the m = 0 wave. The $\dot{v}$ response is particularly interesting because the m = -1 wave still has distinctive wave front behavior, so that it causes a marked jog in the total response.

Results for the displacements at $\theta = \frac{3}{4}\pi$, analogous to those discussed above, are presented in Figures 26 through 29. The modal response for the m = -1 wave has been omitted since it does not show anything new. The correspondence with the long time solution is good, but again, in the case of the circumferential displacement, it would probably be noticeably better if the P4 mode were included in the m = 0 wave.

The results for the displacements and velocities at $\theta = \pi$ are presented in Figures 30 through 34. The results are similar to those for $\theta = \frac{3}{4}\pi$. Note that the m = 0 and m = -1 wave responses are equal for u and $\dot{u}$ and equal but opposite in sign for v and $\dot{v}$. Thus the v and $\dot{v}$ wave sums are zero at $\theta = \pi$. Nevertheless, the $\dot{v}$ responses have been given (Figure 31), since they may be compared to Figures 21 and 23 to see how the $\dot{v}$ pulse decays. Figures 32 and 34 show that the comparison with the long time solution is good.

The qualitative results from the wave front approximations of Friedlander (6) and Gilbert (8) which were pointed out in Section

2.2, namely, smooth diffracted fronts and rapid decay of amplitudes near the wave front, are found to be present in the above results. The smoothness of the velocity fronts is not evident, however, for the $\theta = \frac{3}{4}\pi$ velocity fronts because they are still quite steep just behind the fronts, and the numerical resolution is not fine enough to show the smooth build up.

4.9.3 Comparison with Baron's Fourier Series Results

In Reference 3 Baron and Parnes present extensive numerical results for the displacement and velocities for the present problem, based on the Fourier series form of solution. For points in the shadow zone they gave the velocities at $\theta = \frac{3}{4}\pi$ and $\theta = \pi$ and the displacement at $\theta = \pi$. Baron calculated 3 terms of the Fourier series for the scattered wave and used the exact incident wave.

The comparison between Baron's and the present results for the velocities at $\theta = \frac{3}{4}\pi$ is shown in Figures 35 and 36. The correspondence is fairly good at moderate to long times. For short time the comparison is quite poor. The response using a three-term series for the incident wave also was calculated by the present author, using Baron's results, and it yields considerably better correspondence. The better correspondence using the three-term series is possibly explained by the fact that higher terms in the scattered waves may tend to cancel the corresponding higher terms in the incident wave.

The comparison between Baron's and the present results for the velocities and displacements at $\theta = \pi$ is shown in Figures 32 and 34. In view of the fact that the displacement correspondence

is good it seems quite likely that the poor correspondence between Baron's velocity and the present solution for long time is due to an inadvertent error of some sort on Baron's part.

Since the incident wave has encompassed the entire cavity at $c_d t/a = 1$, a three-term Fourier series on the incident wave is exact, so no changes in Baron's results at $\theta = \pi$ can be made on that basis. However, a different sort of change can be made. Baron apparently set his results to zero arbitrarily ahead of the wave arrival time, but it is clear from Figure 32 that he chose the incident wave arrival time instead of the diffracted P wave arrival time shown. If one cuts off the results ahead of the P arrival, fairly good correspondence is obtained.

Finally, it should be noted that the diffracted wave fronts should be smooth, according to both the general theory of diffracted waves (6) and the wave front approximations (6,8).

5. CONCLUSIONS AND RECOMMENDATIONS

Although the present method might be most correctly classified as a short-time method, the numerical results show that it is good up to times at which the solution is essentially equal to the long-time solution for a step-stress incident wave. Therefore it seems fair to conclude that the method is even more powerful than was anticipated.

The purpose of studying a step-function incident wave is of course so that more general transient behavior can be studied through the use of the Duhamel integral. The short time inaccuracy of the Fourier series method must then be taken into account when the time variations become fairly rapid, and the present method would be even more advantageous.

The great disadvantage of the present work is, of course, that it is limited to the shadow zone insofar as the total response is concerned. In view of the power of the wave sum method in obtaining numerical results for the shadow it would appear to be worthwhile to investigate the possibilities for numerical evaluation in the illuminated zone. In the illuminated zone the inversion of the transform on θ cannot be obtained by residues, and there seems to be no obvious way of avoiding having to invert the θ-transform by numerical integration. Then the inversion of the Laplace and the Fourier transforms would involve the numerical evaluation of repeated infinite integrals, a formidable task, but perhaps possible with the exercise of insight.

A more immediate, and much easier, object of continued

research on the present method would be the extension of Gilbert's shadow zone approximations for the line source case (8) to the present problem. The first step in such a program would be the verification of the conjecture (in Section 3.8) that the next higher term in the large $|p|$ behavior of the roots is $O(p^0)$ instead of $O(p^{-1/3})$, for this would have a major effect on Gilbert's results. It might also be useful to try to extend to the elastodynamic case the higher approximations for the acoustic wave front response obtained by Levey and Mahoney (17). They concluded that the first order approximations obtained by Friedlander and Gilbert were valid in such a short region behind the wave fronts as to be of rather limited usefulness.

Also, more refined numerical methods could be developed to evaluate the σ_θ integrals. It is probable that such refined methods could also be used to speed the convergence of the velocity integrals at short time.

6. REFERENCES

1. M. L. Baron, H. L. Bleich, and P. Weidlinger, "Theoretical Studies on Ground Shock Phenomena," Mitre Corporation Report SR-19, October 1960.

2. M. L. Baron and A. T. Matthews, "Diffraction of a Pressure Wave by a Cylindrical Cavity in an Elastic Medium," J. Appl. Mech., Vol. 28, pp. 347-354, 1961.

3. M. L. Baron and R. Parnes, "Displacements and Velocities Produced by the Diffraction of a Pressure Wave by a Cylindrical Cavity in an Elastic Medium," J. Appl. Mech., Vol. 29, pp. 385-394, 1962.

4. S. L. Paul and A. R. Robinson, "Interaction of Plane Elastic Waves with a Cylindrical Cavity," Air Force Weapons Laboratory Report RTD TDR 63-3021, June 1963.

5. A. M. Soldate and J. F. Hook, "A Theoretical Study of Structure-Medium Interaction," Air Force Special Weapons Center Report SWC TDR 62-30, March 1962.

6. F. G. Friedlander, "Diffraction of Pulses by a Circular Cylinder," Comm. Pure and Appl. Math., Vol. 7, pp. 705-732, 1954; also, Chapter 6 of Sound Pulses, Cambridge University Press, 1958.

7. F. Gilbert and L. Knopoff, "Scattering of Impulsive Elastic Waves by a Circular Cylinder," J. Acoust. Soc. Amer., pp. 1169-1175, 1959.

8. F. Gilbert, "Scattering of Impulsive Elastic Waves by a Smooth Convex Cylinder," J. Acoust. Soc. Amer., pp. 841-857, 1960.

9. J. Miklowitz, "Scattering of Transient Elastic Waves by a Circular Cylindrical Cavity," Air Force Special Weapons Center Report SWC TDR 63-43, November 1963.

10. J. Miklowitz, "Recent Developments in Elastic Wave Propagation," Appl. Mech. Rev., Vol. 13, pp. 865-878, 1960.

11. J. Miklowitz, "Pulse Propagation in a Viscoelastic Solid with Geometric Dispersion," in Stress Waves in Anelastic Solids, Springer-Verlag, Berlin, pp. 255-276, 1964.

12. J. Miklowitz, "Scattering of a Plane Elastic Compressional Pulse by a Cylindrical Cavity," presented at the Eleventh International Congress of Applied Mechanics, Munich, Germany, 1964.

13. J. B. Keller, S. I. Rubinow, and M. Goldstein, "Zeros of Hankel Functions and Poles of Scattering Amplitudes," J. Mathematical Physics, Vol. 4, pp. 829-832, 1963.

14. P. M. Morse and H. Feshbach, Methods of Theoretical Physics, McGraw-Hill, New York, 1953.

15. W. R. LePage, Complex Variables and the Laplace Transform for Engineers, McGraw-Hill, New York, 1961.

16. R. G. Payton, "Transient Interaction of an Acoustic Wave with a Circular Cylindrical Elastic Shell," J. Acoust. Soc. Amer., Vol. 32, pp. 722-729, 1960.

17. H. C. Levey and J. J. Mahoney, "The Interaction of a Plane Shock and a Cylindrical Body," Australian Defense Scientific Service, Aeronautical Research Laboratories, Aerodynamics Report 121, November 1961.

18. C. K. Grimes, "Studies on the Propagation of Elastic Waves in Solid Media," Ph.D. Thesis, Calif. Inst. of Technology, 1964.

19. T. M. Apostol, Mathematical Analysis, Addison-Wesley, Reading, Mass., 1957.

20. J. Miklowitz, "Plane-Stress Unloading Waves Emanating from a Suddenly Punched Hole in a Stretched Elastic Plate," J. Appl. Mech. Vol. 27, pp. 165-171, 1960.

21. I. A. Victorov, "Rayleigh-Type Waves on a Cylindrical Surface," Soviet Physics-Acoustics, Vol. 4, pp. 131-136, 1958.

22. W. M. Ewing, W. S. Jardetzky, and F. Press, Elastic Waves in Layered Media, McGraw-Hill, New York, 1957.

23. F. W. J. Olver, "The Asymptotic Expansion of Bessel Functions of Large Order," Phil. Trans. Roy. Soc. A, Vol. 247, pp. 328-369, 1955.

24. F. W. J. Olver, "The Asymptotic Solution of Linear Differential Equations of the Second Order for Large Values of a Parameter," Phil. Trans. Roy. Soc. A, Vol. 247, pp. 307-327, 1955.

25. F. W. J. Olver, "Some New Asymptotic Expansions for Bessel Functions of Large Order," Proc. Camb. Phil. Soc., Vol. 48, pp. 414-427, 1952.

26. C. Yeh, "An Application of Sommerfeld's Complex-Order Wavefunctions to an Antenna Problem," J. Mathematical Physics, Vol. 5, pp. 344-350, 1964.

27. A. Erdelyi, Asymptotic Expansions, Dover, New York, 1956.

28. I. S. Sokolnikoff, Mathematical Theory of Elasticity, McGraw-Hill, New York, Second Edition, 1956.

29. J. R. Lloyd and J. Miklowitz, "On the Use of Double Integral Transforms in the Study of Dispersive Elastic Wave Propagation," Proc. Fourth U. S. Natl. Cong. Appl. Mech., pp. 255-267, 1962.

30. M. Abramowitz and I. A. Stegun, editors, Handbook of Mathematical Functions, Natl. Bur. Stds. Appl. Math. Series 55, 1964.

APPENDIX A. ASYMPTOTIC APPROXIMATIONS FOR BESSEL FUNCTIONS OF LARGE COMPLEX ORDER

Introduction

The purpose of this appendix is the development of asymptotic approximations for the Hankel function of the first kind, $H_\nu(\nu z)$,* valid as $|\nu| \to \infty$ for $|\arg \nu| < \pi/2$ and various regions in z. The development takes as its starting point the asymptotic expansions given by Olver (23, 24), which are uniform in z. The uniform expressions are too complicated for the application in the text so simpler forms are obtained by restricting the range of variation of z.

Summary of Olver's Results

From Equations 4.25, 4.16, 4.17 and 4.6 of (23) and Equation 4.6 of (24), the expansion for $H_\nu(\nu z)$ is found to be

$$H_\nu(\nu z) \sim 2 e^{-\frac{1}{3}\pi i} \nu^{-\frac{1}{3}} \left(\frac{4\zeta}{1-z^2}\right)^{1/4} \cdot \left\{ Ai(\nu^{2/3} e^{2/3\pi i}\zeta) \sum_{s=0}^{\infty} A_s(\zeta) \nu^{-2s} + Ai'(\nu^{2/3} e^{2/3\pi i}\zeta) \nu^{-4/3} \sum_{s=0}^{\infty} B_s(\zeta) \nu^{-2s} \right\} \tag{A.1}$$

as $|\nu| \to \infty$ in $|\arg \nu| < \frac{\pi}{2}$. The function $\zeta(z)$ is given by

$$\frac{2}{3}\zeta^{3/2} = \log \frac{1+\sqrt{1-z^2}}{z} - \sqrt{1-z^2} \tag{A.2}$$

ζ has branch points at -1, 0 and ∞, hence it is regular on the cut z-plane in Figure A 1(a). The expansion is uniform on the region R

* Since only $H_\nu^{(1)}(\nu, z)$ is considered, the conventional superscript is omitted.

formed by the removal of points within a distance $\delta > 0$ of the cut. The cut from -1 to ∞ is taken as shown to secure the maximum region of validity in z (for details see Reference 23). The branch of ζ is specified by taking ζ real for real positive z.

The coefficients $A_s(\zeta)$ and $B_s(\zeta)$ are also regular on the cut z-plane, with $A_0(\zeta) = 1$. Olver gives expressions for the higher coefficients but they will not be needed for the present analysis.

The following results will be needed.

$$z(\zeta) = 1 - 2^{-1/3}\zeta + O(\zeta^2) \quad \text{as } \zeta \to 0 \tag{A.3}$$

$$\zeta(z) = 2^{1/3}(1-z) + O\left[(1-z)^2\right] \quad \text{as } z \to 1 \tag{A.4}$$

The function $\phi(z)$, given by

$$\phi(z) = \left(\frac{4\zeta}{1-z^2}\right)^{1/4} \tag{A.5}$$

which appears in Equation A.1, is regular on the cut z-plane, since the only possibility of a finite zero or infinity of $4\zeta/(1-z^2)$ on the cut plane is at $\zeta = 0$, $z = 1$, but in this neighborhood

$$\frac{4\zeta}{1-z^2} = 2^{4/3} + O(\zeta) \tag{A.6}$$

The branch of $\phi(z)$ is specified by taking ϕ real for $z > 0$.

The cut z-plane maps onto the ζ-plane as shown in Figure A1(b). The domain K bounded by the branch cut and the lines BPE and BP'E' maps onto part of $|\arg \zeta| < \frac{\pi}{3}$ and E'F' maps onto part of the ray $\arg \zeta = \frac{\pi}{3}$ as shown. The values of z at P and P' are $\pm i\, 0.66\ldots$ so that $|z| < 1$ for z in K. These facts will be needed below.

The asymptotic expansion for $H_\nu'(\nu z)$ may be derived by the differentiation of the expansion for $H_\nu(\nu z)$, giving

$$H_\nu'(\nu z) \sim -\frac{4e^{-\frac{1}{3}\pi i}}{z\phi(\zeta)}\left\{\nu^{-\frac{4}{3}}Ai\left(\nu^{\frac{2}{3}}e^{\frac{2}{3}\pi i}\zeta\right)\cdot\sum_{s=0}^{\infty}\nu^{-2s}\left[\frac{\phi'(\zeta)}{\phi(\zeta)}A_s(\zeta)+A_s'(\zeta)+e^{\frac{4}{3}\pi i}\zeta B_s(\zeta)\right]\right.$$

$$\left.+\nu^{-\frac{2}{3}}Ai'\left(\nu^{\frac{2}{3}}e^{\frac{2}{3}\pi i}\zeta\right)\cdot\sum_{s=0}^{\infty}\nu^{-2s}\left[e^{\frac{2}{3}\pi i}A_s(\zeta)+\frac{\phi'(\zeta)}{\phi(\zeta)}\nu^{-2}B_s(\zeta)+\nu^{-2}B_s'(\zeta)\right]\right\} \tag{A.7}$$

for $|\arg \nu| < \frac{\pi}{2}$, uniformly on the region R defined above.

Properties of the Airy Function

A few properties of the Airy function Ai(z) will be needed in the following analysis. Ai(z) is defined by

$$Ai(z) = \frac{1}{2\pi i}\int_{\infty e^{-\frac{2}{3}\pi i}}^{\infty e^{\frac{2}{3}\pi i}} \exp\left(tz-\tfrac{1}{3}t^3\right)dt$$

Ai(z) is entire, real for z real, and its only zeros are on the real negative z axis. The following asymptotic approximations hold as $|z| \to \infty$.

$|\arg z| < \pi$

$$Ai(z) = \tfrac{1}{2}\pi^{-1/2} z^{-1/4} \exp\left(-\tfrac{2}{3} z^{3/2}\right)\left[1 + O(z^{-3/2})\right] \qquad \text{(A.8)}$$

$$Ai'(z) = -\tfrac{1}{2}\pi^{-1/2} z^{1/4} \exp\left(-\tfrac{2}{3} z^{3/2}\right)\left[1 + O(z^{-3/2})\right] \qquad \text{(A.9)}$$

$|\arg z| < \tfrac{2}{3}\pi$

$$Ai(-z) = \pi^{-1/2} z^{-1/4} \cos\left(\tfrac{2}{3} z^{3/2} - \tfrac{1}{4}\pi\right)\left[1 + O(z^{-3/2})\right] \qquad \text{(A.10)}$$

$$Ai'(-z) = \pi^{-1/2} z^{1/4} \sin\left(\tfrac{2}{3} z^{3/2} - \tfrac{1}{4}\pi\right)\left[1 + O(z^{-3/2})\right] \qquad \text{(A.11)}$$

Dominant Terms of the Expansions

From the approximations given in Equations A.8 through A.11 it is seen that

$$Ai'(z) = O\left[z^{1/2} Ai(z)\right]$$

i.e.,

$$Ai'(\nu^{2/3} e^{2/3\pi i}\zeta) = O\left[\nu^{1/3} e^{1/3\pi i}\zeta^{1/2} Ai(\nu^{2/3} e^{2/3\pi i}\zeta)\right]$$

(except near zeros of Ai). Then the dominant term of the asymptotic expansion for $H_\nu(\nu z)$ is

$$H_\nu(\nu z) \sim 2 e^{-1/3\pi i} \nu^{-1/3} \left(\frac{4\zeta}{1-z^2}\right)^{1/4} Ai(\nu^{2/3} e^{2/3\pi i}\zeta) \qquad \text{(A.12)}$$

and the dominant term of the asymptotic expansion for $H'_\nu(\nu z)$ is

$$H_\nu'(\nu z) \sim -4 e^{\frac{1}{3}\pi i} z^{-1} \nu^{-2/3} \left(\frac{4\zeta}{1-z^2}\right)^{-1/4} Ai'(\nu^{2/3} e^{\frac{2}{3}\pi i}\zeta) \qquad \text{(A.13)}$$

for $|\nu| \to \infty$, $|\arg \nu| < \frac{\pi}{2}$.

Transitional and Non-Transitional Zones

The above approximations are still too complicated for the present application, so further simplification will be achieved by writing separate approximations for the transitional zone

$$z-1 = O(\nu^{-2/3}), \text{ i.e., } \lim_{|\nu|\to\infty} |\nu^{2/3}(z-1)| < \infty$$

and the "non-transitional" zone

$$\lim_{|\nu|\to\infty} |\nu^{2/3}(z-1)| = \infty$$

In the transitional zone the z-ζ relation can be simplified. In the non-transitional zone the Airy functions can be replaced by their asymptotic approximations.

Asymptotic Approximations for the Transitional Zone

Let $z - 1 = \tau \nu^{-2/3}$. Then from Equation A.4

$$\zeta(z) = -2^{1/3} \tau \nu^{-2/3} + O(\nu^{-4/3})$$

and

$$\left(\frac{4\zeta}{1-z^2}\right)^{1/4} = 2^{1/3} + O(\nu^{-2/3})$$

Hence, from Equations A.12 and A.13,

$$H_\nu(\nu z) = H_\nu(\nu + \tau\nu^{1/3}) \sim 2^{4/3} e^{-\frac{1}{3}\pi i} \nu^{-1/3} Ai(-2^{1/3}\tau e^{2/3\pi i}) \qquad \text{(A.14)}$$

$$H'_\nu(\nu z) = H'_\nu(\nu + \tau\nu^{1/3}) \sim -2^{5/3} e^{\frac{1}{3}\pi i} z^{-1} \nu^{-2/3} Ai'(-2^{1/3}\tau e^{2/3\pi i}) \qquad \text{(A.15)}$$

These approximations are in agreement with those given in an earlier paper by Olver (25), where they were obtained by a different method.

Asymptotic Approximations in the Non-Transitional Zone

The non-transitional zone is defined by

$$\lim_{|\nu|\to\infty} |\nu^{2/3}(z-1)| = \infty$$

Then, from Equation A.4,

$$\lim_{|\nu|\to\infty} |\nu^{2/3}\zeta| = \infty$$

and the asymptotic approximations given in Equations A.8 and A.9 for the Airy functions can be used in Equations A.12 and A.13 to give

$$H_\nu(\nu z) \sim \pi^{-1/2} e^{-\frac{1}{3}\pi i} \left(\frac{4\zeta}{1-z^2}\right)^{1/4} \nu^{-1/3} \left(\nu^{2/3} e^{2/3\pi i}\zeta\right)^{-1/4} \exp\left[-\frac{2}{3}\left(\nu^{2/3} e^{2/3\pi i}\zeta\right)^{3/2}\right] \qquad \text{(A.16)}$$

$$H'_\nu(\nu z) \sim 2\pi^{-1/2} e^{\frac{1}{3}\pi i} z^{-1} \left(\frac{4\zeta}{1-z^2}\right)^{-1/4} \nu^{-2/3} \left(\nu^{2/3} e^{2/3\pi i}\zeta\right)^{1/4} \exp\left[-\frac{2}{3}\left(\nu^{2/3} e^{2/3\pi i}\zeta\right)^{3/2}\right] \qquad \text{(A.17)}$$

where

$$|\arg(\nu^{2/3} e^{2/3\pi i}\zeta)| < \pi \qquad \text{(A.18)}$$

is required for the validity of the Airy function approximations. Equations A.16 and A.17 are valid as $|\nu| \to \infty$ in $|\arg \nu| < \frac{\pi}{2}$ and z in the non-transitional zone.

It is seen that Equations A.16 and A.17 will be simplified if the products raised to fractional powers can be expressed as the product of each factor raised to the fractional power, for then the $\zeta^{1/4}$ factors will cancel. However, this process is complicated by the fact that, according to Equation A.18, the principal value of $\nu^{2/3} e^{2/3\pi i} \zeta$ must be taken, and principal values of products are not in general equal to products of principal values. This difficulty can be resolved by writing the principal value of the argument of $\nu^{2/3} e^{2/3\pi i} \zeta$ as the sum of the principal values of the argument of each factor plus the proper multiple of 2π. This process is carried out as follows.

Let Arg denote the principal value of the argument. Then

$$\operatorname{Arg}\left(\nu^{2/3} e^{2/3\pi i} \zeta\right) = \tfrac{2}{3} \operatorname{Arg} \nu + \tfrac{2}{3}\pi + \operatorname{Arg} \zeta + 2n\pi$$

$$= \tfrac{2}{3} \arg \nu + \tfrac{2}{3}\pi + \operatorname{Arg} \zeta + 2n\pi$$

the last equation arising from the fact that the restriction $|\arg \nu| < \frac{\pi}{2}$ has already been imposed. The range of n for the present problem is easily obtained since $|\arg \nu| < \frac{\pi}{2}$, and $-\pi < \operatorname{Arg} \zeta \leq \pi$ by definition. Then

$$-\tfrac{2}{3}\pi < \left(\tfrac{2}{3} \arg \nu + \tfrac{2}{3}\pi + \operatorname{Arg} \zeta\right) < 2\pi$$

so the only values of n required are 0 and -1, selected as follows:

$$n = \begin{cases} 0, & -\frac{2}{3}\pi < \left(\frac{2}{3} \arg \nu + \frac{2}{3}\pi + \operatorname{Arg} \zeta\right) < \pi \\ -1, & \pi < \left(\frac{2}{3} \arg \nu + \frac{2}{3}\pi + \operatorname{Arg} \zeta\right) < 2\pi \end{cases} \qquad \text{(A.19)}$$

The case $(\frac{2}{3} \arg \nu + \frac{2}{3}\pi + \operatorname{Arg} \zeta) = \pi$ is excluded since it would require the use of different Airy function approximations, and is

not required for the application in the text.

The application in the text considers z to be of the form

$$z = \frac{\Omega}{\nu}$$

where Ω is real, so that arg z = -arg ν. In this case some useful further delineation of the behavior of n can be made. The reasoning is based on the domain K defined in the paragraph following Equation A.5 on the z-ζ transformation depicted in Figure A1. For convenience in writing the notation

$$x \in (a,b) \Rightarrow a < x < b$$
$$x \in [a,b) \Rightarrow a \leq x < b$$
$$etc.$$

will be used. The discussion is broken down into three parts which cover the range of interest.

(i) For $\arg\nu \in [0, \frac{\pi}{2})$ and z not in K, $\arg z \in (-\frac{\pi}{2}, 0]$ so $\text{Arg}\zeta \in (\frac{\pi}{3}, \pi]$ and $(\frac{2}{3}\arg\nu + \frac{2}{3}\pi + \text{Arg}\zeta) \in (\pi, 2\pi)$, hence n = -1.

(ii) For $\arg\nu \in [0, \frac{\pi}{2})$ and z in K, $\arg z \in (-\frac{\pi}{2}, 0]$ so $\text{Arg}\zeta \in [0, \frac{\pi}{3})$ and $(\frac{2}{3}\arg\nu + \frac{2}{3}\pi + \text{Arg}\zeta) \in (\frac{2}{3}\pi, \frac{4}{3}\pi)$ hence n may be 0 or -1. However, for sufficiently small $\arg\nu$, $\arg z$ is small and $\text{Arg}\zeta$ is small, in which case $(\frac{2}{3}\arg\nu + \frac{2}{3}\pi + \text{Arg}\zeta) < \pi$, so that n = 0.

(iii) For $\arg\nu \in (-\frac{\pi}{2}, 0)$, $\arg z \in (0, \frac{\pi}{2})$ so $\text{Arg}\zeta \in (-\pi, 0)$ and $(\frac{2}{3}\arg\nu + \frac{2}{3}\pi + \text{Arg}\zeta) \in (-\frac{2}{3}\pi, \frac{2}{3}\pi)$, hence n = 0.

The definition of n allows the quantity $(\nu^{2/3} e^{2/3\pi i_\zeta})^{\pm 1/4}$ to be split up into its factors, so that if the same can be done for $[4\zeta/(1-z^2)]^{\pm 1/4}$ the ζ's outside the exponential can be cancelled, effecting a desirable simplification. This can be done, but requires

further delicate reasoning.

The function $[4\zeta/(1-z^2)]^{1/4}$ has previously been defined as $\phi(z)$, see Equation A.5. Let

$$\gamma \equiv \frac{4\zeta}{1-z^2}$$

Anticipating the application in the text, the range of z will be limited to argz $(-\pi/2, \pi/2)$. The discussion is broken down into four parts:

(i) z in K, argz$\varepsilon[0, \pi/2)$. It follows that $-\text{Arg}(1-z^2)\varepsilon[0, \pi/2)$ and $\text{Arg}\zeta\varepsilon(-\pi/3, 0]$, so arg$\gamma\varepsilon(-\pi/3, \pi/2)$.

(ii) z in K, argz$\varepsilon(-\pi/2, 0]$. Then $-\text{Arg}(1-z^2)\varepsilon(-\pi/2, 0]$ and $\text{Arg}\zeta\varepsilon[0, \pi/3)$, so arg$\gamma\varepsilon(-\pi/2, \pi/3)$.

(iii) z not in K, argz$\varepsilon(0, \pi/2)$. Then $-\text{Arg}(1-z^2)\varepsilon(0, \pi)$ and $\text{Arg}\zeta\varepsilon(-\pi, -\pi/3)$, so arg$\gamma\varepsilon(-\pi, 2\pi/3)$.

(iv) z not in K, argz$\varepsilon(-\pi/2, 0]$. Then $-\text{Arg}(1-z^2)\varepsilon[-\pi, 0)$ and $\text{Arg}\zeta\varepsilon(\pi/3, \pi]$, so arg$\gamma\varepsilon(-2\pi/3, \pi)$.

From the above discussion it is seen that

$$\arg\gamma = \arg\zeta - \arg(1-z^2) \qquad \text{(A.20)}$$

Hence in breaking up ϕ into its factors $\zeta^{1/4}$ and $(1-z^2)^{-1/4}$ the principal values of the fractional powers may be used. The intervals on argz in (iii) and (iv) are chosen so that argz can reach zero only from negative values (for z not in K). This is equivalent to introducing a branch cut from z = 1 to z = ∞ along the real axis, in which the surrounding region is open above the cut and closed below the cut. (It should be noted that the necessity for the cut arises from choosing to describe $\phi(z)$ by the principal arguments of its factors,

not because ϕ has a branch point at z = 1.)

On the basis of the above discussions, the factors raised to fractional powers in Equations A.16 and A.17 may be separated, and advantage taken of the cancellation of $\zeta^{1/4}$, resulting in

$$H_\nu(\nu z) \sim 2^{1/2}\pi^{-1/2}(1-z^2)^{-1/4}\nu^{-1/2}\exp\left[(-1)^n\frac{2}{3}\zeta^{3/2}\nu - (n+1)\frac{\pi}{2}i\right] \qquad \text{(A.21)}$$

$$H_\nu'(\nu z) \sim 2^{1/2}\pi^{-1/2}z^{-1}(1-z^2)^{1/4}\nu^{-1/2}\exp\left[(-1)^n\frac{2}{3}\zeta^{3/2}\nu + (n+1)\frac{\pi}{2}i\right] \qquad \text{(A.22)}$$

where $|\nu| \to \infty$, $|\arg \nu| < \frac{\pi}{2}$ and $|\arg z| < \frac{\pi}{2}$. The principal value of $(1 - z^2)^{1/4}$ is to be taken. The special case $(2/3 \arg \nu + 2/3\ \pi + \text{Arg } \zeta) = \pi$ is excluded.

APPENDIX B. APPROXIMATIONS FOR $\bar{f}_j^*$ AS $p \to 0$

Introduction

In Chapter 2 the solution for the response functions $f_j^*(r,\theta,t)$ was reduced to the following integral on the contour C in Figure 6:

$$f_j^*(r,\theta,t) = -\frac{1}{2\pi i}\int_C \bar{f}_j^*(r,\theta,p)e^{pt}dp \qquad (B.1)$$

where $\bar{f}_j^*$ is given by

$$\bar{f}_j^*(r,\theta,p)\Big|_{\theta<0} = -i\tilde{f}_{sc}^*(r,\nu_j^+,p)e^{-i\nu_j^+\theta}\frac{D(\nu_j^+,p)}{Dp(\nu_j^+,p)}\frac{d\nu_j^+}{dp} \qquad (B.2)$$

in which ν_j^+ denotes the roots ν_j having Im $\nu_j > 0$.

The radius of the C_0 part of the contour C will be taken to zero, so a study of the behavior of $\bar{f}_j^*$ as $p \to 0$ is required. The necessary information about the roots ν_j as $p \to 0$ was obtained in Chapter 3. There it was found that ν_j^+ approached $\nu = \pm 1$ as $p \to 0$, and approximations were written in terms of ϵ_j, where

$$\nu_j = 1 + \epsilon_j$$

and from Equation 3.21 it was seen that

$$Im\,\epsilon_j \begin{cases} > 0, & \text{for } j \geq 0 \\ < 0, & \text{for } j < 0 \end{cases}$$

Thus,

$$\nu_j^+ = \begin{cases} 1+\epsilon_j, & \text{for } j \geq 0 \\ -1-\epsilon_j, & \text{for } j < 0 \end{cases}$$

according to the symmetry of the roots in $\nu = 0$.

In view of the above, approximations for $\tilde{f}^*_{sc}(r, \nu_j, p)$ for $\nu_j = 1 + \epsilon_j$ will not be directly applicable for $j < 0$. However, it is proven below that $\tilde{f}^*_{sc}$ satisfies the simple symmetry rule

$$\tilde{f}^*_{sc}(r, \nu_j^+, p) = S(f)\, \tilde{f}^*_{sc}(r, -\nu_j^+, p) \tag{B.3}$$

where

$$S(f) = \begin{cases} +1, & \text{for } f \text{ even in } \theta \\ -1, & \text{for } f \text{ odd in } \theta \end{cases} \tag{B.4}$$

Therefore, the approximations for $\nu_j = 1 + \epsilon_j$ can be converted to those for ν_j^+, and this is the procedure that will be followed.

Symmetry of $\tilde{f}^*_{sc}$ in $\nu = 0$

Although the proof of Equation B.3 can be based on a detailed examination of the various expressions for $\tilde{f}^*_{sc}$, it is shorter to argue as follows.

The residue evaluation yielding the form given by Equation B.2 is based on $\theta < 0$, which requires Im $\nu_j > 0$. Considering instead $\theta > 0$, the ν-inversion contour must be closed in Im $\nu < 0$, which yields

$$\bar{f}^*_j(r, \theta, p)\Big|_{\theta>0} = i \tilde{f}^*_{sc}(r, \nu_j^-, p) e^{-i\nu_j^- \theta} \frac{D(\nu_j^-, p)}{D_p(\nu_j^-, p)} \frac{d\nu_j^-}{dp} \tag{B.5}$$

where ν_j^- denotes those ν_j satisfying Im $\nu_j < 0$. Note a sign change between Equations B.2 and B.5 arising from encircling the poles of $\tilde{f}^*_{sc}$ in directions of opposite sense.

Since the roots of ν_j are symmetric in $\nu = 0$, no generality

is lost by taking

$$\nu_j^- = -\nu_j^+ \tag{B.6}$$

Furthermore,

$$D(-\nu,p) = D(\nu,p)$$

$$D_p(-\nu,p) = D_p(\nu,p)$$

$$\frac{d(-\nu)}{dp} = -\frac{d\nu}{dp}$$

so Equation B.5 can be written

$$\bar{f}_j^*(\lambda,\theta,p)\Big|_{\theta>0} = -i\,\tilde{f}_{sc}^*(\lambda,-\nu_j^+,p)\,e^{i\nu_j^+\theta}\,\frac{D(\nu_j^+,p)}{D_p(\nu_j^+,p)}\,\frac{d\nu_j^+}{dp} \tag{B.7}$$

Now, from Equation B.4,

$$\bar{f}_j^*(\lambda,\theta,p)\Big|_{\theta>0} = S(f)\,\bar{f}_j^*(\lambda,-\theta,p)\Big|_{\theta>0} \tag{B.8}$$

so combining Equations B.2, B.7 and B.8 gives the desired result, Equation B.3.

Approximations for $\bar{f}_j^*$

The first step is the development of approximations for K_ν, I_ν, and their derivatives for $p \to 0$ and $\epsilon \to 0$. To simplify the writing, the subscript j on ϵ_j and ν_j will be dropped when no loss of clarity results. The dependence of ϵ on p is given in sufficient detail to make order of magnitude assessments by the following approximations,

$$\epsilon \sim \text{const}\,(\log p)^{-1}$$

$$p^\epsilon \sim \text{const} + \text{const}\,\epsilon$$

derived from Equations 3.21 and 3.16a, respectively. Then using the power series definitions for the Bessel functions, the two

term approximations are found to be

$$I_{1+\epsilon}(z) = \frac{1}{(1+\epsilon)!}\left(\frac{z}{2}\right)^{1+\epsilon}\left[1 + \frac{1}{2+\epsilon}\left(\frac{z}{2}\right)^2 + O(z^4)\right] \qquad \text{(B.9a)}$$

$$I'_{1+\epsilon}(z) = \frac{1}{2\epsilon!}\left(\frac{z}{2}\right)^{\epsilon}\left[1 + \frac{3+\epsilon}{(1+\epsilon)(2+\epsilon)}\left(\frac{z}{2}\right)^2 + O(z^4)\right] \qquad \text{(B.9b)}$$

$$K_{1+\epsilon}(z) = \frac{\epsilon!}{2}\left(\frac{z}{2}\right)^{-1-\epsilon}\left\{1 + \left[-\frac{1}{\epsilon} + \frac{\pi \csc \epsilon\pi}{\epsilon!(1+\epsilon)!}\left(\frac{z}{2}\right)^{2\epsilon}\right]\left(\frac{z}{2}\right)^2 + O(\epsilon^{-1}z^4)\right\} \qquad \text{(B.10a)}$$

$$K'_{1+\epsilon}(z) = -\frac{(1+\epsilon)!}{4}\left(\frac{z}{2}\right)^{-2-\epsilon}\left\{1 + \left[\frac{1-\epsilon}{\epsilon(1+\epsilon)} - \frac{\pi \csc \epsilon\pi}{\epsilon!(1+\epsilon)!}\left(\frac{z}{2}\right)^{2\epsilon}\right]\left(\frac{z}{2}\right)^2 + O(\epsilon^{-1}z^4)\right\} \qquad \text{(B.10b)}$$

where $z = k_d a = pa/c_d$ or $z = k_s a = pa/c_s$.

Using just the first terms of Equations B.10 the approximation for D_p is found to be

$$D_p(\nu,p) = -\frac{a}{c_d} 4\epsilon(1+\epsilon)(2+\epsilon)\frac{\pi\epsilon}{\sin \pi\epsilon}\alpha^{-1-\epsilon}(\alpha^{2+2\epsilon}+1)(k_d a)^{-1} \cdot \left[1 + O(\epsilon^{-1}p^2)\right] \qquad \text{(B.11)}$$

For the function $A(\nu, p)$, defined in Equation 2.21, it turns out a two term approximation is required, since the lower order term cancels when A is inserted into the $\tilde{f}^*_{sc}$. Thus, using both terms in Equations B.9 and B.10 one finds

$$D(\nu,p)\,A(\nu,p) = 8\pi\,\bar{\varphi}_o(p)\,\epsilon(1+\epsilon)(2+\epsilon)\,\alpha^{-1-\epsilon}$$

$$\cdot\left[1+\frac{\alpha^2(2-\epsilon)^2+\epsilon(2+\epsilon)}{4\epsilon(1+\epsilon)(2+\epsilon)}\,(k_d a)^2+O(\epsilon^{-1}p^4)\right] \qquad \text{(B.12)}$$

The approximations for the response functions $\tilde{f}^*_{sc}$ will be written only for $\tilde{u}^*_{sc}$, $\tilde{v}^*_{sc}$, and $\tilde{\sigma}^*_{\theta sc}$. The stresses σ_r and $\tau_{r\theta}$ will no longer be considered because attention will later be focussed on r = a, where the latter stresses are zero. Using the approximations for the Bessel functions, A(ν,p), and the exact elementary expression for B(ν,p), Equation 2.22, yields

$$D(\nu,p)\,\tilde{u}^*_{sc}(a,\nu,p) = \left\{-4\pi\bar{\varphi}_o(p)\,a^{-1}(1+\epsilon)(2+\epsilon)\left(\frac{\pi\epsilon}{\sin\pi\epsilon}\right)^{1/2}\alpha^{-1-\epsilon}\right.$$

$$\left.\cdot\left(-\frac{\alpha^{2+2\epsilon}+1}{\alpha^2-1}\right)^{1/2} k_d a\left[1+O(\epsilon^{-1}p^2)\right]\right\} \qquad \text{(B.13)}$$

$$D(\nu,p)\,\tilde{v}^*_{sc}(a,\nu,p) = -i\left\{\text{same as Eqn. B.13}\right\} \qquad \text{(B.14)}$$

$$D(\nu,p)\,\tilde{\sigma}^*_{\theta_{sc}}(a,\nu,p) = 16\pi\,\bar{\varphi}_o(p)\,a^{-2}\mu\epsilon(1+\epsilon)(2+\epsilon)\,\alpha^{-1-\epsilon}(\alpha^2-1)^{1/2}$$

$$\cdot\left[-(\alpha^{2+2\epsilon}+1)\right]^{1/2}\left(\frac{\epsilon\pi}{\sin\epsilon\pi}\right)^{1/2} k_d a\left[1+O(\epsilon^{-1}p^2)\right] \qquad \text{(B.15)}$$

In Chapter 3, the argument of $-(\alpha^2+1)$ was taken to be $(2j+1)\pi i$, so since ϵ is small,

$$\left[-(\alpha^{2+2\epsilon}+1)\right]^{1/2} = (\alpha^{2+2\epsilon}+1)^{1/2}\,e^{\frac{1}{2}(2j+1)\pi i} \qquad \text{(B.16)}$$

Combining the above results the approximations for $\bar{f}_j^*$ for $\theta > 0$ are found to be

$$\bar{u}_j^*(a,\theta,p) = \left\{(-1)^j \pi \bar{\varphi}_o(p) a^{-1} e^{i\nu_j^+\theta} \frac{d\nu_j^+}{d\left(\frac{pa}{c_d}\right)} (\alpha^{2+2\epsilon_j}+1)^{-1/2} (\alpha^2-1)^{-1/2}\right.$$

$$\left. \cdot \left(\frac{\sin \epsilon_j \pi}{\epsilon_j \pi}\right)^{1/2} \epsilon_j^{-1} \left(\frac{pa}{c_d}\right)^2 \left[1 + O(\epsilon^{-1}p^2)\right]\right\} \qquad \text{(B.17)}$$

$$\bar{v}_j^*(a,\theta,p) = -i\, \mathrm{sgn}(j) \left\{ \text{same as Eqn. B.17} \right\} \qquad \text{(B.18)}$$

$$\bar{\sigma}_{\theta_j}^*(a,\theta,p) = -(-1)^j 4\pi \bar{\varphi}_c(p) a^{-2} \mu e^{i\nu_j^+\theta} \frac{d\nu_j^+}{d\left(\frac{pa}{c_d}\right)} (\alpha^{2+2\epsilon_j}+1)^{-1/2}$$

$$\cdot (\alpha^2-1)^{1/2} \left(\frac{\sin \epsilon_j \pi}{\epsilon_j \pi}\right)^{1/2} \left(\frac{pa}{c_d}\right)^2 \left[1 + O(\epsilon^{-1}p^2)\right] \qquad \text{(B.19)}$$

where

$$\mathrm{sgn}(j) \equiv \begin{cases} +1, & j \geq 0 \\ -1, & j < 0 \end{cases}$$

The sgn function arises from the oddness of v with respect to zero, which must be accounted for according to Equation B.3 for $j < 0$. The approximations given in Equations B.17, B.18 and B.19 have been compared with numerical results for the Rayleigh mode ($j = 0$) at $\Omega = ipa/c_d = 0.01$. Using exact values for ν_j and ϵ_j the errors are about 5%.

The expressions for $\bar{f}_j^*$ can be written entirely in terms of p by using

$$\epsilon_j(p) \sim -\frac{1}{2}\left[\log\frac{\alpha^2+1}{\alpha^2-1} + (2j+1)\pi i\right]\left(\log\frac{pa}{c_d}\right)^{-1}$$

from Equation 3.21,

$$\frac{dv_j}{d\left(\frac{pa}{c_d}\right)} \sim \frac{1}{2}\left[\log\frac{\alpha^2+1}{\alpha^2-1} + (2j+1)\pi i\right]\left(\log\frac{pa}{c_d}\right)^{-2}\left(\frac{pa}{c_d}\right)^{-1}$$

from Equation 3.22, and

$$\bar{\varphi}_0(p) = \frac{\sigma_0 c_d^2 p^{-3}}{\lambda+2\mu}$$

from Equation 2.17b. Then the $\bar{\Gamma}_j^*$, normalized on u_0 (defined by Equation 4.1) and σ_0 are

$$\frac{\bar{u}_j^*(a,\theta,p)}{u_0} \sim \left\{-(-1)^j \pi a c_d^{-1}(\alpha^4-1)^{-1/2} e^{i\,\mathrm{sgn}(j)\theta}\left(\log\frac{pa}{c_d}\right)^{-1}\left(\frac{pa}{c_d}\right)^{-2}\right\} \qquad \text{(B.20)}$$

$$\frac{\bar{v}_j^*(a,\theta,p)}{u_0} \sim -i\,\mathrm{sgn}(j)\left\{\text{same as Eqn. B.20}\right\} \qquad \text{(B.21)}$$

$$\frac{\bar{\sigma}_{\theta j}^*(a,\theta,p)}{\sigma_0} \sim -(-1)^j 2\pi a c_d^{-1} e^{i\,\mathrm{sgn}(j)\theta}\alpha^{-2}\left(\frac{\alpha^2-1}{\alpha^2+1}\right)^{1/2}$$

$$\cdot\left[\log\frac{\alpha^2+1}{\alpha^2-1} + (2j+1)\pi i\right]\left(\log\frac{pa}{c_d}\right)^{-2}\left(\frac{pa}{c_d}\right)^{-2} \qquad \text{(B.22)}$$

The asymptotic approximations for the functions $\hat{f}_j(a,\Omega)$, defined by Equation 4.13, are

$$\frac{\hat{u}_j(a,\Omega)}{u_o} \sim \left\{(-1)^j (i)^{1+\mathrm{sgn}(j)} (\alpha^4-1)^{-1/2} (\log\Omega)^{-1} \Omega^{-2}\right\} \qquad \text{(B.23)}$$

$$\frac{\hat{v}_j(a,\Omega)}{u_o} \sim i\,\mathrm{sgn}(j)\left\{\text{same as Eqn. B.23}\right\} \qquad \text{(B.24)}$$

$$\frac{\hat{\sigma}_{\theta_j}(a,\Omega)}{\sigma_o} \sim (-1)^j (i)^{1+\mathrm{sgn}(j)} 2\alpha^{-2} \left(\frac{\alpha^2-1}{\alpha^2+1}\right)^{1/2}$$

$$\cdot\left[\log\frac{\alpha^2+1}{\alpha^2-1} + (2j+1)\pi i\right](\log\Omega)^{-2}\Omega^{-2} \qquad \text{(B.25)}$$

APPENDIX C. ASYMPTOTIC APPROXIMATIONS FOR LOGARITHMIC INTEGRALS

In the text the integrals

$$\int_0^{\Delta} \frac{d\Omega}{\log\Omega} , \qquad \int_0^{\Delta} \frac{d\Omega}{(\log\Omega)^2}$$

occur, where Δ is small. Asymptotic approximations for $\Delta \to 0$ will now be derived, by the straightforward application of the properties of the exponential and logarithmic integrals, as given, for example, in (30). For $\Delta < 1$ the logarithmic integral $li(\Delta)$ is defined by

$$li(\Delta) \equiv \int_0^{\Delta} \frac{d\Omega}{\log\Omega} \tag{C.1}$$

The change of variables $\Omega = e^{-t}$ gives

$$li(\Delta) = -\int_{-\log\Delta}^{\infty} \frac{e^{-t}}{t} dt = -E_1(-\log\Delta)$$

where $E_1(x)$ is an exponential integral, defined by

$$E_1(x) \equiv \int_x^{\infty} \frac{e^{-t}}{t} dt$$

Reference 30 gives, for large real x,

$$E_1(x) \sim \frac{e^{-x}}{x}\left[1 + \sum_{s=1}^{\infty} s!\,(-x)^{-s}\right]$$

Therefore, for $\Delta \to 0$

$$li(\Delta) \sim \frac{\Delta}{\log\Delta}\left[1 + \sum_{s=1}^{\infty} s!\,(\log\Delta)^{-s}\right] \tag{C.2}$$

Now consider

$$I(\Delta) \equiv \int_0^{\Delta} \frac{d\Omega}{(\log \Omega)^2}$$

$$= -\int_0^{\Delta} \Omega \frac{d}{d\Omega}\left[\frac{1}{\log \Omega}\right] d\Omega$$

$$= -\left[\frac{\Omega}{\log \Omega}\right]_0^{\Delta} + \int_0^{\Delta} \frac{d\Omega}{\log \Omega}$$

$$= li(\Delta) - \frac{\Delta}{\log \Delta}$$

Then, from Equation C.2

$$I(\Delta) \sim \frac{\Delta}{(\log \Delta)^2}\left[1 + \sum_{s=2}^{\infty} s!\,(\log \Delta)^{1-s}\right] \qquad (C.3)$$

APPENDIX D. LONG-TIME SOLUTION

The displacement, velocity, and stress fields as $t \to \infty$ can be found by considering an equivalent static problem. First, consider the response caused by the incident wave alone. Then, from Equations 2.5,

$$\varphi_{inc}(x,y,t) = \frac{\sigma_0 c_d^2}{\lambda+2\mu} \frac{\tau^2}{2} H(\tau)$$

where $\tau = t + \frac{x}{c_d}$. Then

$$u_{x_{inc}} = \frac{\partial \varphi_{inc}}{\partial x} = \frac{\sigma_0 c_d}{\lambda+2\mu} \tau H(\tau) = u_0 \left(T + \frac{x}{a}\right) H(\tau) \qquad \text{(D.1a)}$$

$$u_{y_{inc}} = 0 \qquad \text{(D.1b)}$$

$$e_{x_{inc}} = \frac{\partial u_{x_{inc}}}{\partial x} = \frac{\sigma_0}{\lambda+2\mu} H(\tau) \qquad \text{(D.2)}$$

the remaining strain components being zero. The normalization constant u_0 is defined by Equation 4.1 and $T \equiv c_d t/a$. The stresses and velocities are

$$\sigma_{x_{inc}} = \lambda(e_x+e_y+e_z) + 2\mu e_x = \sigma_0 H(\tau) \qquad \text{(D.3a)}$$

$$\sigma_{y_{inc}} = \lambda(e_x+e_y+e_z) + 2\mu e_y = \frac{\lambda}{\lambda+2\mu} \sigma_0 H(\tau) \qquad \text{(D.3b)}$$

$$\tau_{xy_{inc}} = 0 \qquad \text{(D.3c)}$$

$$\dot{u}_{x_{inc}} = \frac{\sigma_0 c_d}{\lambda+2\mu} H(\tau) = \dot{u}_0 H(\tau) \qquad \text{(D.4a)}$$

$$\dot{u}_{y_{inc}} = 0 \qquad \text{(D.4b)}$$

where $\dot{u}_0$ is the normalization constant defined by Equation 4.2.

These same response fields apply at large distances from the cavity long after the incident wave has passed the cavity. Therefore the long-time solution is the sum of the following:

(i) the stresses and displacements for the static problem where the stresses $\sigma_x = \sigma_0$ and $\sigma_y = [\lambda/(\lambda + 2\mu)]\,\sigma_0$ are applied at $r = \infty$ and the displacement at $r = 0$ is zero,

(ii) the displacements and velocity of the center of the cavity, derived from Equations D.1 and D.4.

The solution to the static problem can be constructed from the uniaxial load solution given, for example, on p. 291 of Reference 28. At $r = a$, the results for $\lambda = \mu$ ($a^2 = 3$) are

$$\sigma_{\theta_{st}}(a,\theta)/\sigma_0 = \frac{8}{3}\sin^2\theta$$

$$u_{st}(a,\theta)/u_0 = 3\cos^2\theta$$

$$v_{st}(a,\theta)/u_0 = -\frac{3}{2}\sin 2\theta$$

where $(\ )_{st}$ denotes the static solution. The total long-time response at $r = a$ is given by

$$\sigma_\theta(a,\theta,t)/\sigma_0 \sim \frac{8}{3}\sin^2\theta \qquad \text{(D.5)}$$

$$u(a,\theta,t)/u_0 \sim T\cos\theta + 3\cos^2\theta \qquad \text{(D.6a)}$$

$$v(a,\theta,t)/u_0 \sim -T\sin\theta - \frac{3}{2}\sin 2\theta \qquad \text{(D.6b)}$$

$$\dot{u}(a,\theta,t)/\dot{u}_0 \sim \cos\theta \qquad \text{(D.7a)}$$

$$\dot{v}(a,\theta,t)/\dot{u}_0 \sim -\sin\theta \qquad \text{(D.7b)}$$

APPENDIX E. DISCUSSION OF NUMERICAL TECHNIQUES

Programs for Bessel Functions of Complex Order

SHARE Program 979 was the basic program used for the computation of the Bessel functions. This program can handle complex arguments and orders of absolute value of 75 or less and 85 or less, respectively. This means that the maximum value of Ω that can be used in the present work is 43, since $\Omega_s = \alpha\Omega \doteq 75$ for $\alpha^2 = 3$.

The results for the roots ν_j and the integrands $\hat{f}_j$ were checked against SHARE Program 1315 for $\Omega < 5$ and agreement to 4 or more significant figures was found for $\Omega > 0.1$. At $\Omega = 0.01$ the agreement for the roots is 3 or more figures and for the integrands, 2 or more figures.

The program was checked for large Ω by finding the first two zeros of $H_\nu(\Omega)$ for $\Omega \leq 40$. Agreement with asymptotic expansions for the roots was very close. For example, the numerical values of the lowest two zeros at $\Omega = 40$ are 43.173 + 5.496i and 45.458 + 9.610i, whereas the asymptotic expansion to $O(\Omega^{1/3})$ gives 43.157 + 5.525i and 45.499 + 9.699i, respectively.

Rootfinder Program

The method of false position was used, with complex arithmetic. Convergence usually occurs in about ten iterations when the original guess is good. In order to economize on computer time, the integrands $\hat{f}_j$ were calculated at the same time as the root, and punched on cards. The derivative $d\nu_j/dp$ was calculated using a quadratic polynomial approximation.

Calculating both the roots and the integrands, the time required for each root was about 5 minutes for the points $\Omega = 0.01(0.01)0.1(0.1)1(0.2)2(0.5)5(1)20$,* and one minute for the points $\Omega = 20(1)40$.

Integration Program

In order to avoid recalculation of the Bessel functions and interpolation during integration, the integrands were tabulated on punched cards at a fixed set of integration points. It was found through trial and error that the points $\Omega = 0.01(0.01)0.1(0.1)1(0.2)\Omega_{upper}$ (where $\Omega_{upper} = 20$ for the R and S modes and 40 for the P modes) gave satisfactory results. The integrands at non-integral values of Ω between 2 and Ω_{upper} were found by interpolation. Simpson's rule was used to evaluate the integrals over even numbers of increments, and the trapezoidal rule was used to fill in odd intervals as required. The 7094 time required to calculate the P1, P2, P3, R, S1 and S2 mode response for the displacements and velocities at one θ point and 40 time points was about 10 minutes.

In retrospect, it appears that a great deal of convenience would have been gained by using built-in step size control and built-in upper limit convergence controls. This would require interpolating to find the values of the integrands, but the time required for this would probably be made up by avoiding unnecessary calculations.

---

* Numbers in parentheses are the increments between numbers on either side of parentheses.

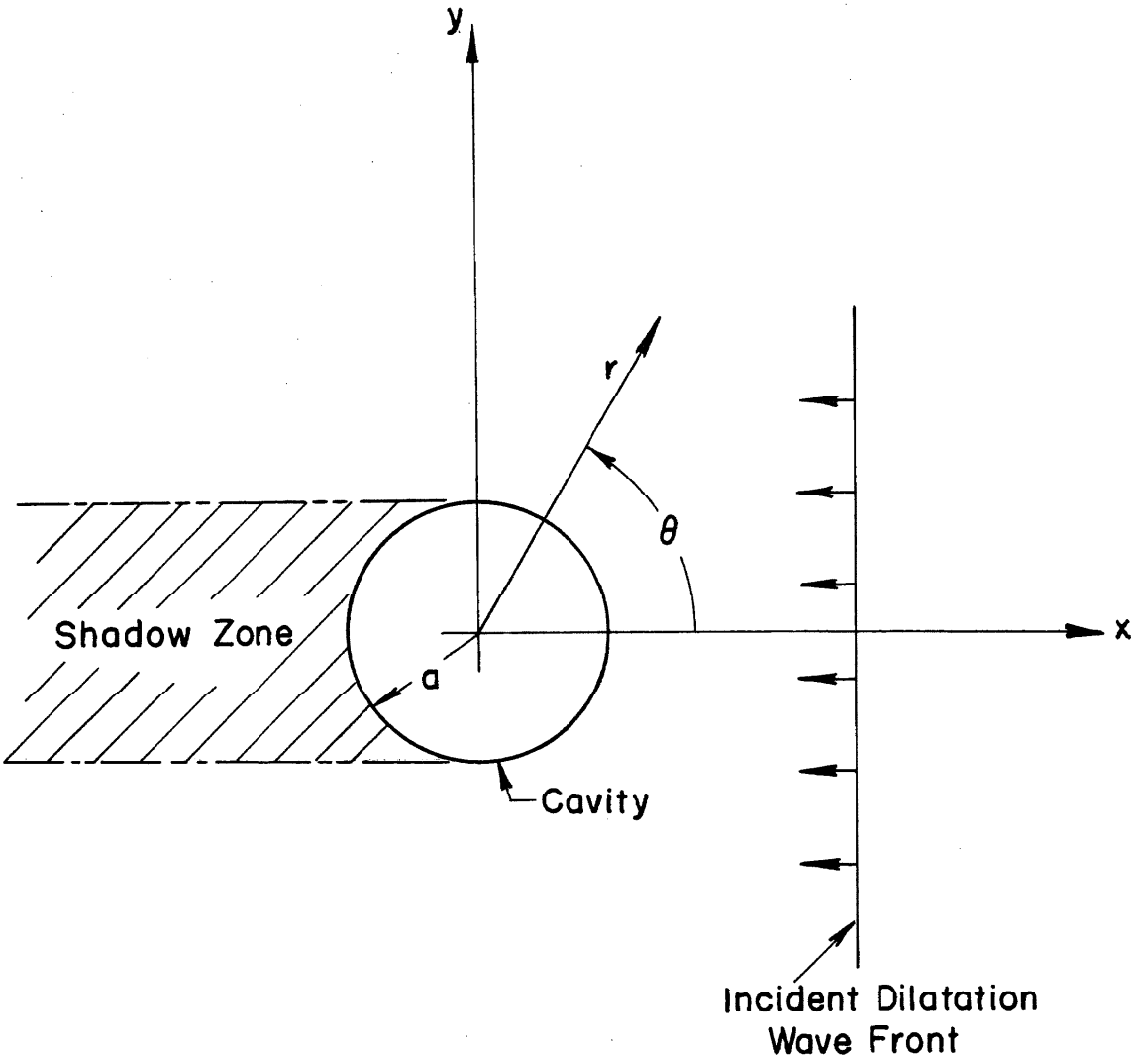

Fig. 1. Geometry of the Problem.

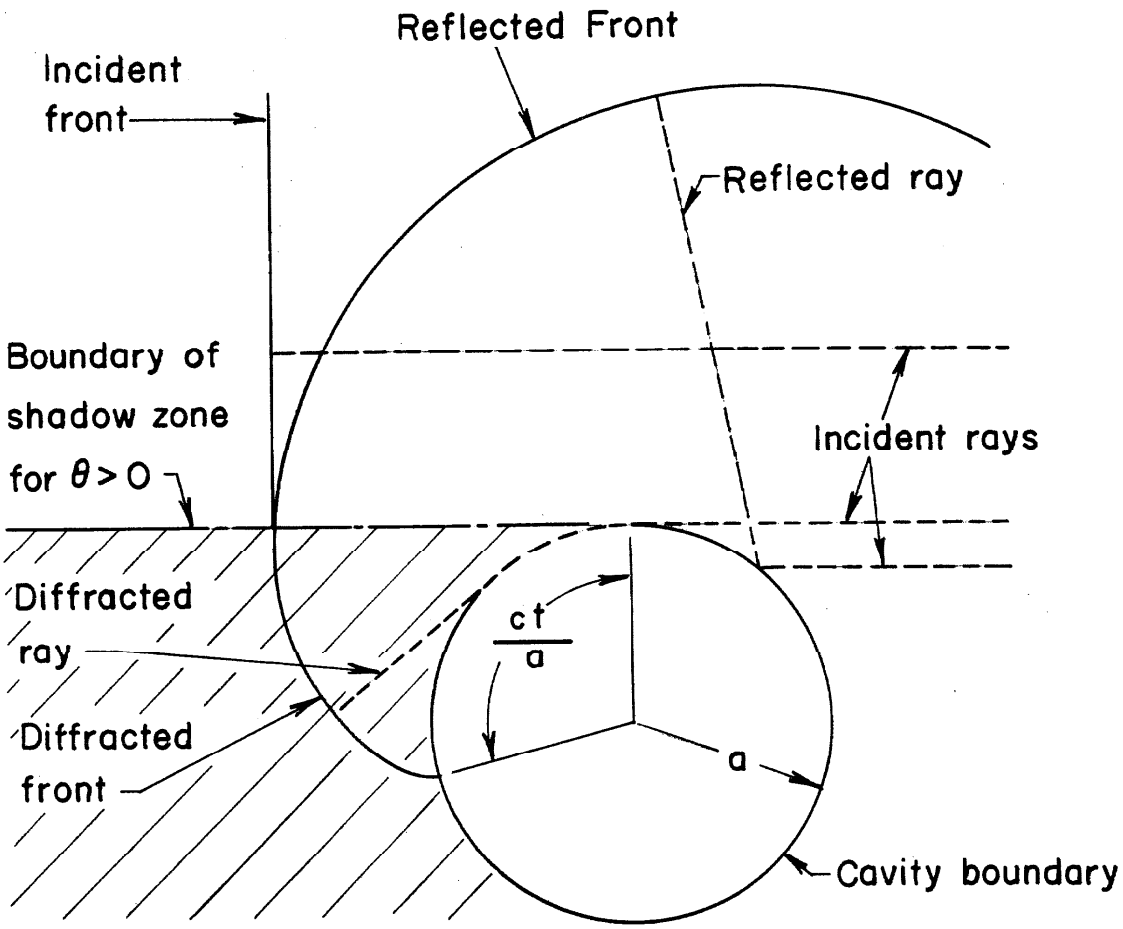

Fig. 2. Geometry of Rays.

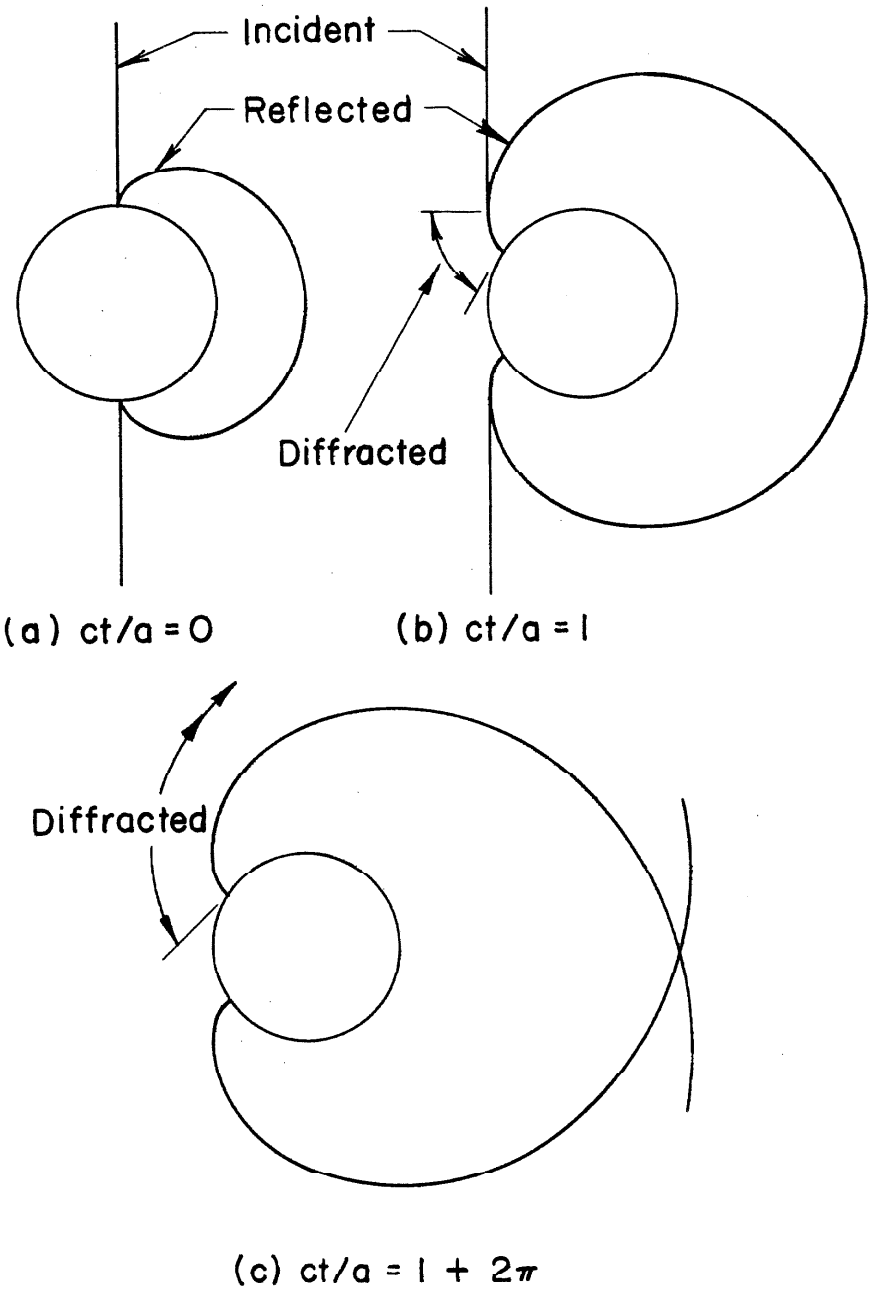

Fig. 3. Geometry of Wave Fronts.

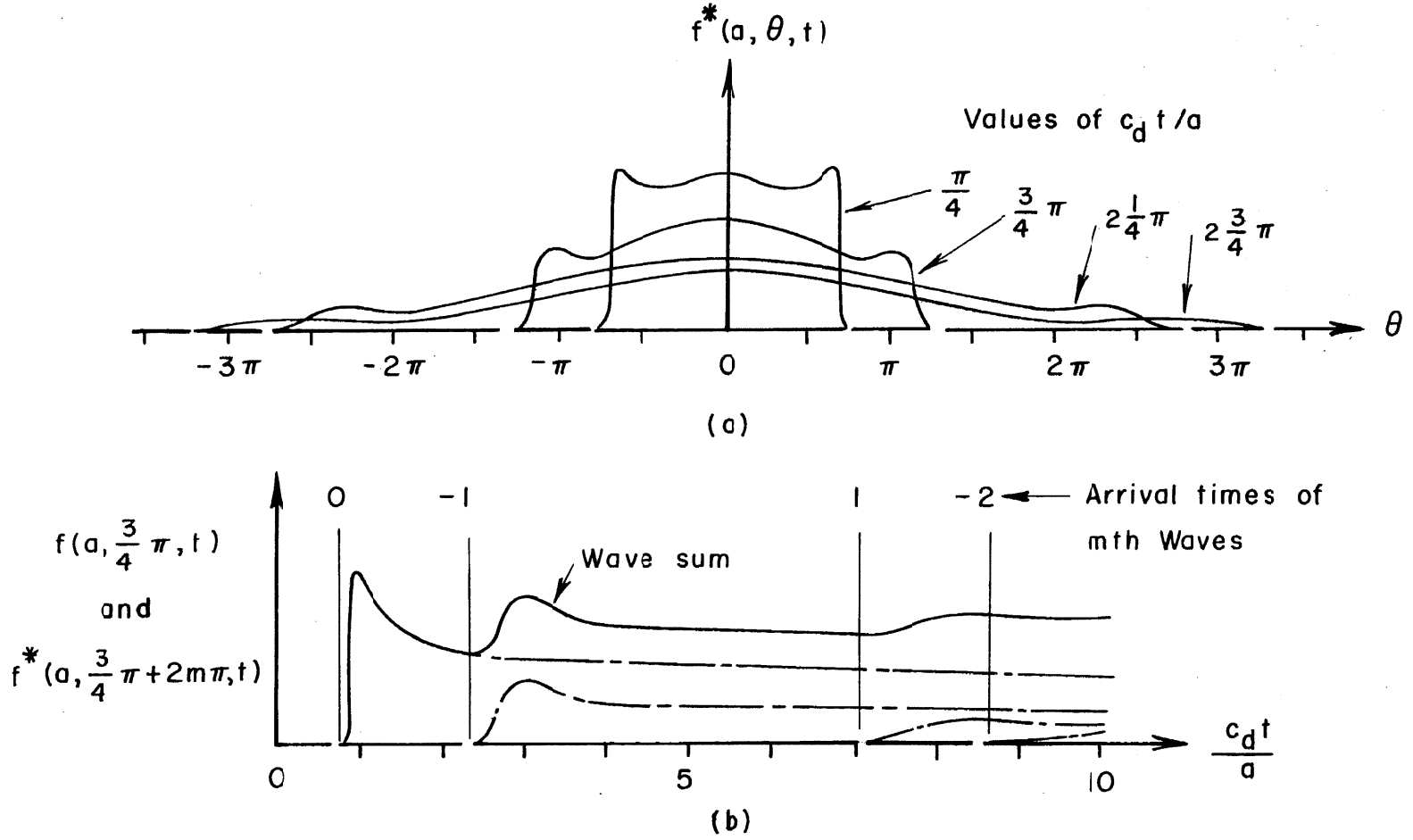

Fig. 4. Illustration of Waves f^* and Wave Sum f.

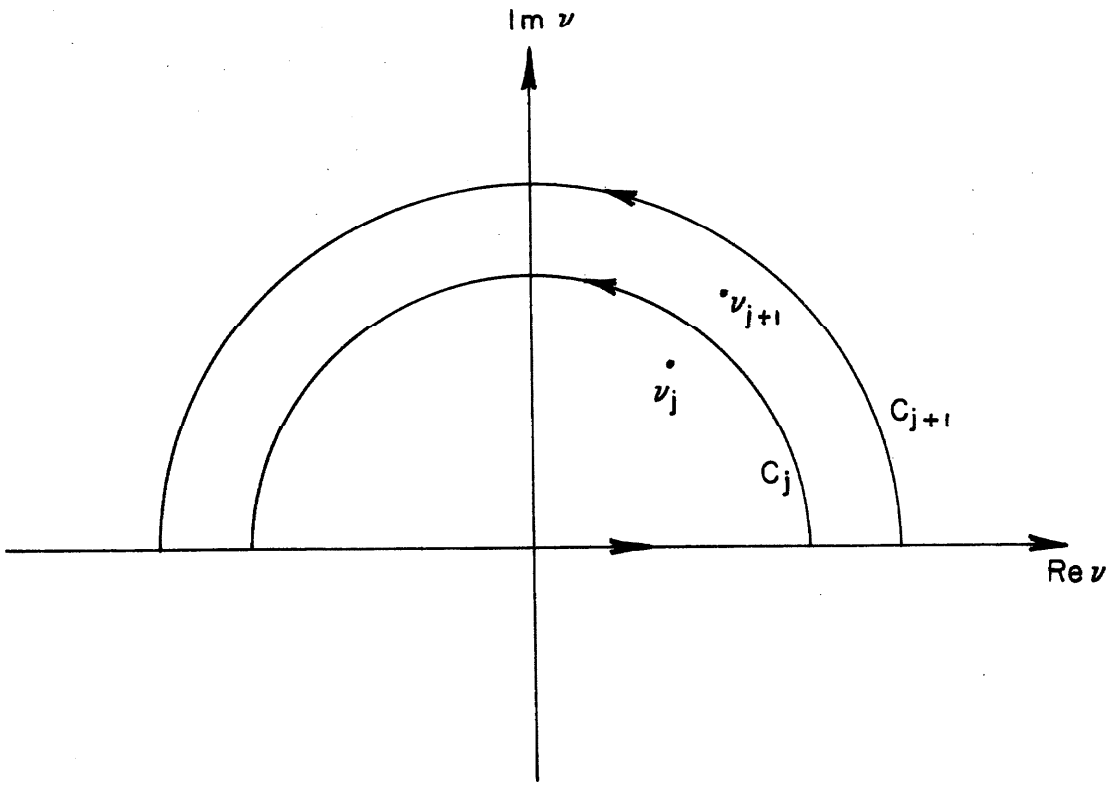

Fig. 5. Completion of the ν - Contour.

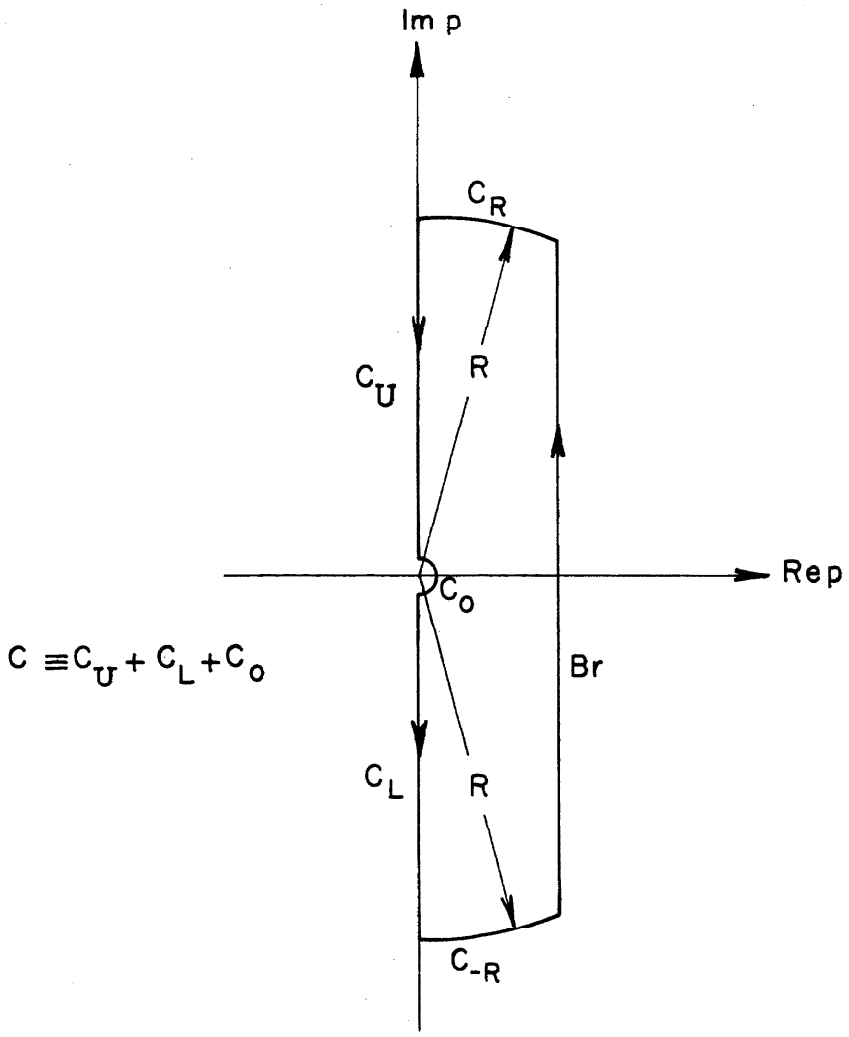

Fig. 6. Completion of Inversion Contour for Laplace Transform.

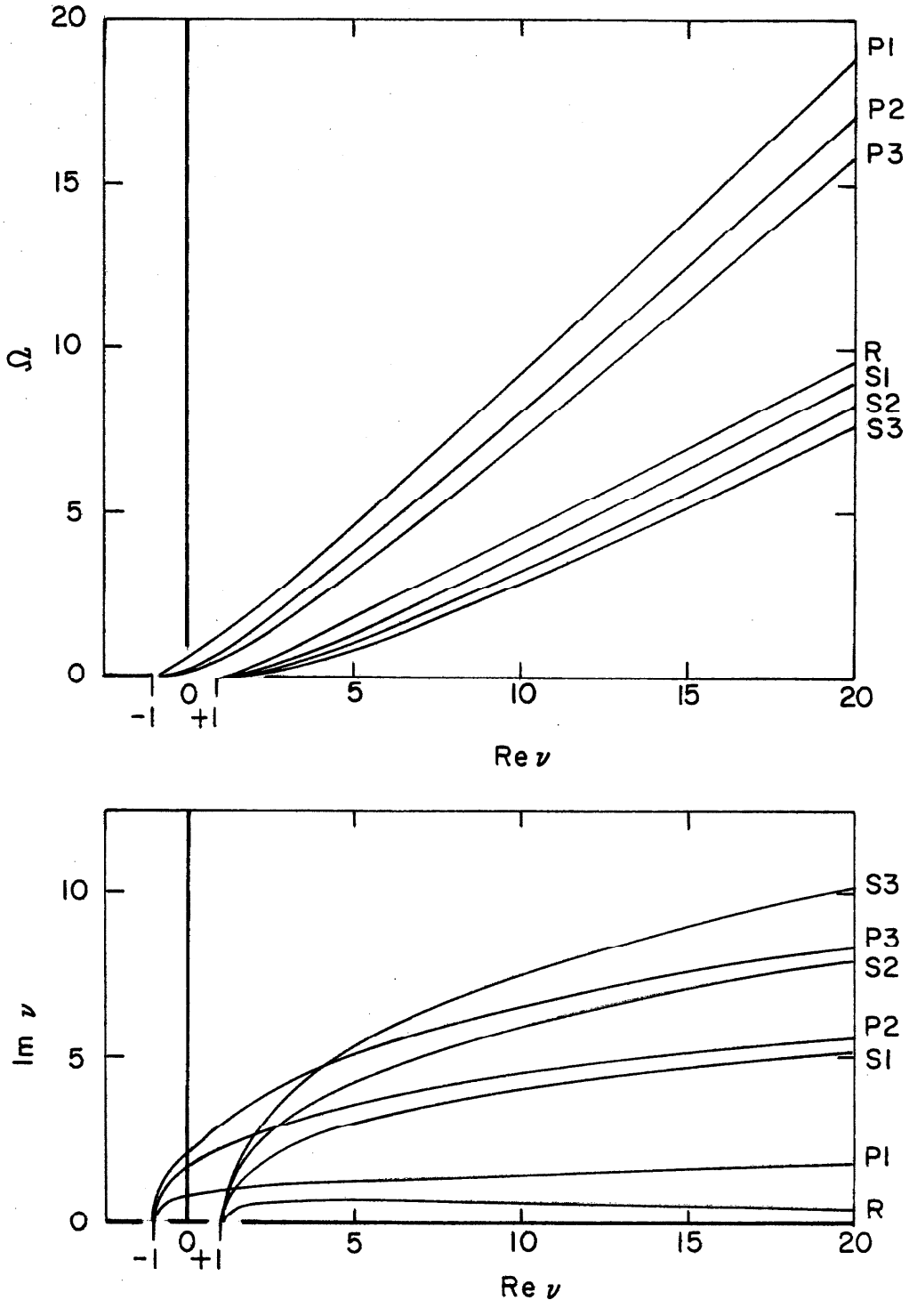

Fig. 7. Projections of the Roots.

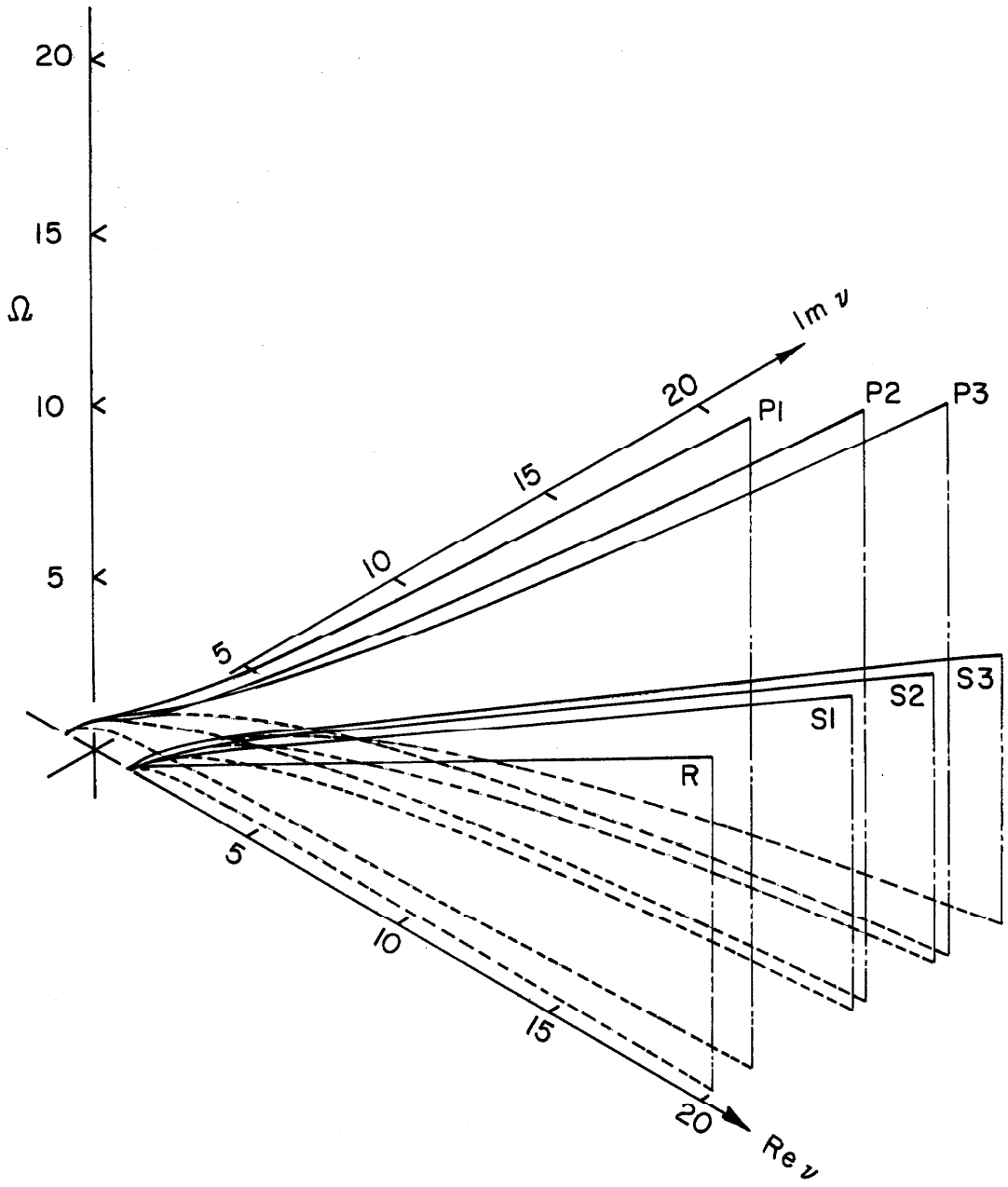

Fig. 8. Isometric Projection of the Roots.

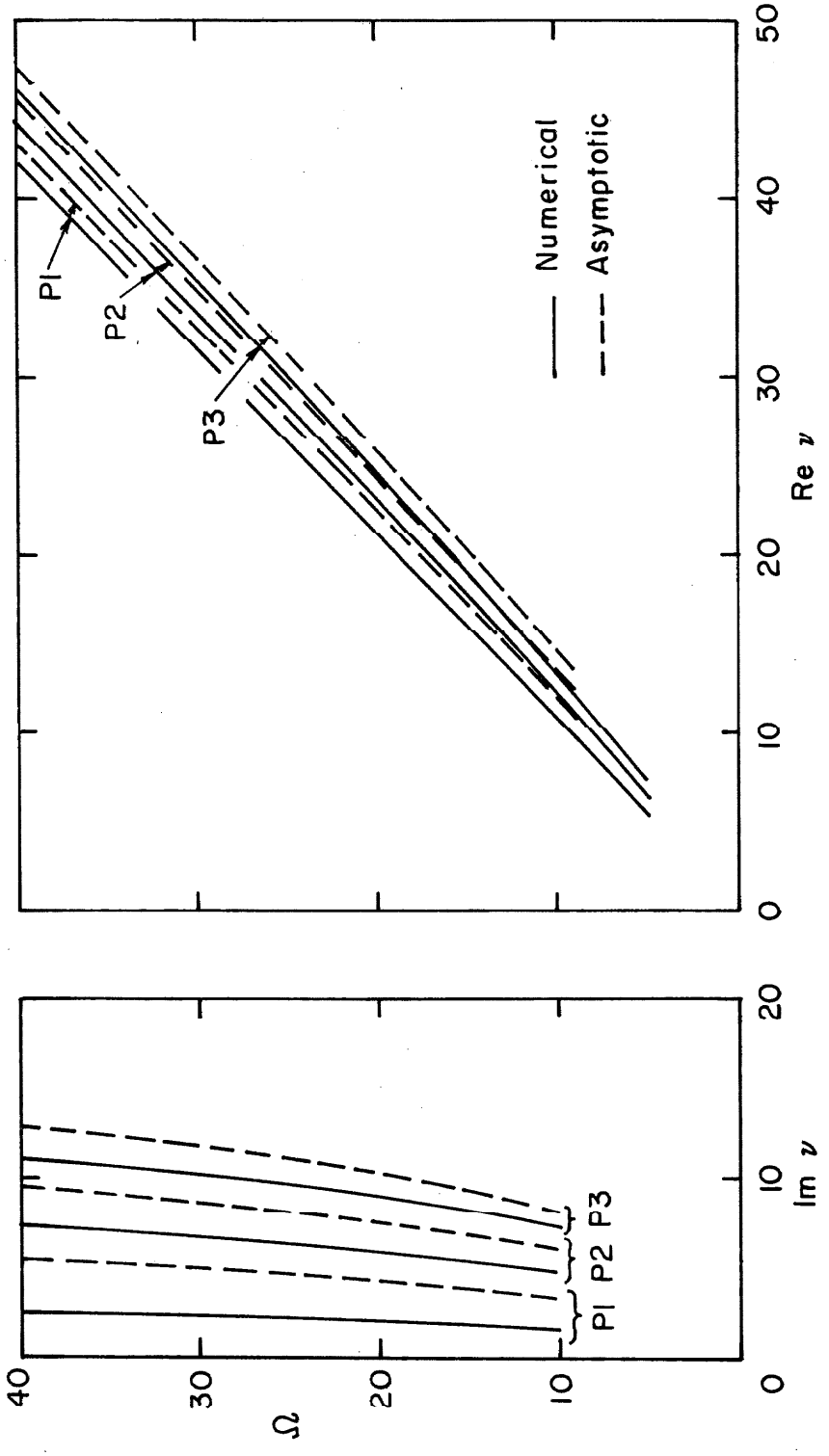

Fig. 9. Comparison of Asymptotic and Numerical Results for P Roots.

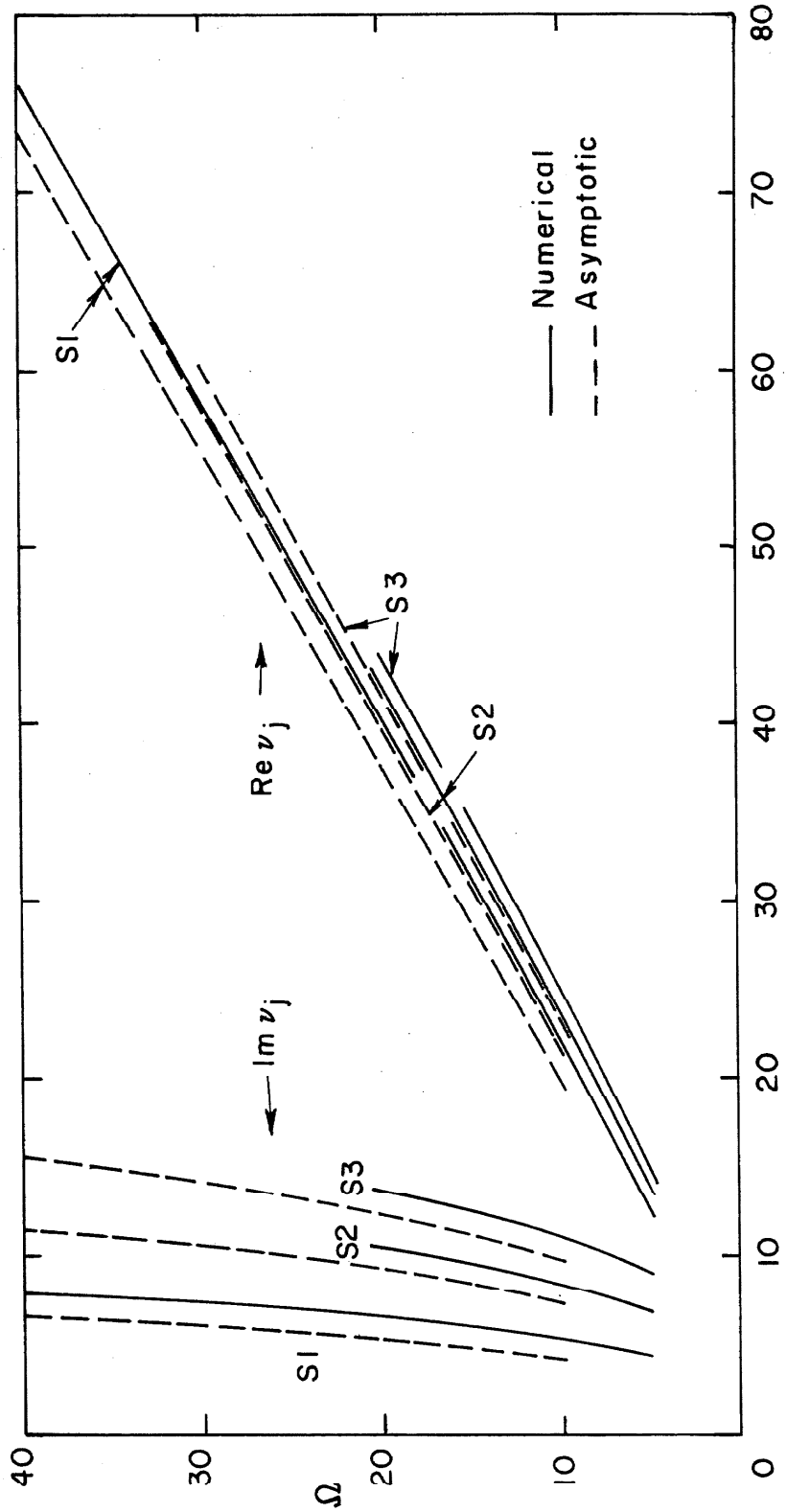

Fig. 10. Comparison of Asymptotic and Numerical Results for S Roots.

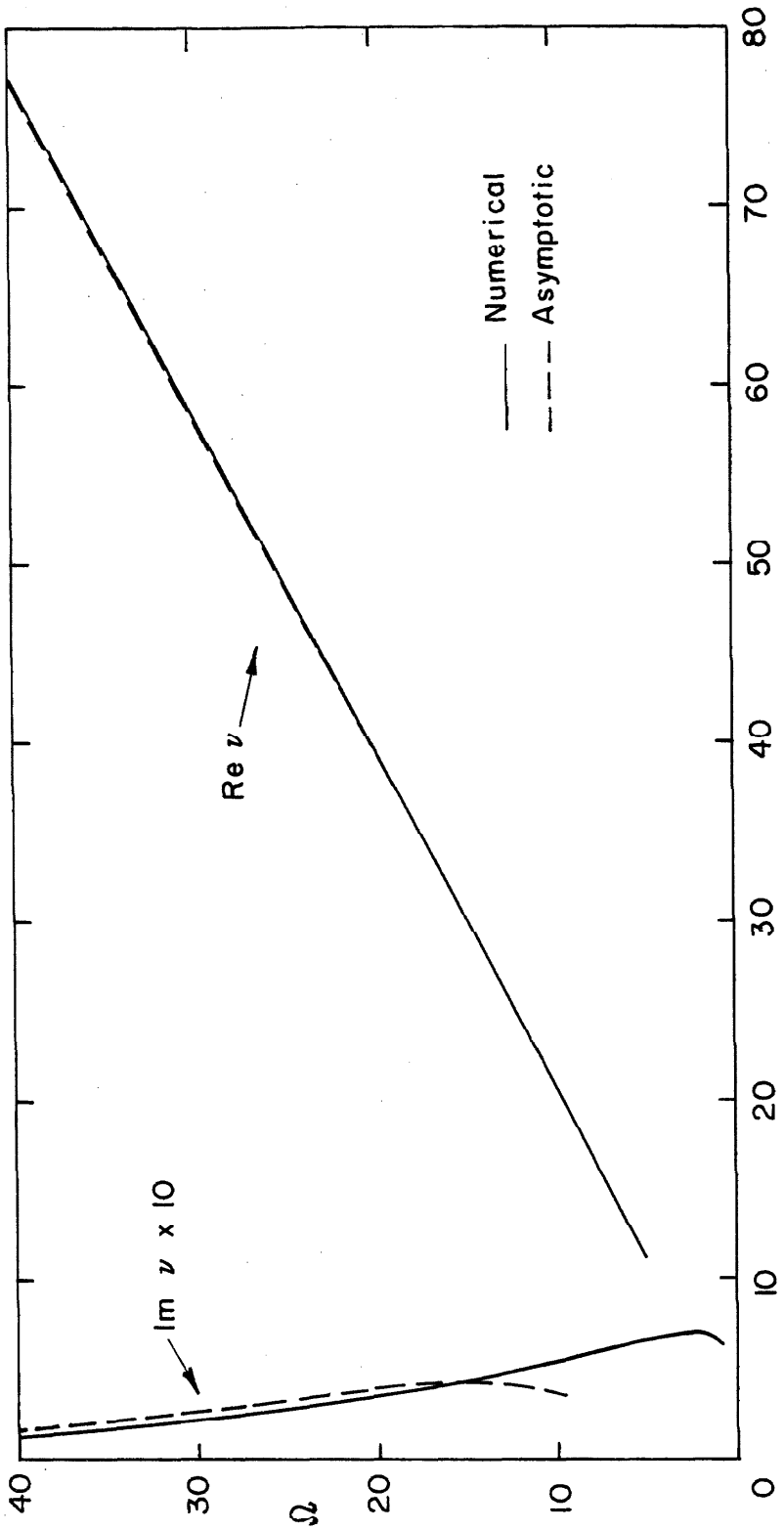

Fig. 11. Comparison of Asymptotic and Numerical Results for Rayleigh Root.

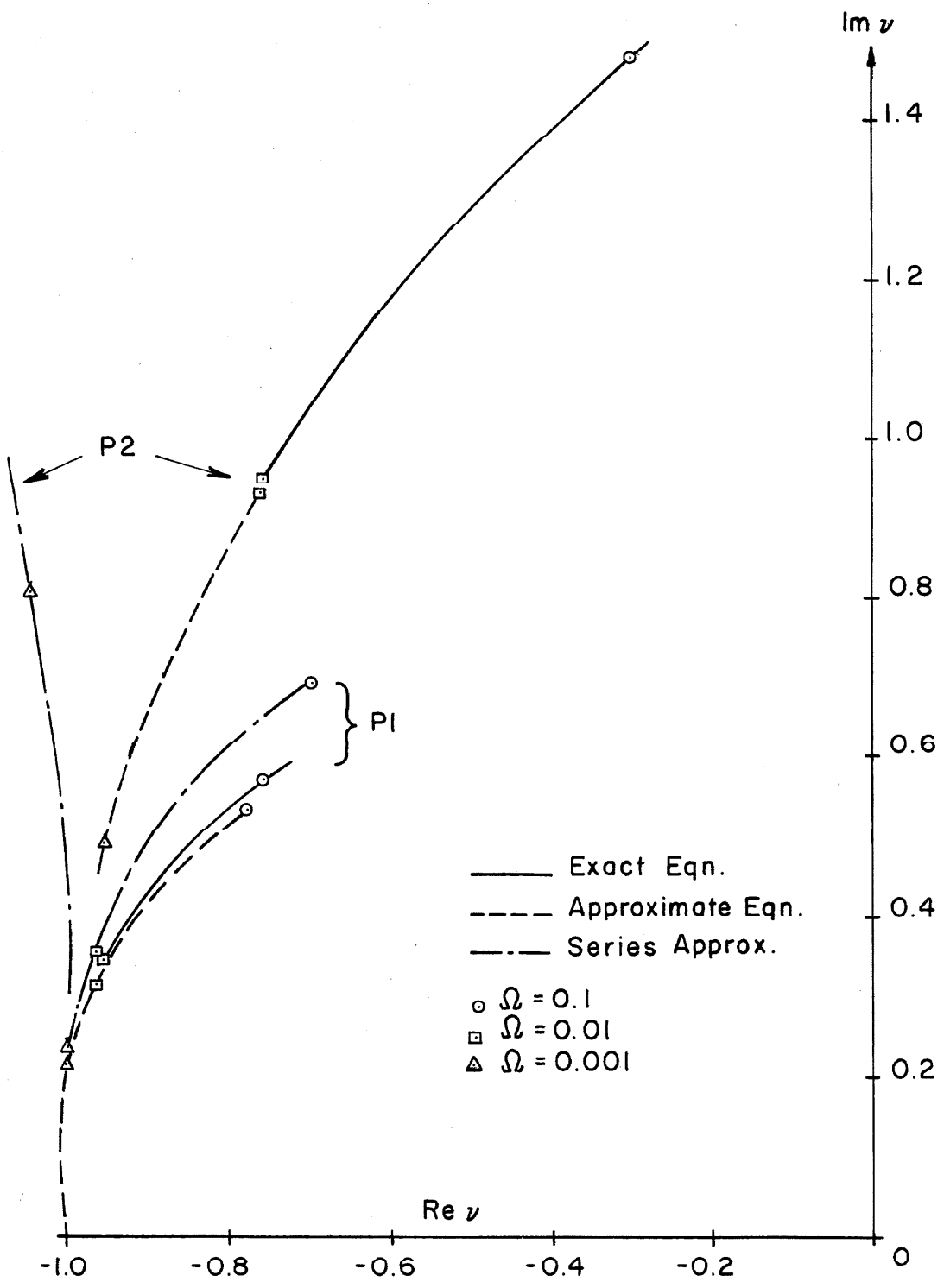

Fig. 12. Comparison of Asymptotic and Numerical Results for the P Roots as $\Omega \to 0$.

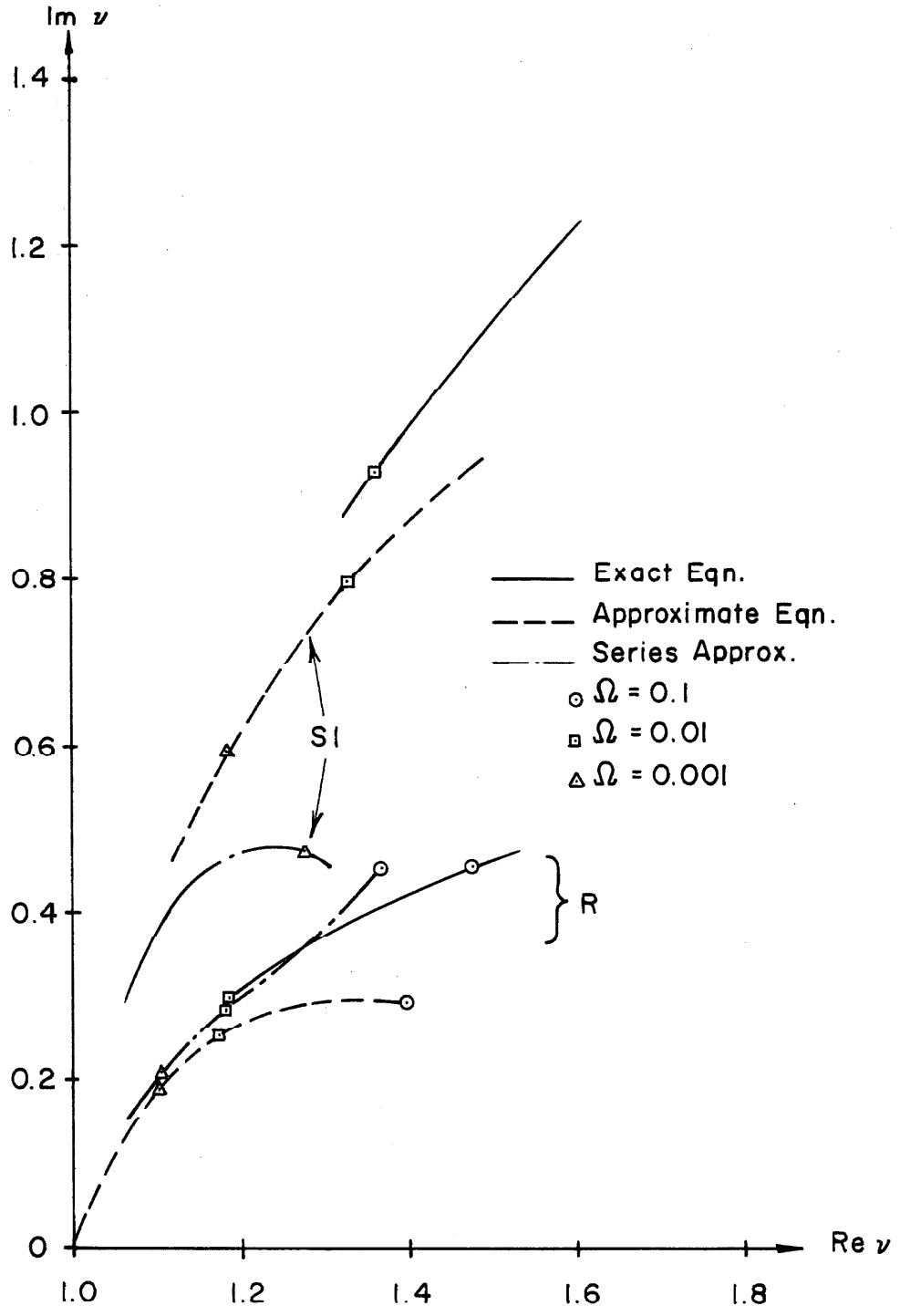

Fig.13. Comparison of Asymptotic and Numerical Results for the R and S Roots as $\Omega \to 0$.

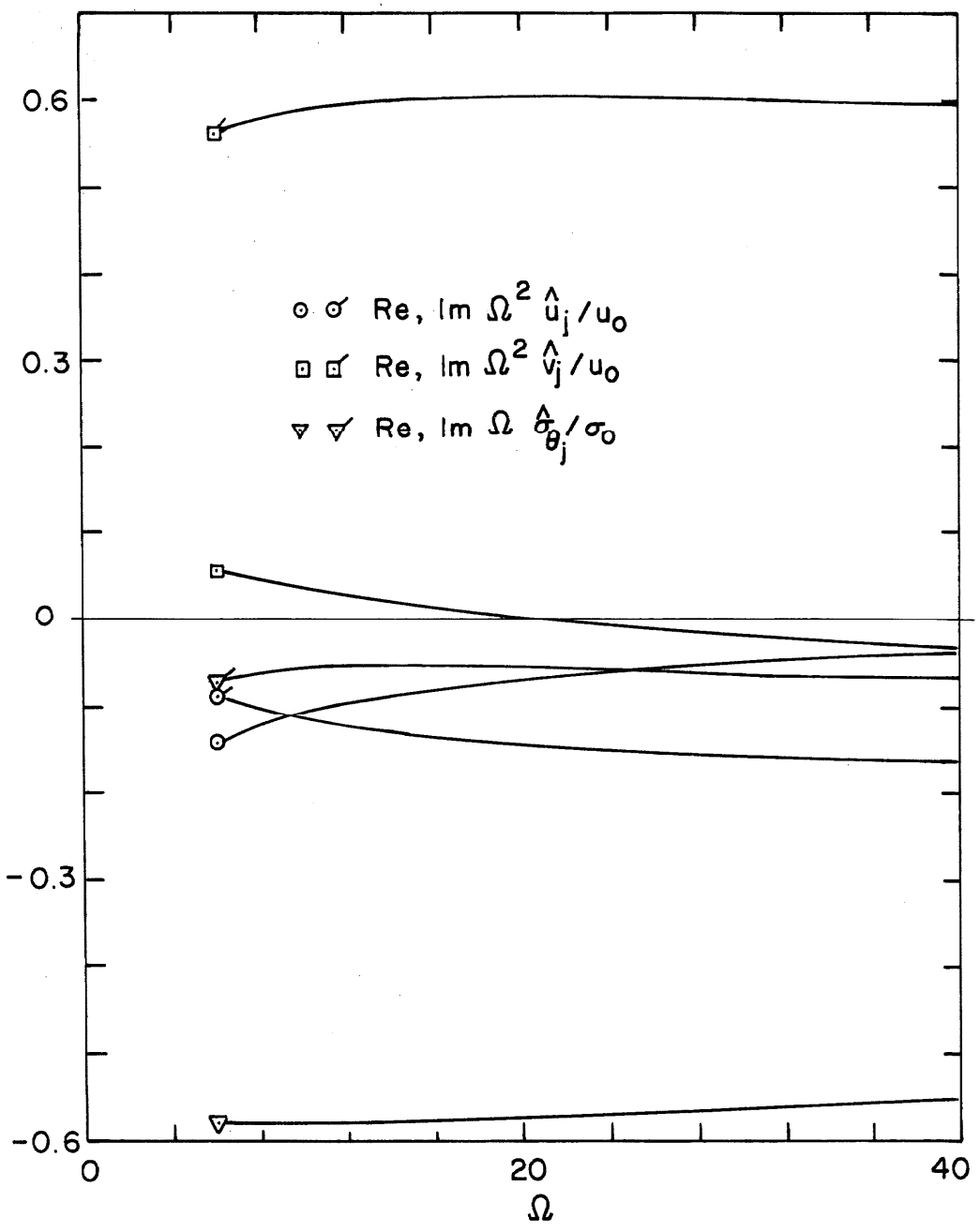

Fig. 14. Behavior of Integrand Functions $\hat{f}_j(a, \Omega)$ for Large Ω, PI Mode.

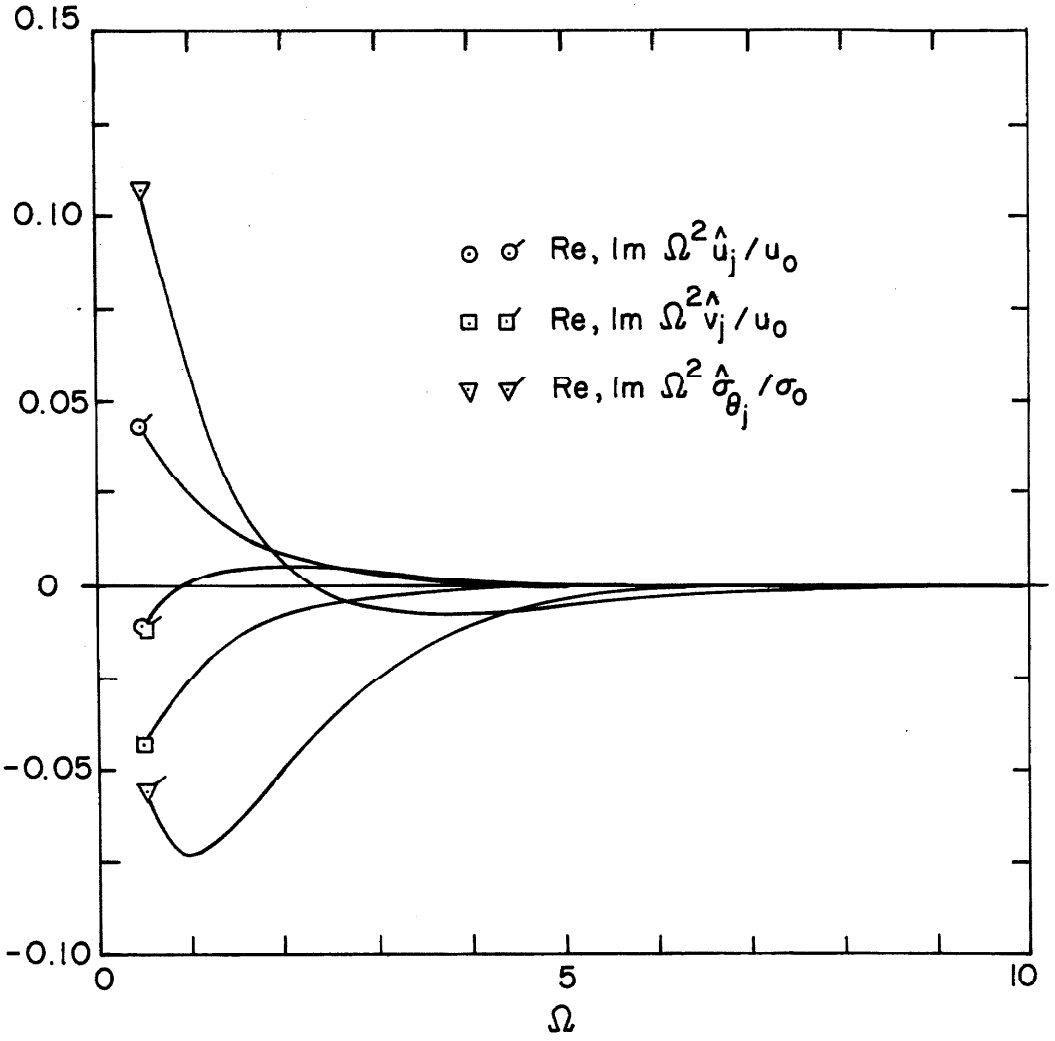

Fig. 15. Behavior of Integrand Functions $\hat{f}_j(a, \Omega)$ for Large Ω, SI Mode.

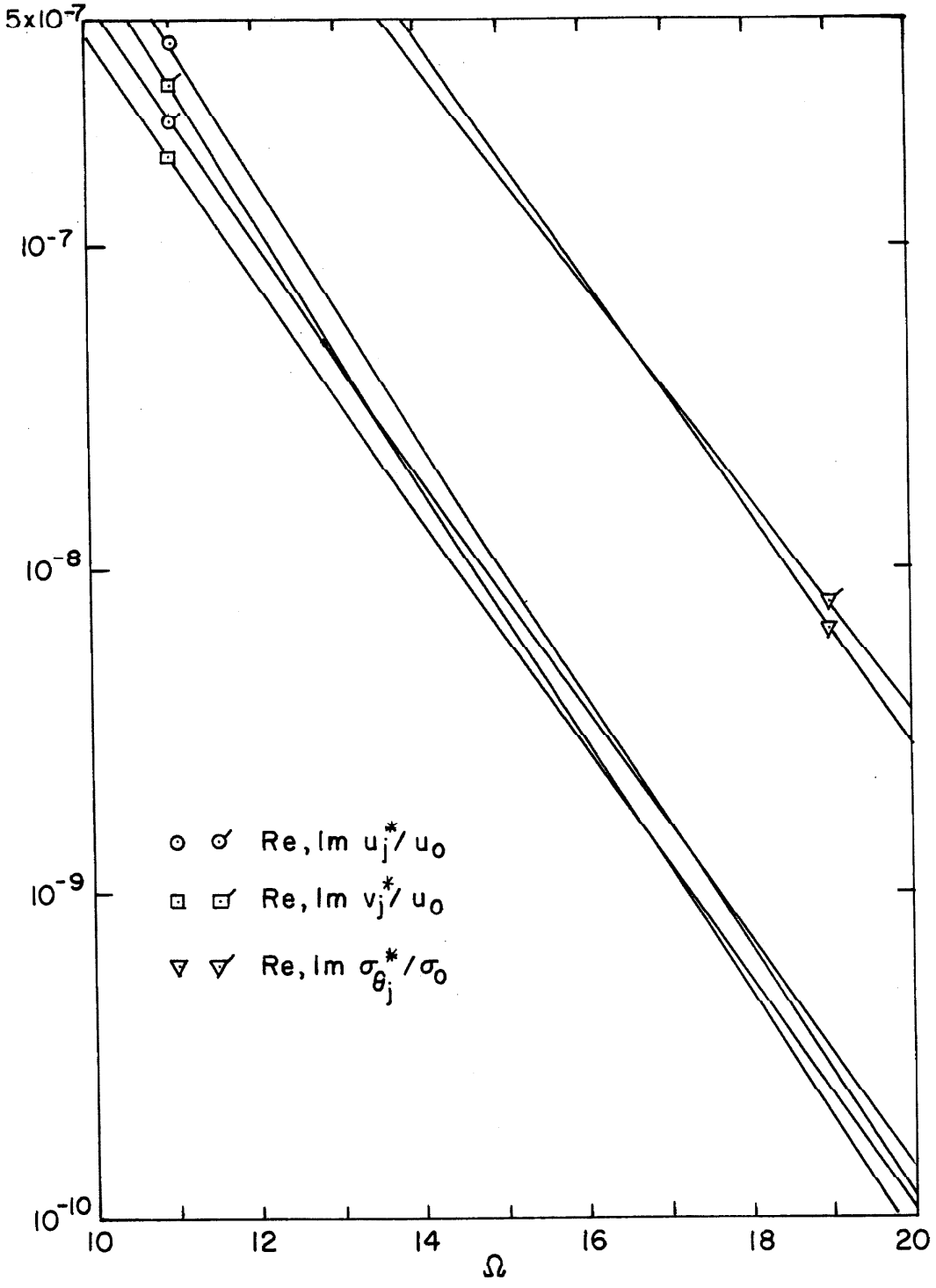

Fig. 16. Behavior of Integrand Functions $\hat{f}_j(a, \Omega)$ for Large Ω, R Mode.

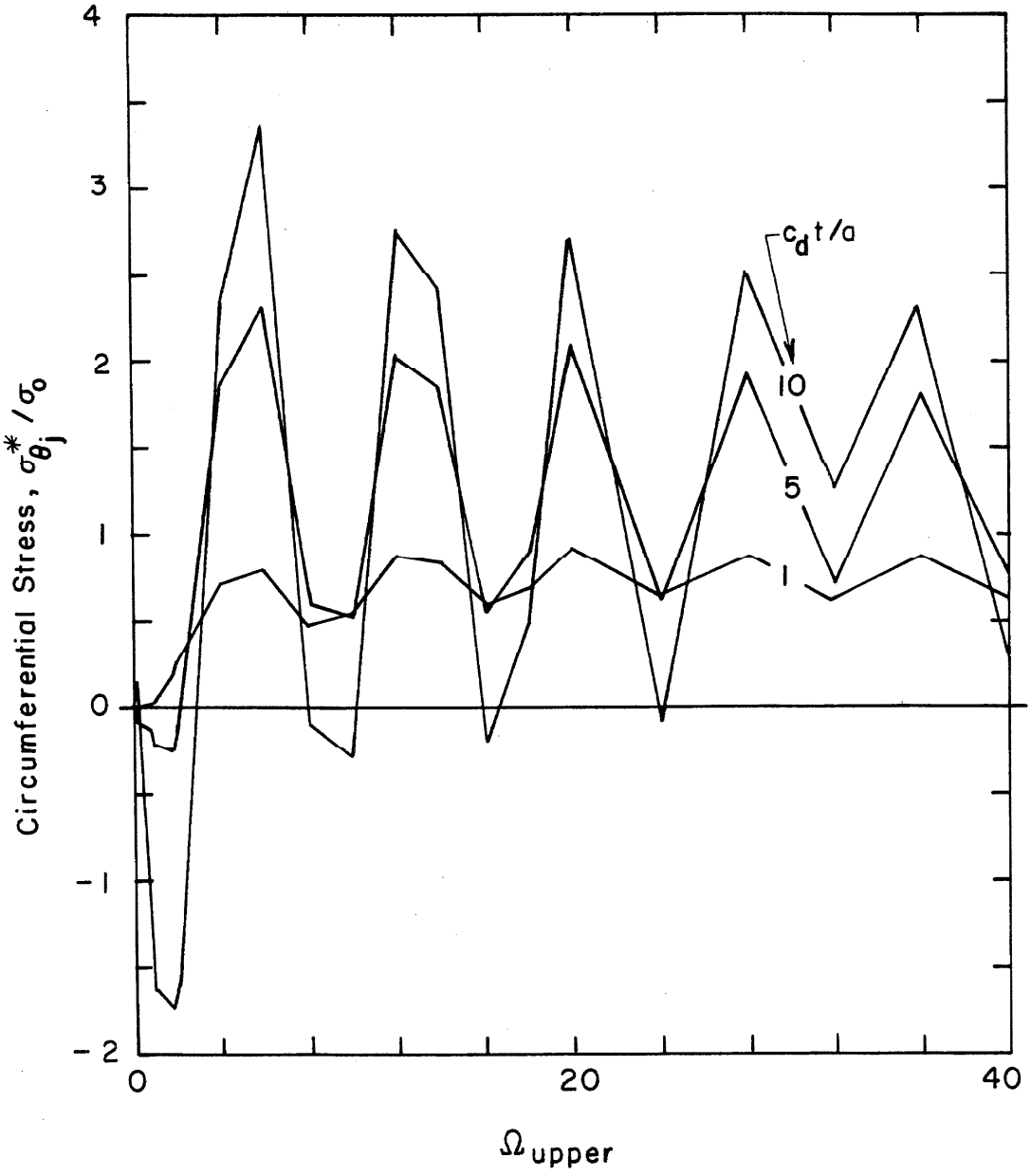

Fig. 17. Convergence at Upper Limit, PI Mode, $\theta = \frac{3}{4}\pi$.

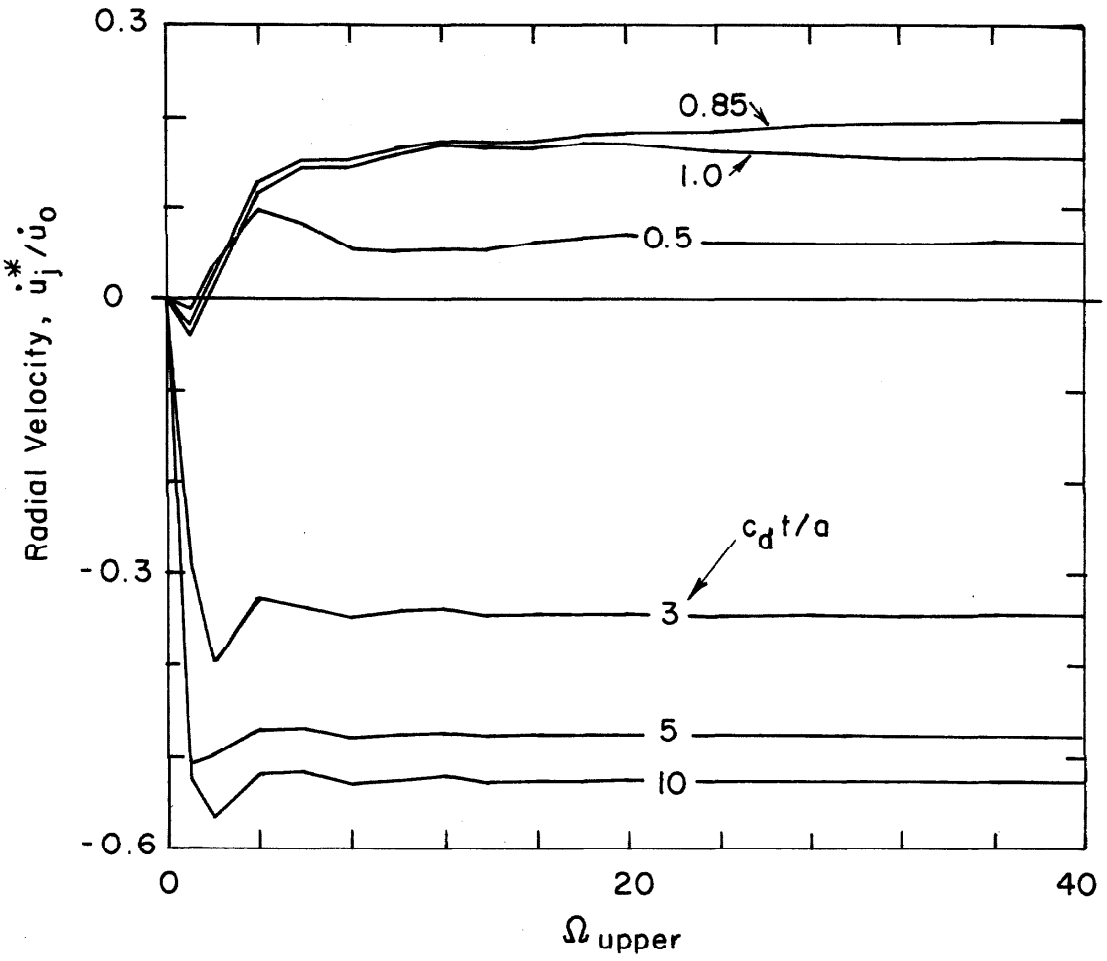

Fig. 18. Convergence at Upper Limit, PI mode, $\theta = \frac{3}{4}\pi$.

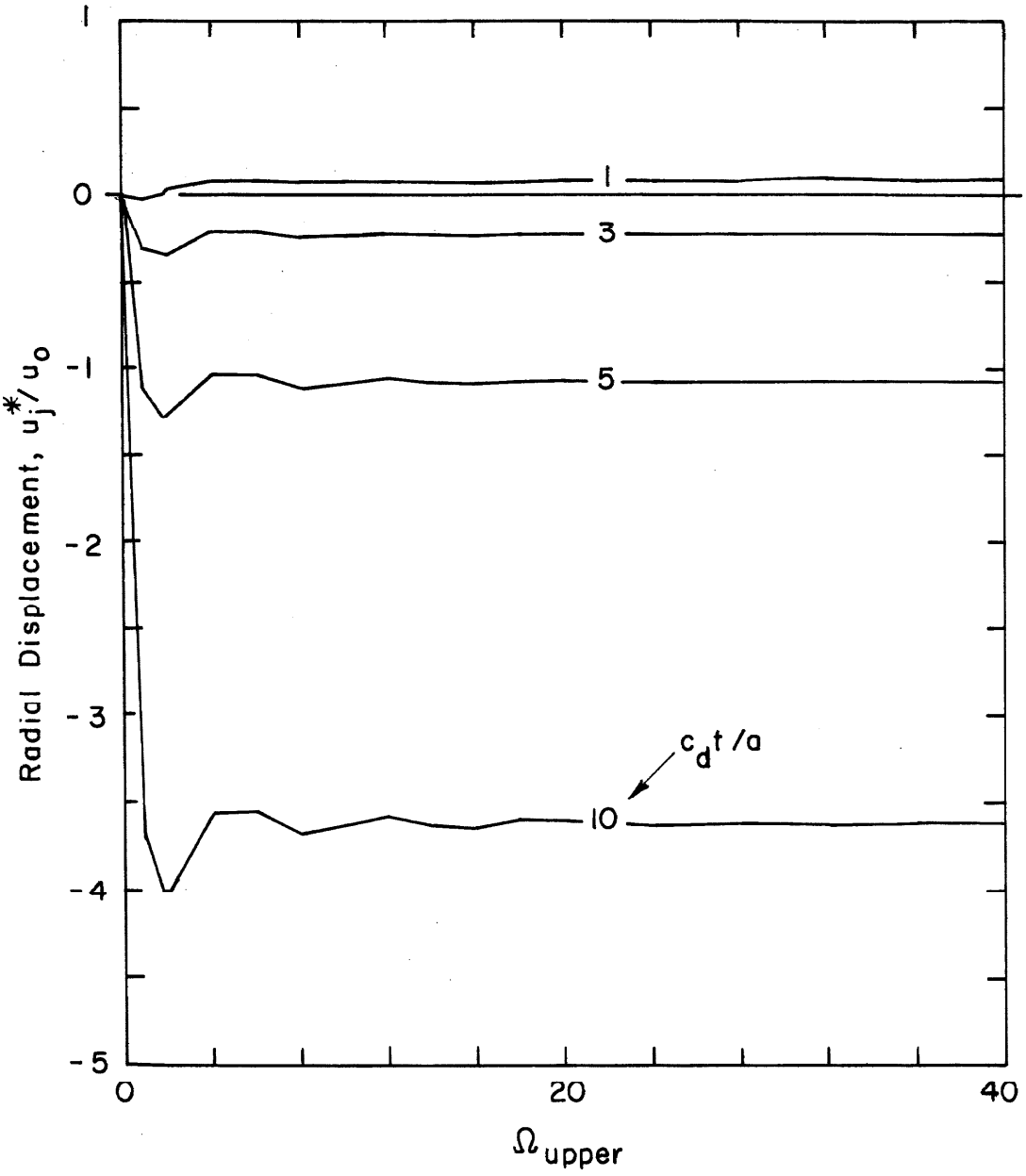

Fig. 19. Convergence at Upper Limit, P1 Mode, $\theta = \frac{3}{4}\pi$.

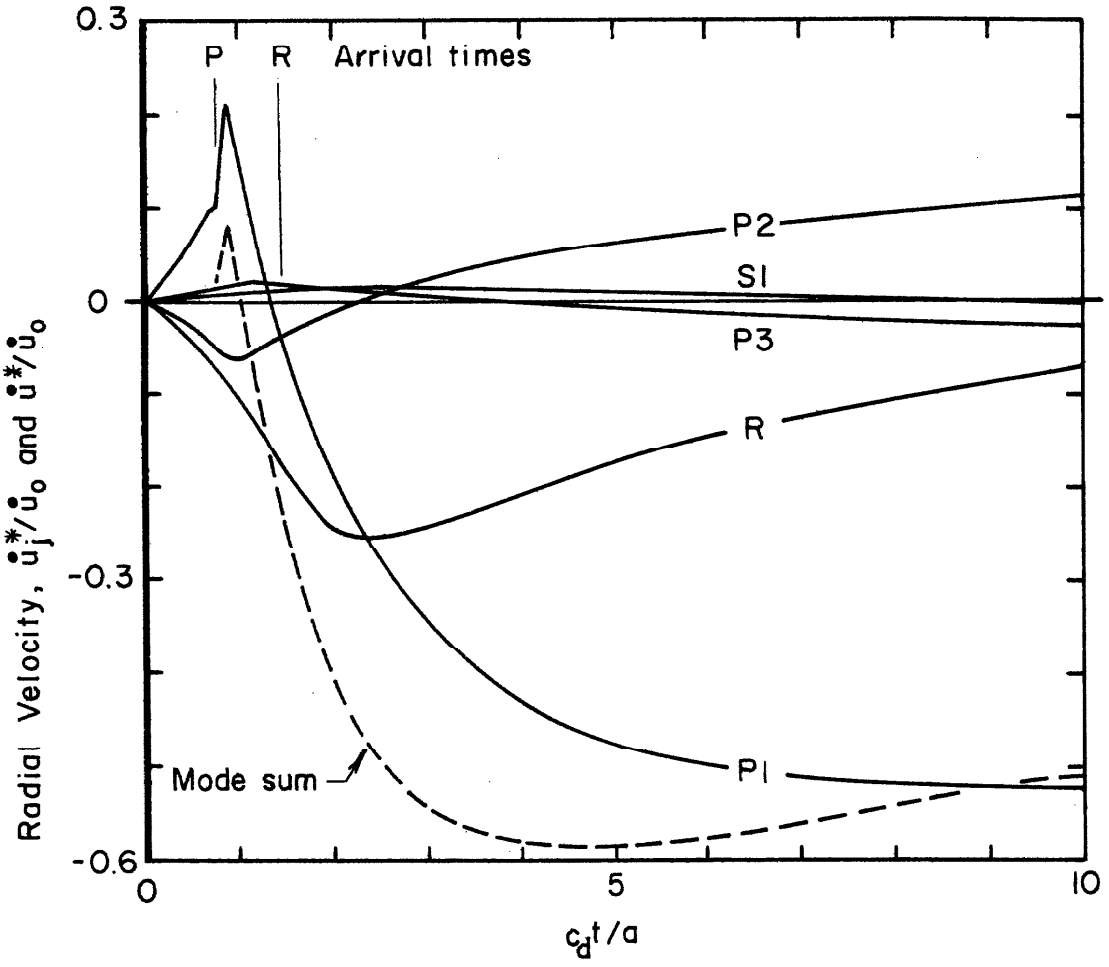

Fig. 20. Modal Response $\dot{u}_j^*$ and Mode Sum $\dot{u}^*$ at $r = a$, $\theta = \frac{3}{4}\pi$.

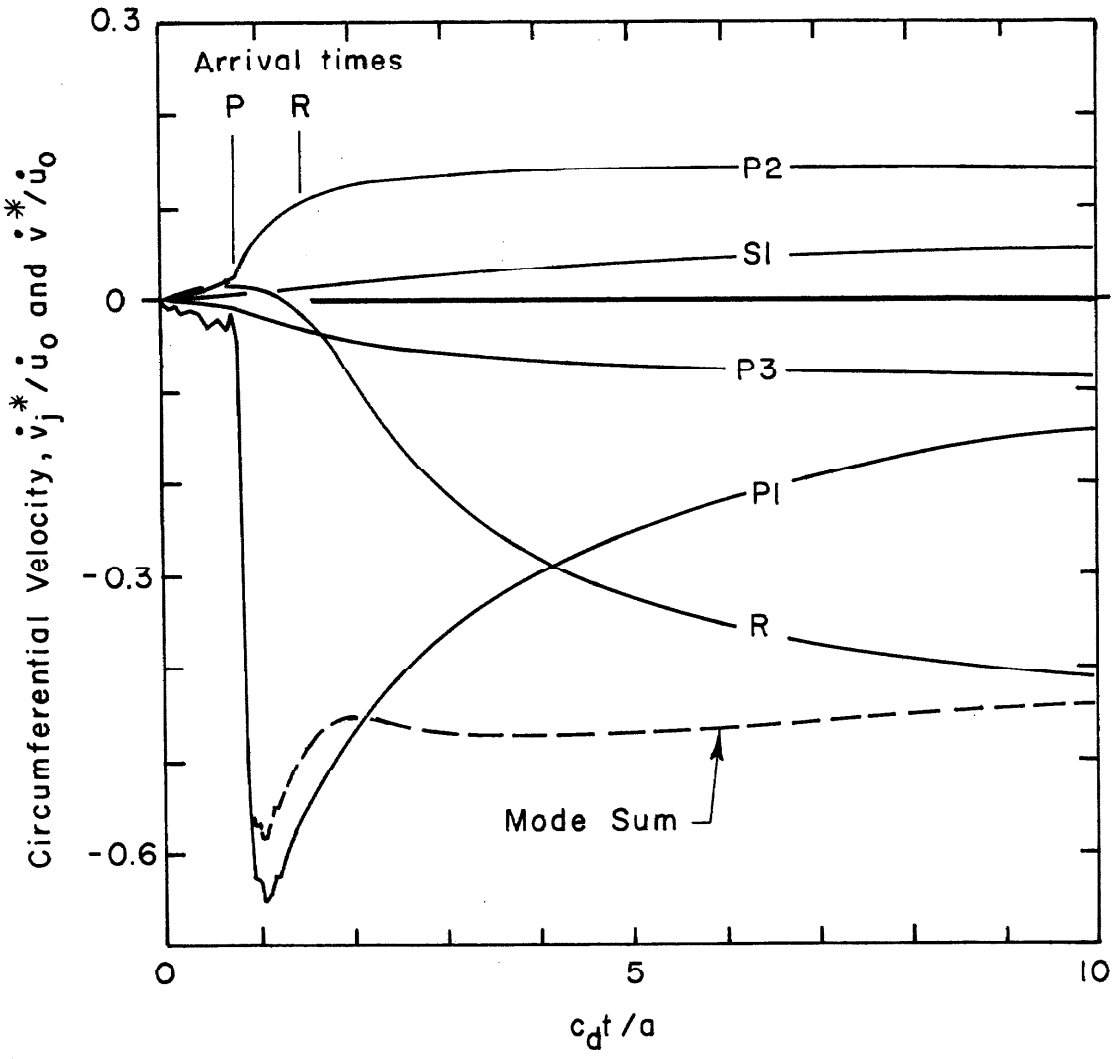

Fig. 21. Modal Response $\dot{v}_j^*$ and Mode Sum $\dot{v}^*$ at $r = a$, $\theta = \frac{3}{4}\pi$.

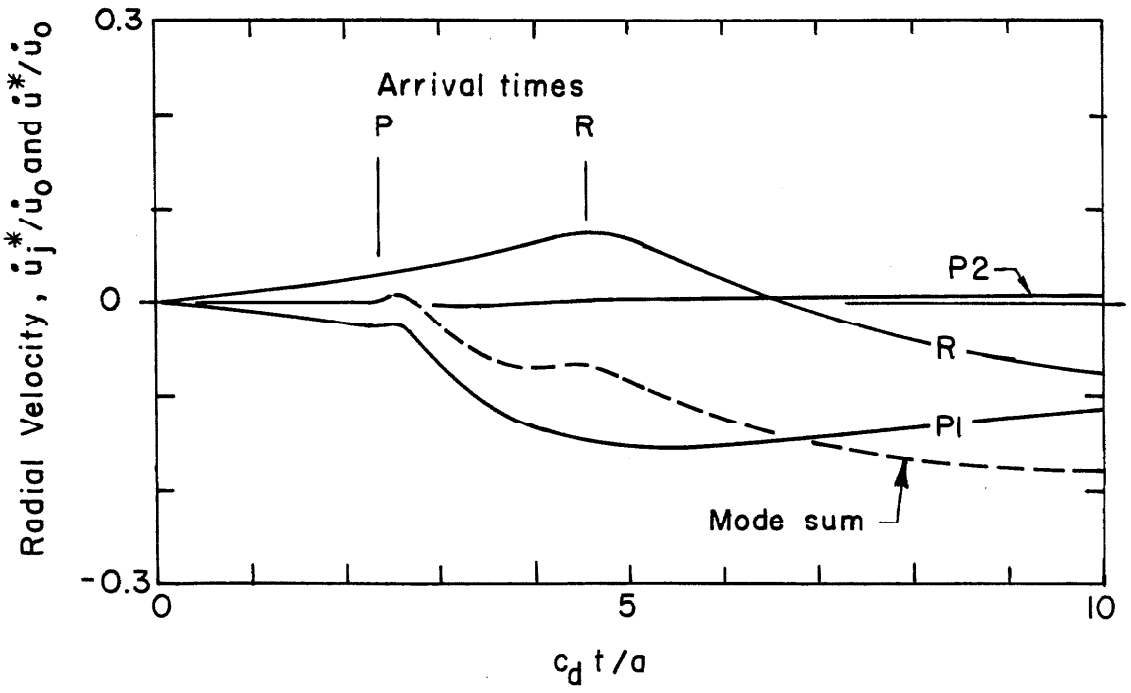

Fig. 22. Modal Response $\dot{u}_j^*$ and Mode Sum $\dot{u}^*$ at $r = a$, $\theta = \frac{5}{4}\pi$.

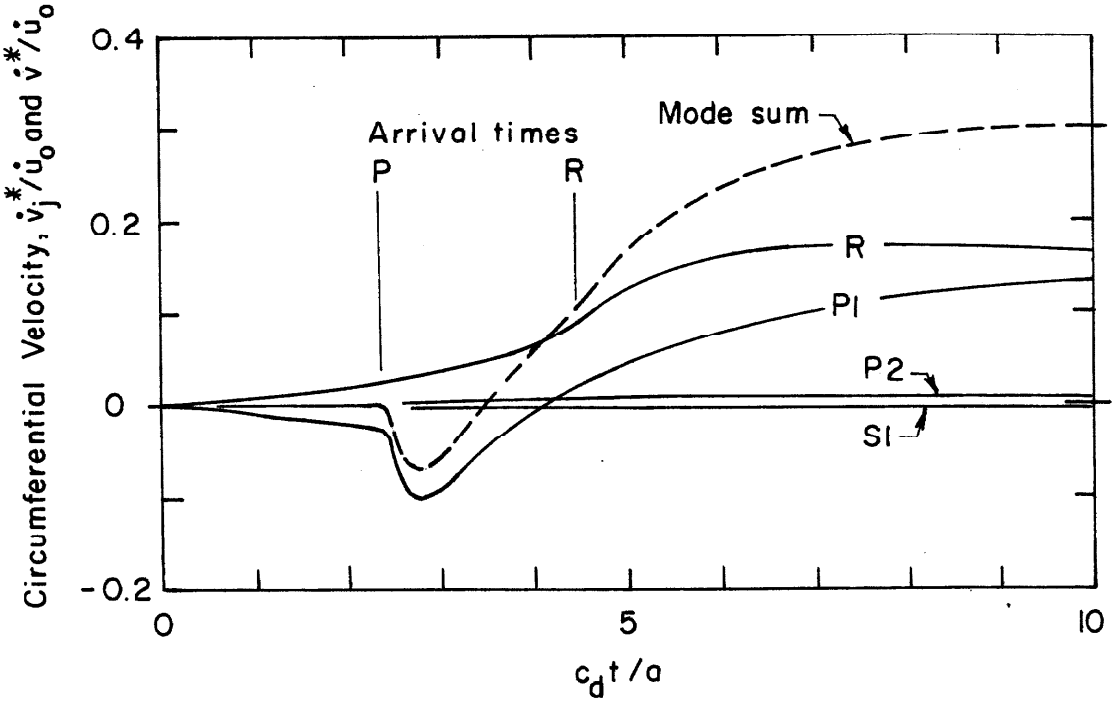

Fig. 23. Modal Response $\dot{v}_j^*$ and Mode Sum $\dot{v}^*$ at $r = a$, $\theta = \frac{5}{4}\pi$.

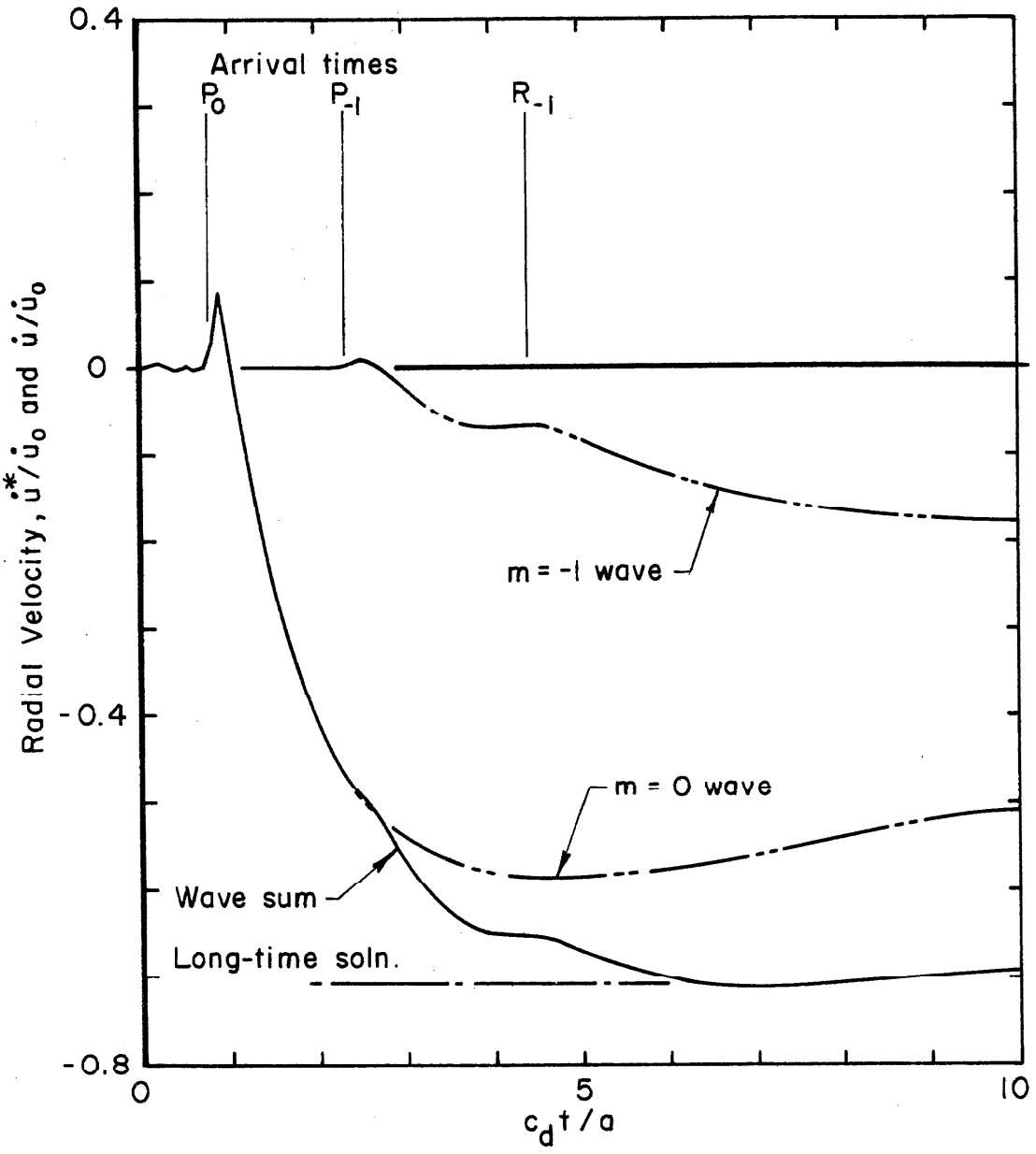

Fig.24. Waves $\dot{u}^*$ and Wave Sum $\dot{u}$ at $r=a$, $\theta=\frac{3}{4}\pi$.

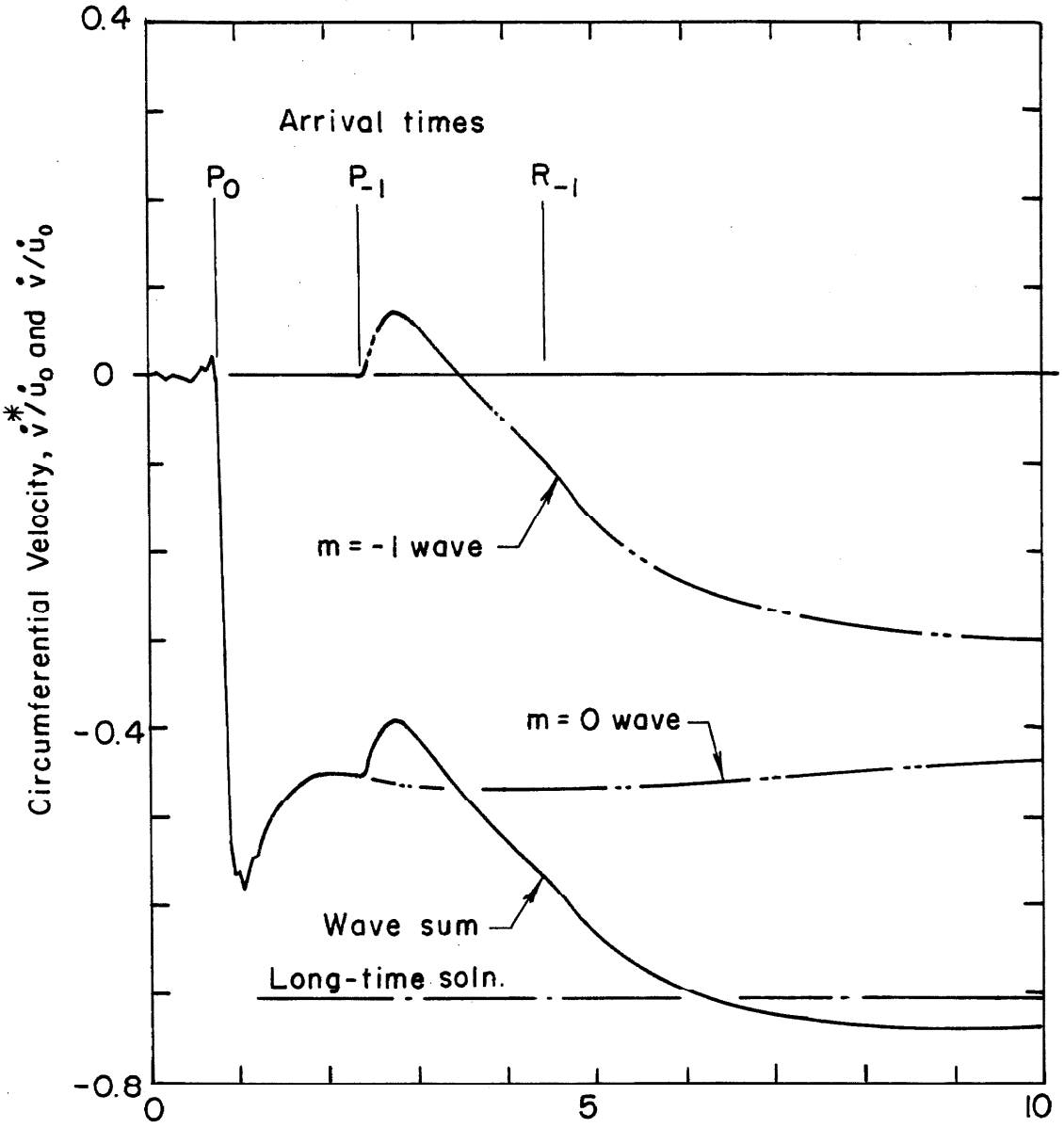

Fig. 25. Waves $\dot{v}^*$ and Wave Sum $\dot{v}$ at $r=a$, $\theta=\frac{3}{4}\pi$.

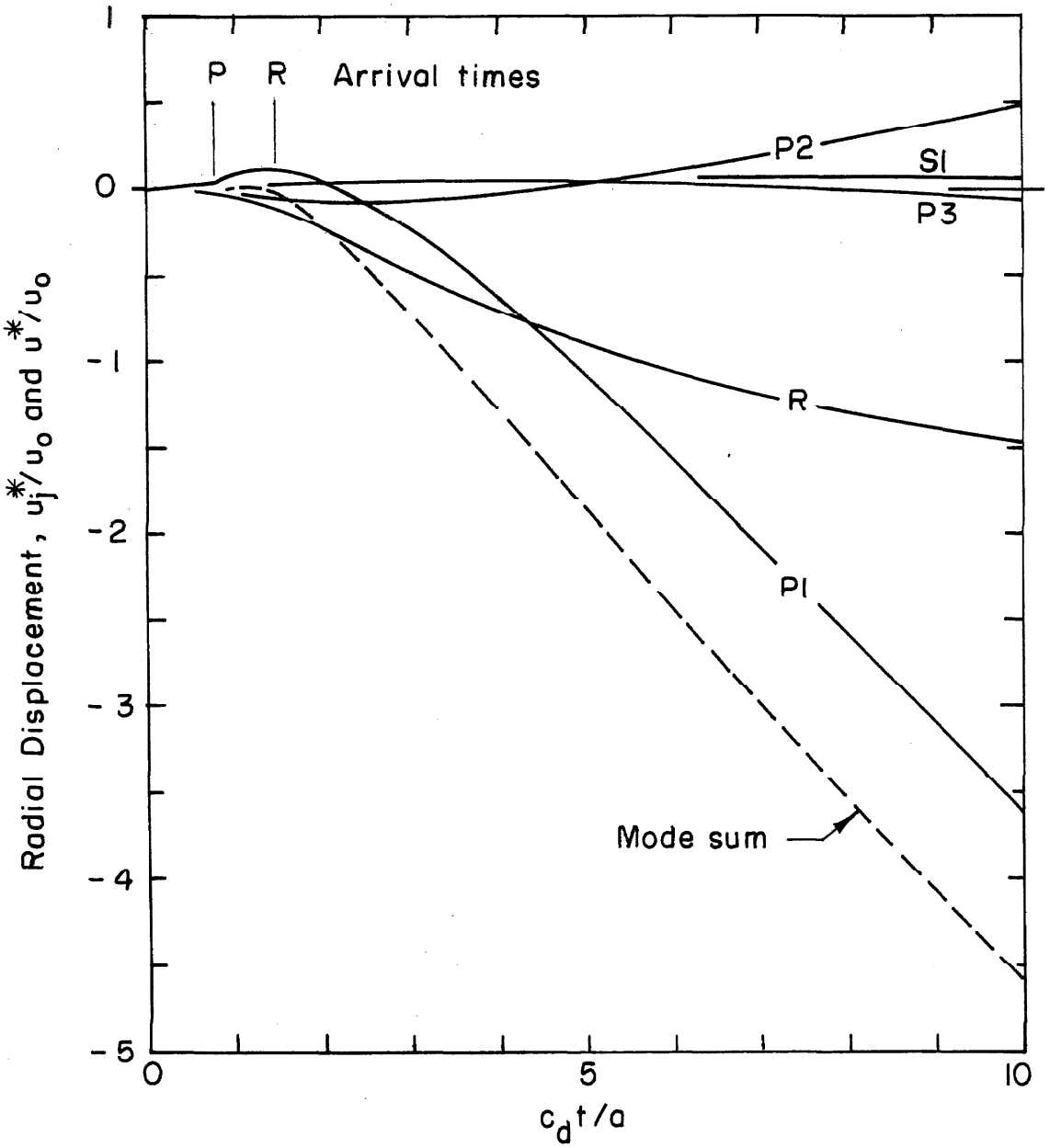

Fig. 26. Modal Response u_j^* and Mode Sum u^* at $r = a$, $\theta = \frac{3}{4}\pi$.

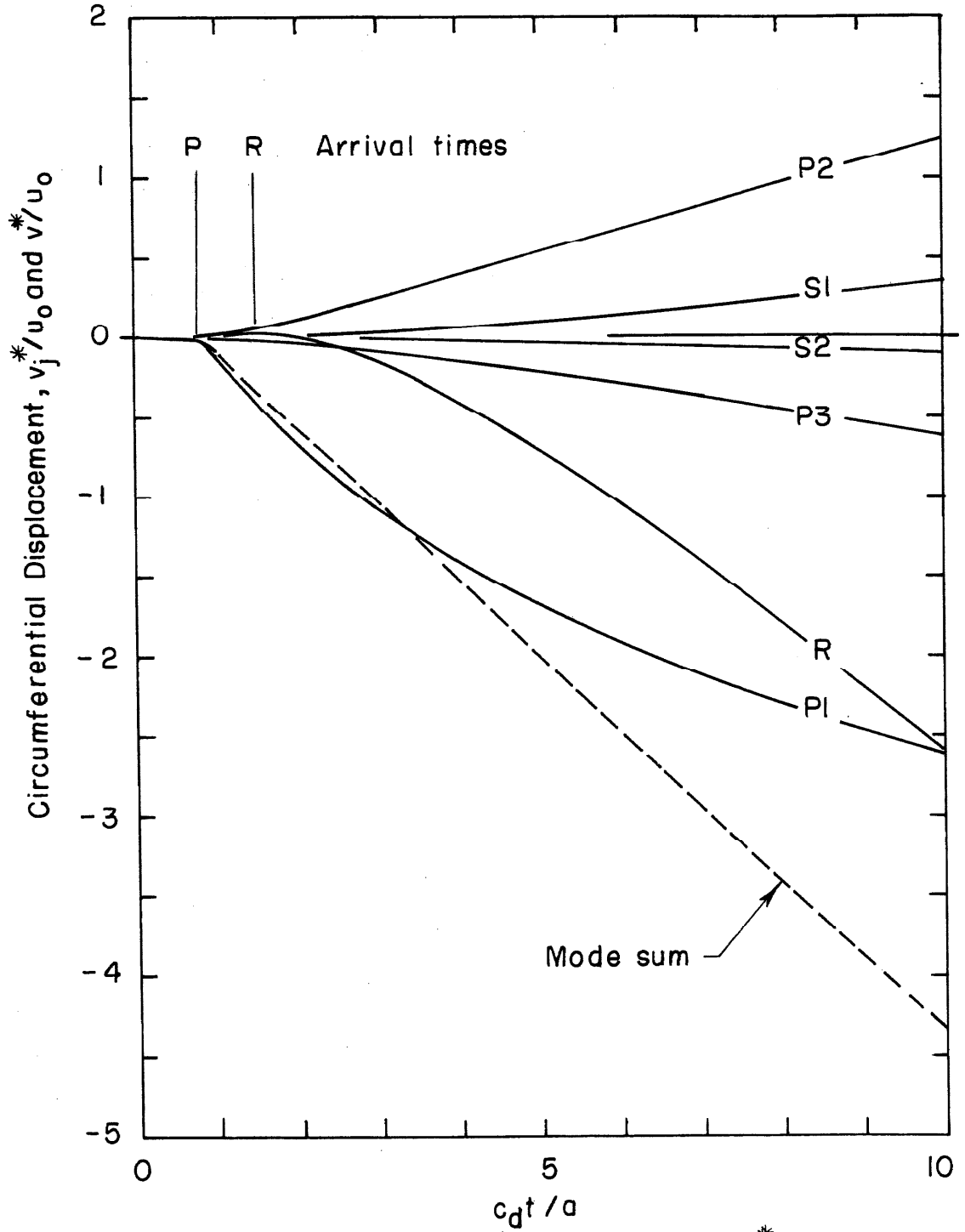

Fig. 27. Modal Response v_j^* and Mode Sum v^* at $r = a$, $\theta = \frac{3}{4}\pi$.

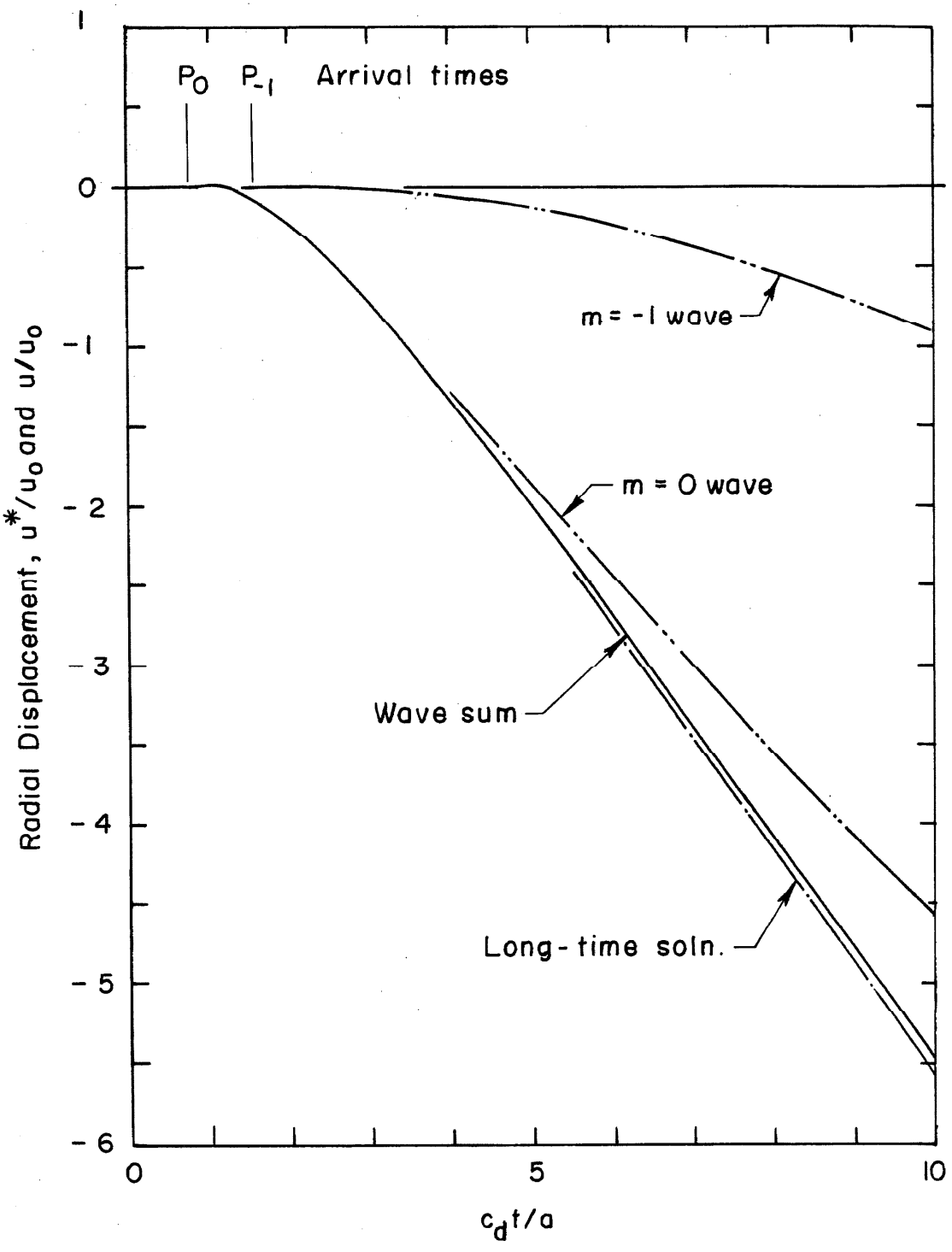

Fig. 28. Waves u^* and Wave Sum u at $r = a, \theta = \frac{3}{4}\pi$.

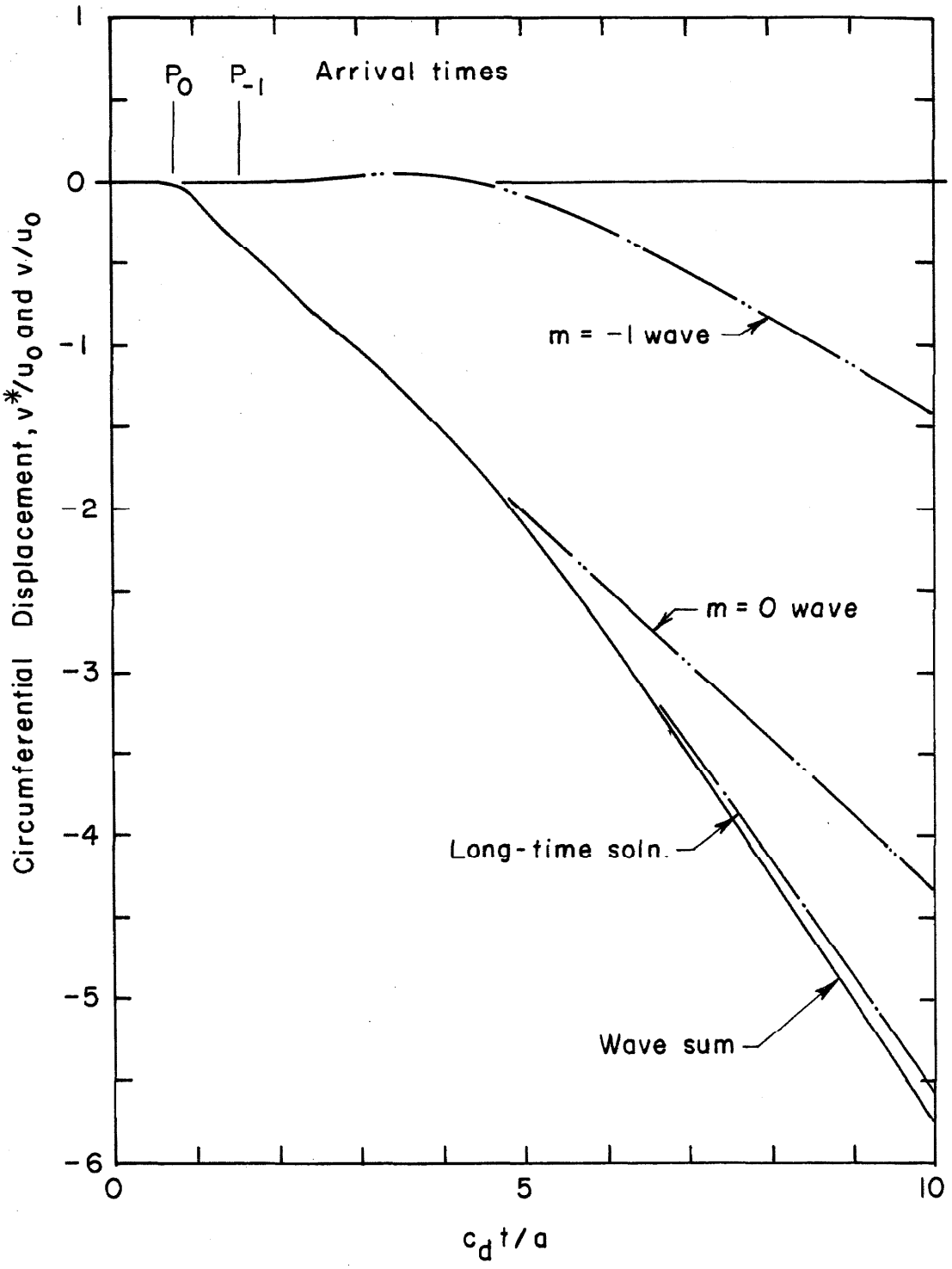

Fig. 29. Waves v^* and Wave Sum v at r = a, $\theta = \frac{3}{4}\pi$.

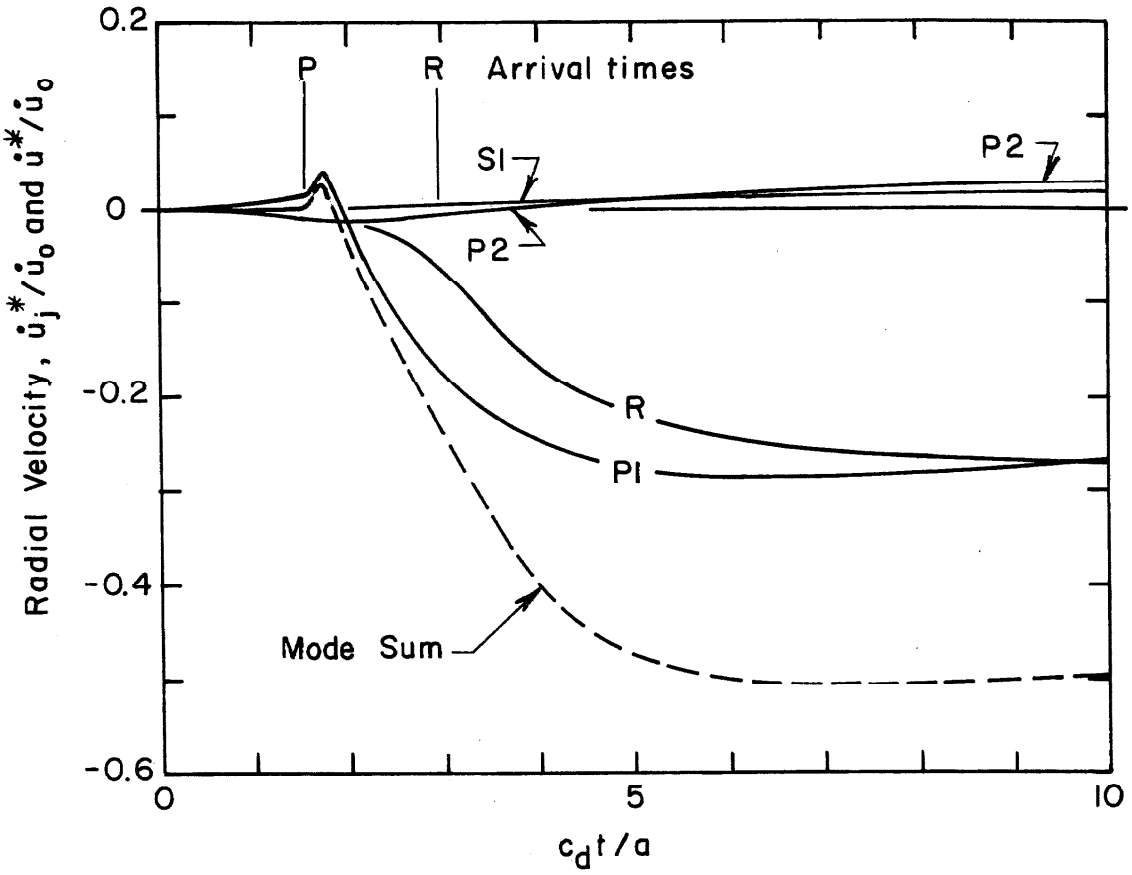

Fig. 30. Modal Response $\dot{u}_j^*$ and Mode Sum $\dot{u}^*$ at $r = a$, $\theta = \pi$.

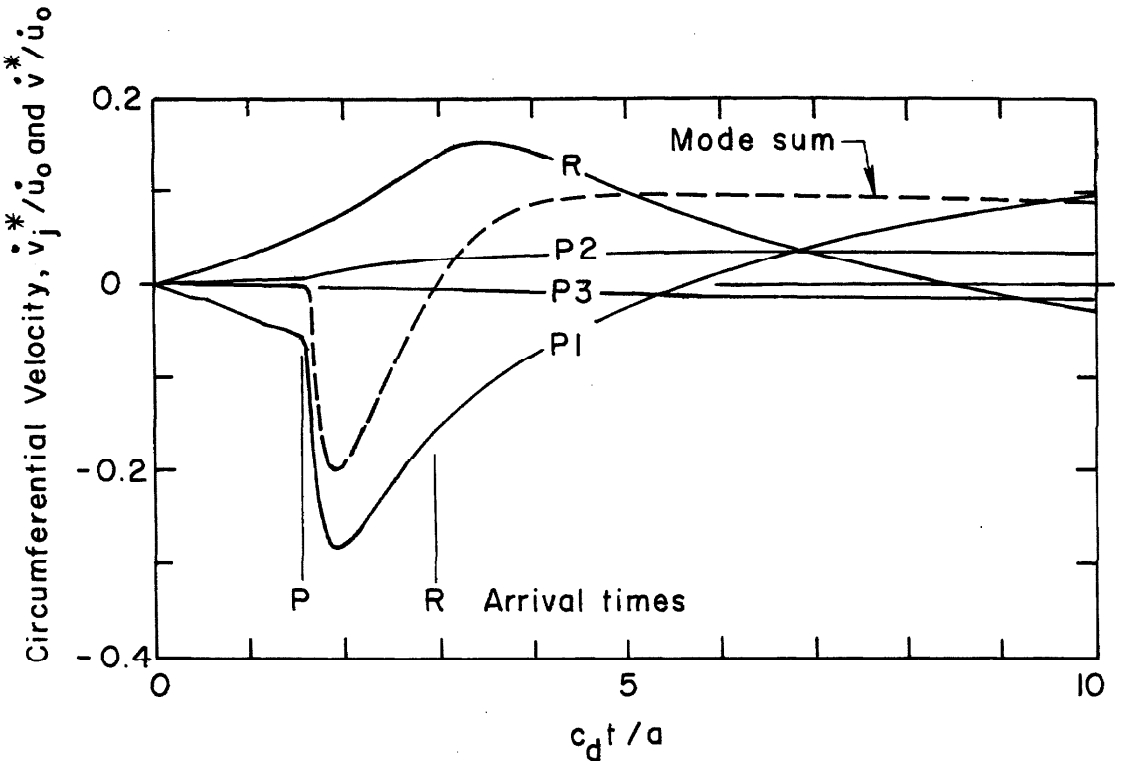

Fig. 31. Modal Response $\dot{v}_j^*$ and Mode Sum $\dot{v}^*$ at $r=a$, $\theta=\pi$.

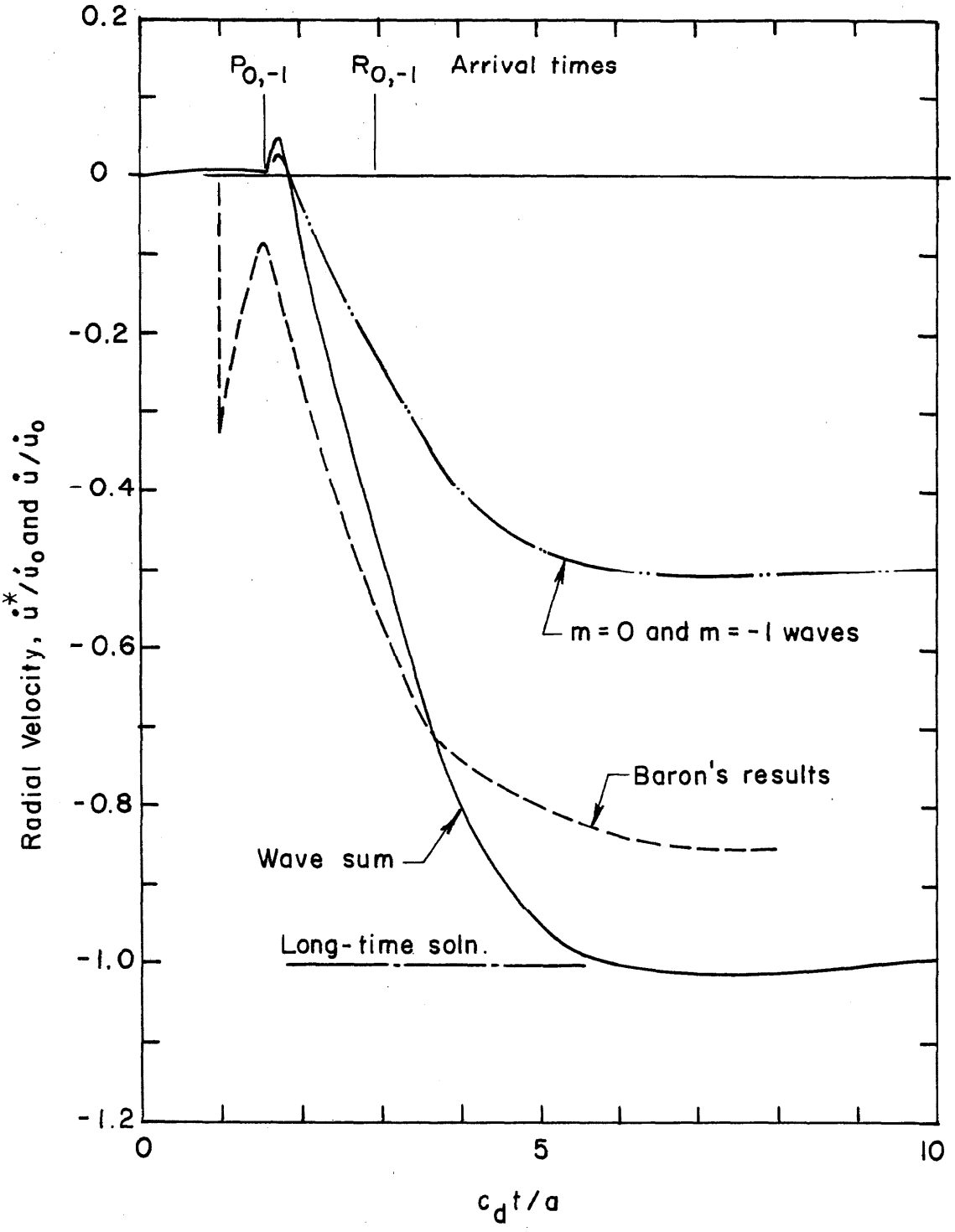

Fig. 32. Waves $\dot{u}^*$ and Wave Sum $\dot{u}$ at $r = a$, $\theta = \pi$.

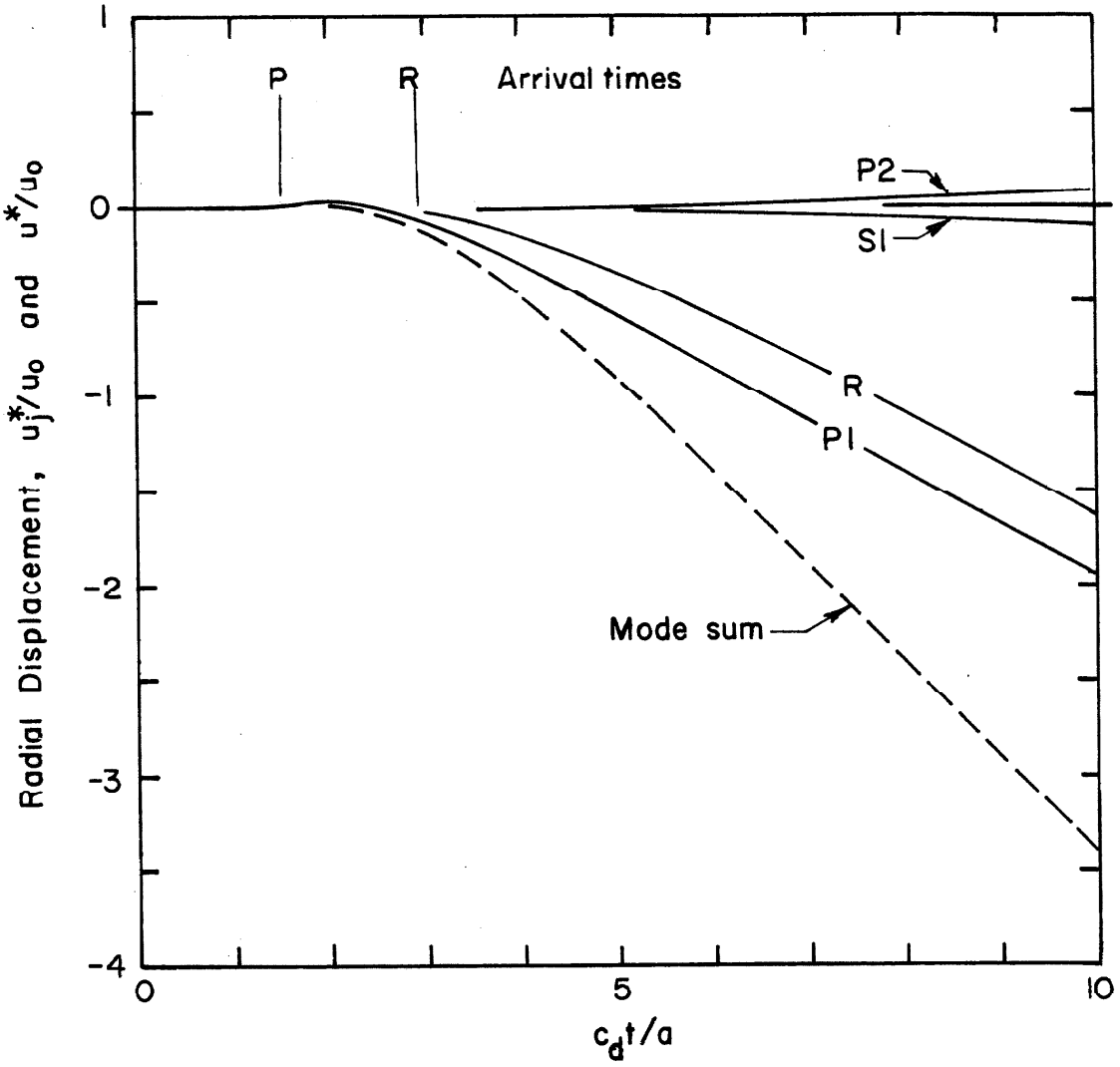

Fig. 33. Modal Response u_j^* and Mode Sum u^* at $r=a$, $\theta = \pi$.

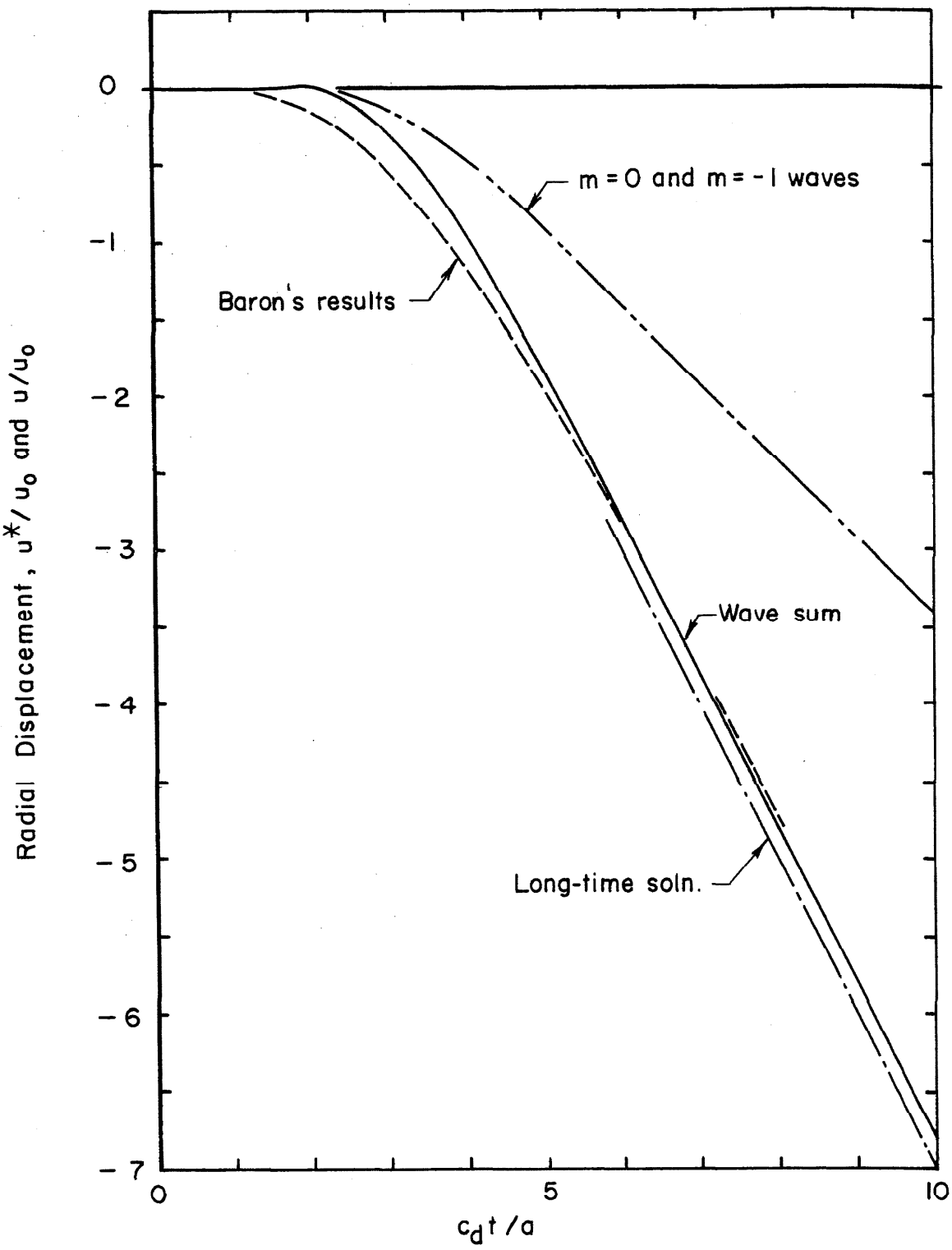

Fig. 34. Waves u^* and Wave Sum u at $r = a$, $\theta = \pi$.

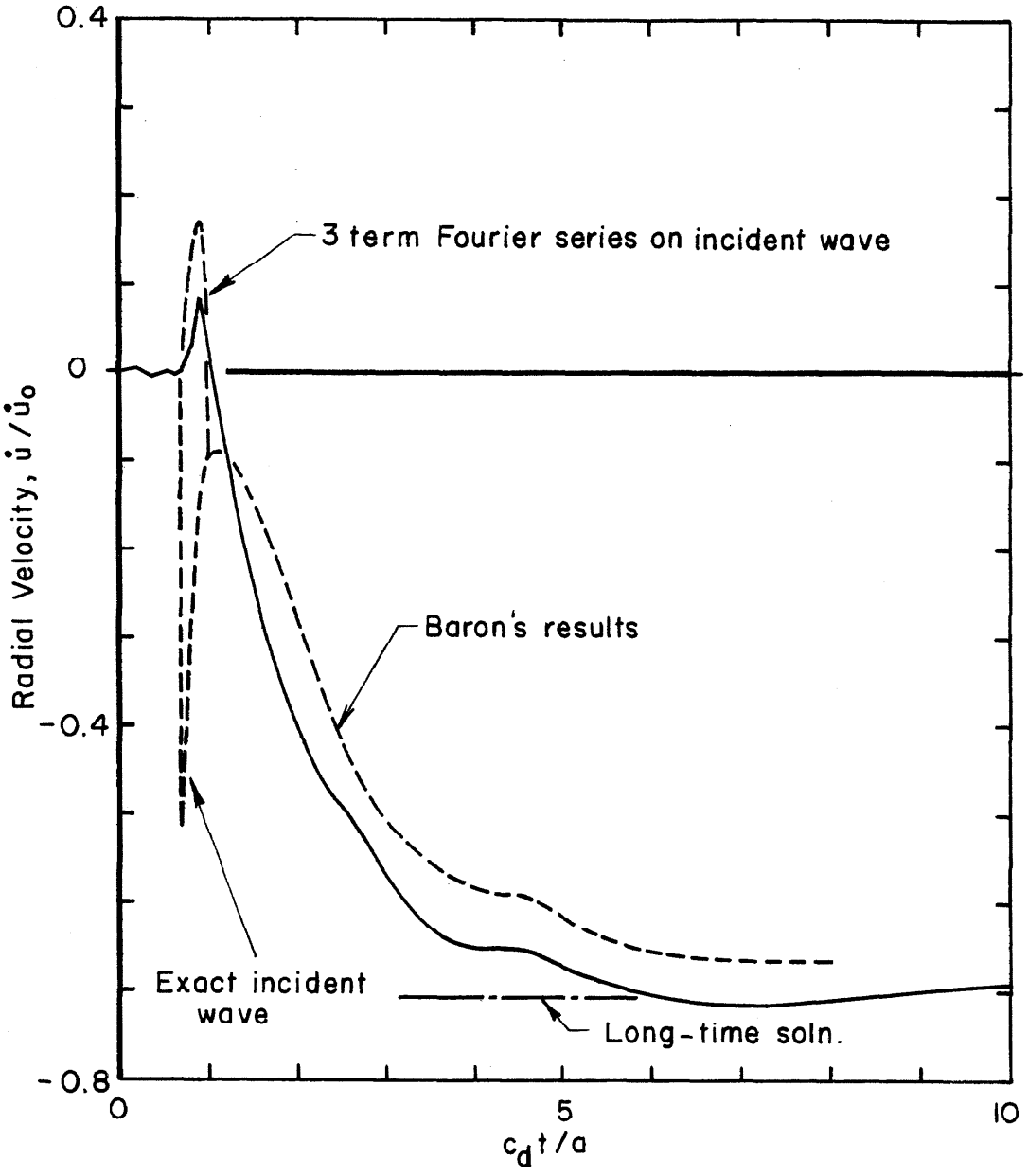

Fig. 35. Comparison with Baron's Results.

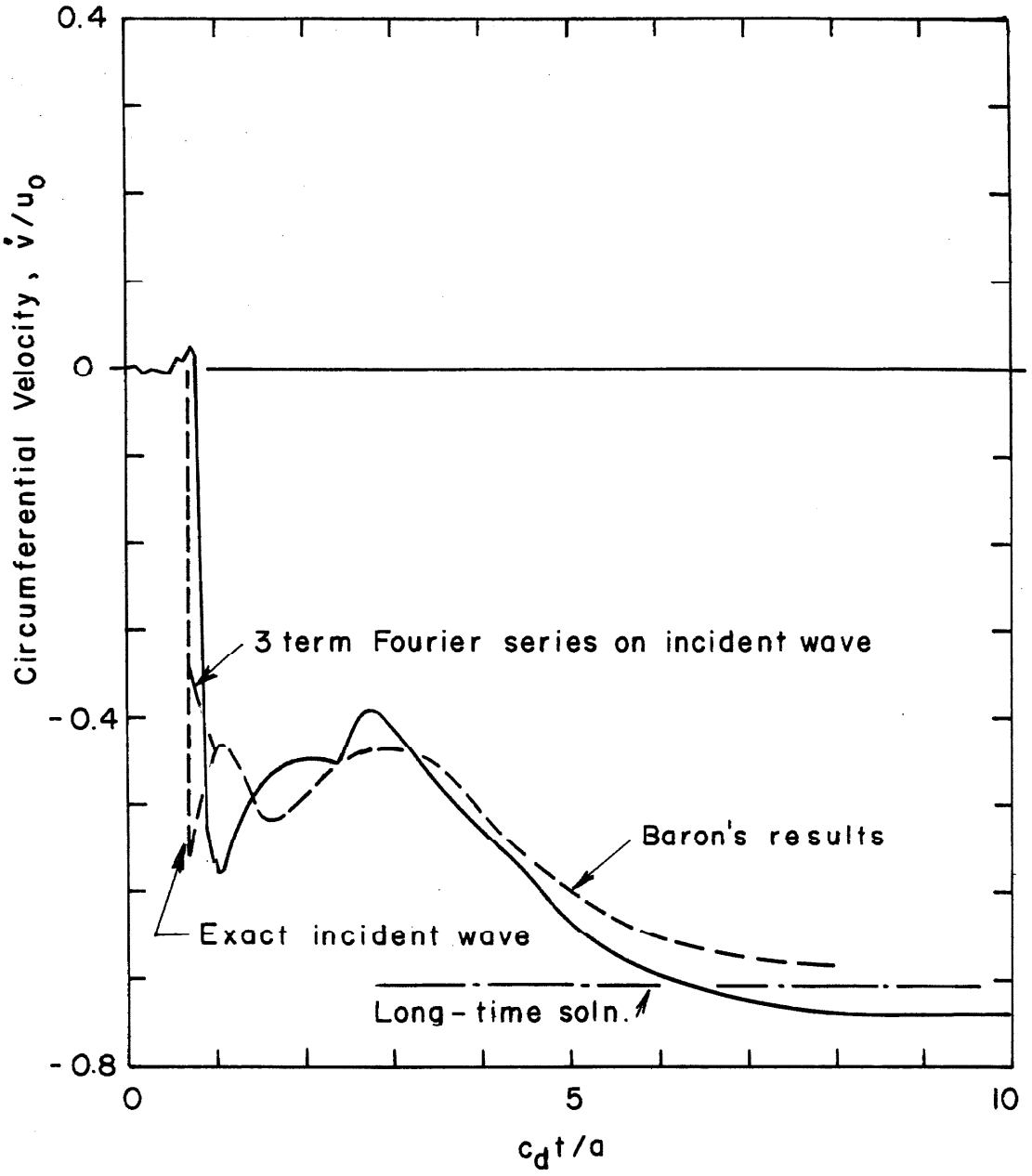

Fig. 36. Comparison with Baron's Results.

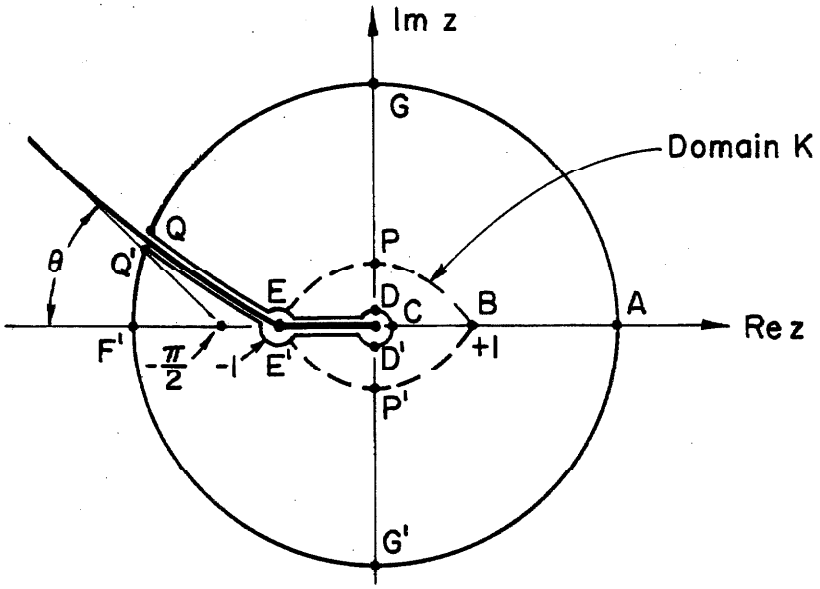

(a) The z-plane. $\theta = \arg \nu$.

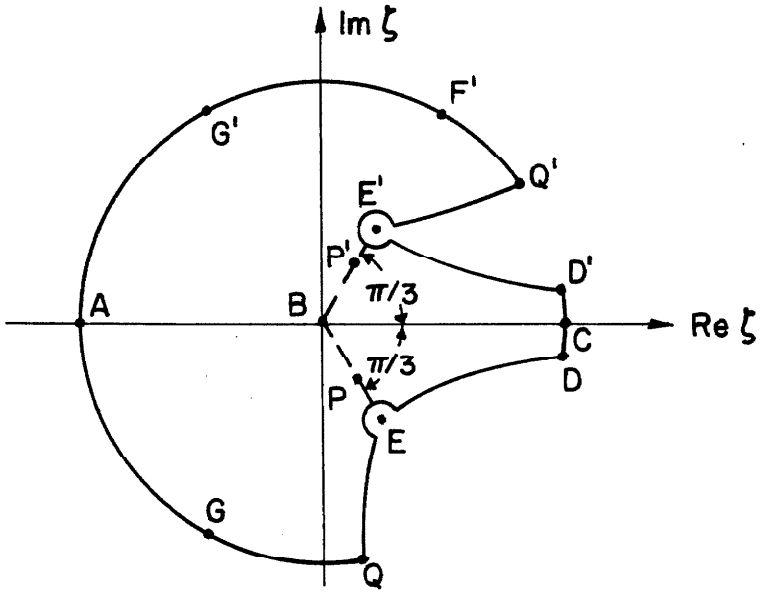

(b) The ζ-plane.

Fig. A1. The $z-\zeta$ Transformation.